A Novel Cryogenic CO_2 Capture Technology Based on Free Piston Stirling Coolers (FPSCs)

May 2013

Chunfeng SONG

A Novel Cryogenic CO_2 Capture Technology Based on Free Piston Stirling Coolers (FPSCs)

A Dissertation Submitted to

the Graduate School of Life and Environmental Sciences,

the University of Tsukuba

in Partial Fulfillment of the Requirements

for the Degree of Doctor of Philosophy in Biotechnology

(Doctoral Program in Bioindustrial Sciences)

Chunfeng SONG

CONTENT

ABBREVIATIONS

ASU	air separation unit
BFPT	boiler feed pump turbine
CCS	CO_2 capture and storage
CFC	chlorofluorocarbon
CLC	chemical-looping combustion
COP	coefficient of performance
COPS	coefficient of performance for the system
COS	carbonyl sulphide
EC	energy consumption
EPA	environmental protection agency
ESA	electric swing adsorption
ESP	electrostatic Precipitators
FGD	flue gas desulphurization
FPSC	free piston Stirling cooler
SCR	selective catalytic reduction
GHG	greenhouse gases
GT	gas turbine
HCFC	hydrochlorofluorocarbon
HFC	hydrofluorocarbon
HHV	high heat value
HP	high pressure
HRSG	heat recover steam generator
IEA	international energy agency

IGCC	integrated gasification combined cycle
IP	intermediate pressure
LHV	low heat value
LN2	liquid nitrogen
LNG	liquefied natural gas
LP	low pressure
IPCC	intergovernmental panel on climate change
LPLT	low pressure low temperature
MDEA	methyl diethanol amine
MEA	mono ethanol amine
NGCC	natural gas combined cycle
PC	pulverized coal
PCC	post-combustion CO_2 capture
PFC	perfluorocarbon
PSA	pressure swing adsorption
SF_6	sulphur hexafluoride
SWS	sour water steam
TBAB	Tetra-no-butyl ammonium bromide
TBAF	tetra-n-butyl ammonium fluoride
THF	tetrahydrofuran
TSA	temperature swing adsorption
VS	venturi scrubber
VSA	vacuum swing adsorption
VT	vapor turbine

CHAPTER 1

INTRODUCTION

The issue of global warming which was mainly caused by CO_2 emission is extremely urgent. Under this situation, CO_2 capture and storage has been proposed as a crucial strategy. There are three main strategies to capture CO_2 from coal-fired power plants, including: post combustion, pre-combustion and oxy-combustion. Compared to pre-combustion and oxy-fuel combustion, post-combustion can be retrofitted to existing power plants with only minimal effort. At present, the most mature technologies for CO_2 capture are absorption and adsorption methods. On the other hand, new technologies (e.g. membrane and cryogenic) for the reduction of CO_2 emissions are also positively investigated. However, there still are some defects for the existing technologies. 1) For absorption processes, high energy demand for solvent regeneration and degradation of the solvent and corrosion; 2) for adsorption, high energy requirement for regeneration and pressure drop; 3) for membrane, high membrane cost and increased pressure drop; 4) for cryogenic, high energy demand for cryogenic and compression condition. In light of these concerns, the investigation on the novel CO_2 capture process is significant.

1. BACKGROUND

Carbon dioxide (CO_2), methane (CH_4), nitrous oxide (N_2O), hydrofluorocarbons (HFCs), perfluorocarbons (PFCs) and sulphur hexafluoride (SF_6) have been listed in Kyoto Protocol 1998 as greenhouse gases (GHGs) (EPA, 2008). Figure 1-1 shows the comparison of the anthropogenic GHG emission. CO_2 is the most important GHG because its emission is notably high compare to the others. Apparently, CO_2 gave the highest impact to global warming among all the listed GHGs.

In nature, CO_2 will be absorbed by earth, either by weathering of rocks, photosynthesis of plants or ocean sinks by photosynthesis of marine plankton (Thiruvenkatachari et al., 2009). These natural sinks phenomena have balanced the natural source of CO_2 emission into the atmosphere over centuries. Excessive emission of CO_2 since industrial era has made these natural removals became insufficient anymore to maintain the CO_2 concentration in the atmosphere.

2. MAIN CO_2 EMISSIONS

According to the report of International Energy Agency (IEA, 2007), nearly a third of the world's energy consumption and 36% of CO_2 emissions are attributable to manufacturing industries. The large primary materials industries (e.g. chemical, petrochemicals, iron and steel, cement, paper and pulp, and other minerals and metals) account for more than two-thirds of this amount. Overall, the energy consumption of these industries has grown by 61% between 1971 and 2004. The detail CO_2 emission of the industrial sources is illustrated in Figure 1-2. It can be found that the emission of power plants is the most dominant and it will be introduced in detail.

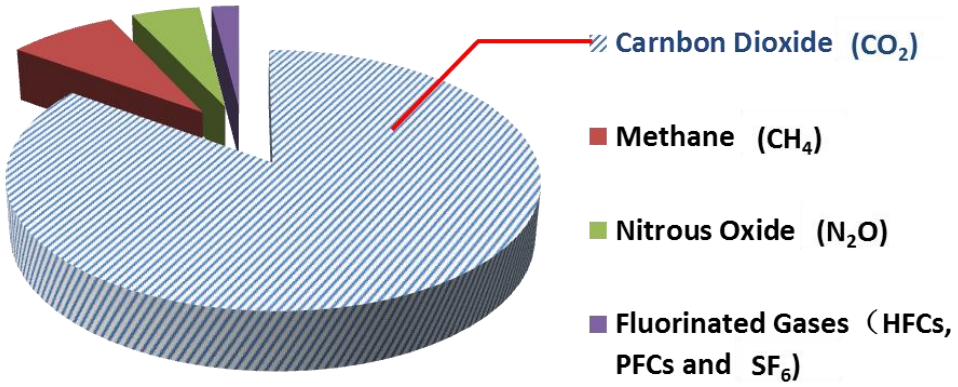

Figure 1-1 Main types and composition of greenhouse gas (GHG). (EPA, 2008)

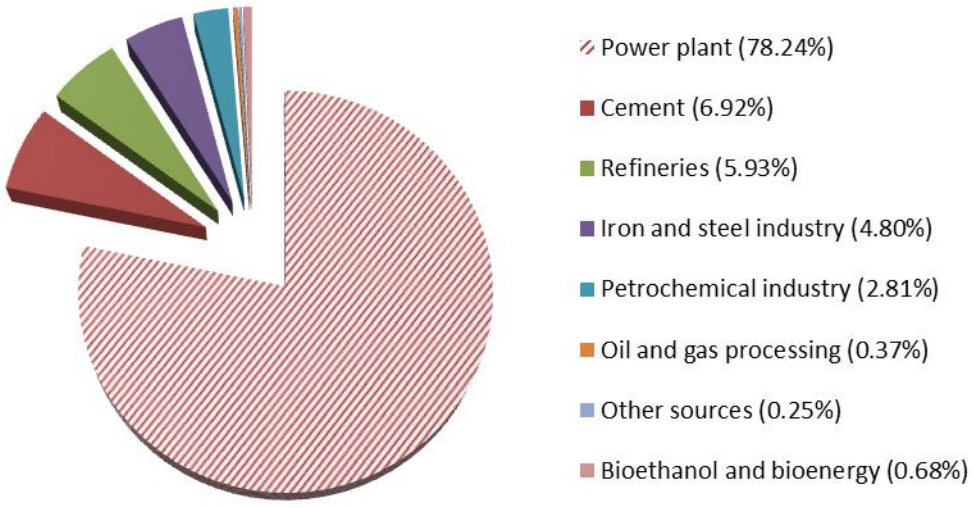

Figure 1-2 Breakdown of the dominant CO_2 emission sources. (IEA, 2007)

2.1 Pulverized coal (PC) fired power plant

The schematic of a pulverized coal-fired power plant is shown in Figure 1-3. Electricity is produced using steam-driven turbo-generators. Three-stage turbines with high-pressure (HP), intermediate-pressure (IP) and low-pressure (LP) cylinders were simulated in line. The milled black coal is combusted with preheated air and the resulting flue gas heats up feed-water in water-tubes inside the boiler producing sub-critical steam. The steam leaves the boiler to the first turbine, i.e. HP. A steam is bled from an appropriate section of the HP turbine to heat up feed water before entering the boiler. It is also partly used to run boiler feed pump turbine (BFPT). The steam from the outlet of the turbine is returned back to the boiler to be pre-heated and move to the next turbine in steam cycle, i.e. IP. This turbine may also have some bleeds to supply heat for feed water heating or deaerator. The exiting steam from the IP turbine is directed to the LP turbine(s). LP turbines have usually different bleeds for primary heating of feed water. The low pressure low temperature (LPLT) steam at the outlet of the turbine is condensed, heated, deaerated, chemically adjusted, pressurized and returned back to the boiler.

2.2 Natural gas combined cycle (NGCC) power plant

The relatively low carbon-to-hydrogen ratio content in natural gas compared to coal and oil, as well as the low investment cost for natural gas combined cycles (NGCC) along with their high efficiencies, ensures that NGCCs will have an important role in the future power generation mix (Sipöcz and Tobiesen, 2012).

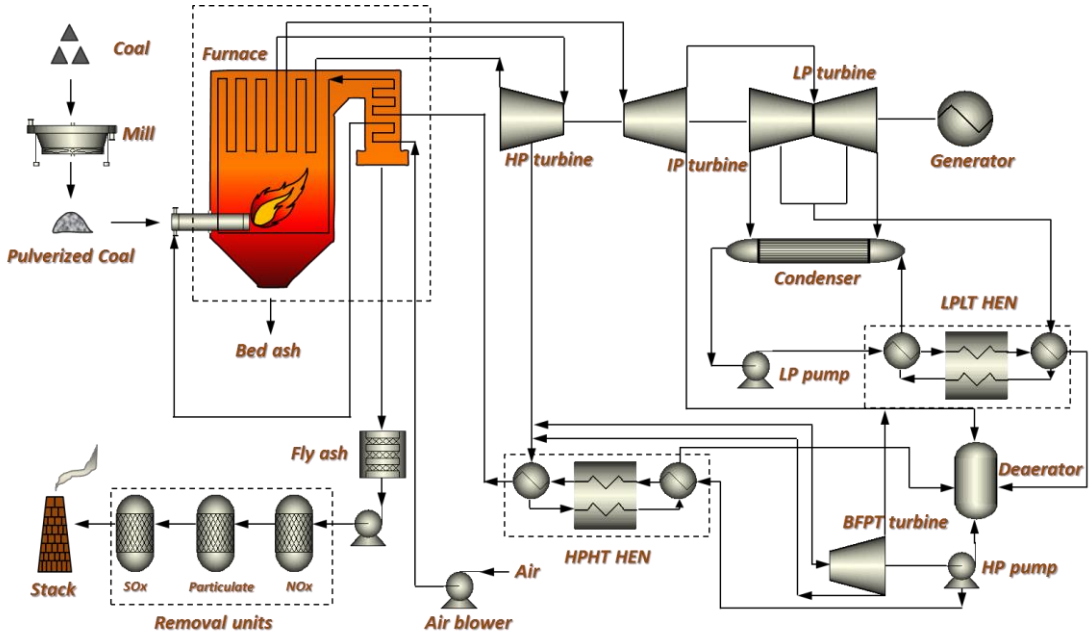

Figure 1-3 A typical flow diagram of pulverized coal fired power plant (Khalilpour and Abbas, 2011).

The overall of a typical NGCC plant is shown schematically in Figure 1-4. The inlet air for the plant is compressed in a single spool compressor to the design basis discharge pressure, and then passes directly on to the burner assembly. The hot combustion gases exit the burners and pass to the inlet of the turbine section of the machine, where they enter and expand through the turbine to produce power to drive the compressor and electric generator. The turbine exhaust gases are conveyed through a HRSG to recover the large quantities of thermal energy. The HRSG exhausts to the plant stack.

2.3 Integrated Gasification Combined Cycle (IGCC) power plant

The global flow diagram of a typical IGCC power plant is depicted in Figure 1-5, which includes a gasifier and a series of gas purification units. These purification units are ceramic filters, a Venturi Scrubber (VS), a Carbonyl Sulphide (COS) hydrolysis reactor, a Sour Water Steam stripper (SWS), a N-Methyl Diethanol Amine (MDEA) absorber and a sulfur recovery Claus plant. An air separation unit (ASU) is used to obtain O_2 at a purity of 85%wt. Steam, O_2 and fuel raw materials enter the gasifier and are converted into synthesis gas, which is cooled before it enters the purification units. Noncombustible materials (ashes) are removed efficiently as slag in the gasification reactor due to high pressure and temperature conditions, and the remaining dust particles are extracted from the synthesis gas by means of ceramic filters. Heat is recovered by producing steam in the HRSG unit. Further downstream, this steam is used in a Vapor Turbine (VT) to produce power. In the VS, syngas is placed in contact with a water stream that absorbs and removes acid (mainly H_2S) and basic (mainly NH_3) pollutants. Polluted water is treated in the SWS stripper and recycled back to the

VS, which closes a water loop and decreases the overall plant-wide water consumption. The SWS stripper unit needs to be purged due to the built up of pollutants. The purged water is then treated and disposed of. Synthesis gas is further purified through the COS hydrolysis reactor. This unit converts COS into H_2S, which is removed in the MDEA absorber. SO_2 emissions are controlled due to the removal of sulfur species from the syngas before combustion in the GT. Polluted gas streams from the SWS stripper, COS hydrolysis section and MDEA absorber are sent to a Claus plant, where sulfur, mainly from H_2S, is recovered in liquid form. The clean gas obtained, after the MDEA absorber, is sent to the GT. NOx emissions are partially avoided here: combustor geometry is specifically designed for NOx control. Also these emissions are controlled by decreasing the relation combustor/air, diminishing the flame temperature and the residence time at top temperatures: that is achieved with clean gas saturation with water vapor and N_2 addition from the ASU. Heat from the exhaust gas after the GT is recovered in the HRSG system. CO_2 emissions are mainly produced in the GT cycle, while CO emissions are minimized as they are oxidized completely in the GT.

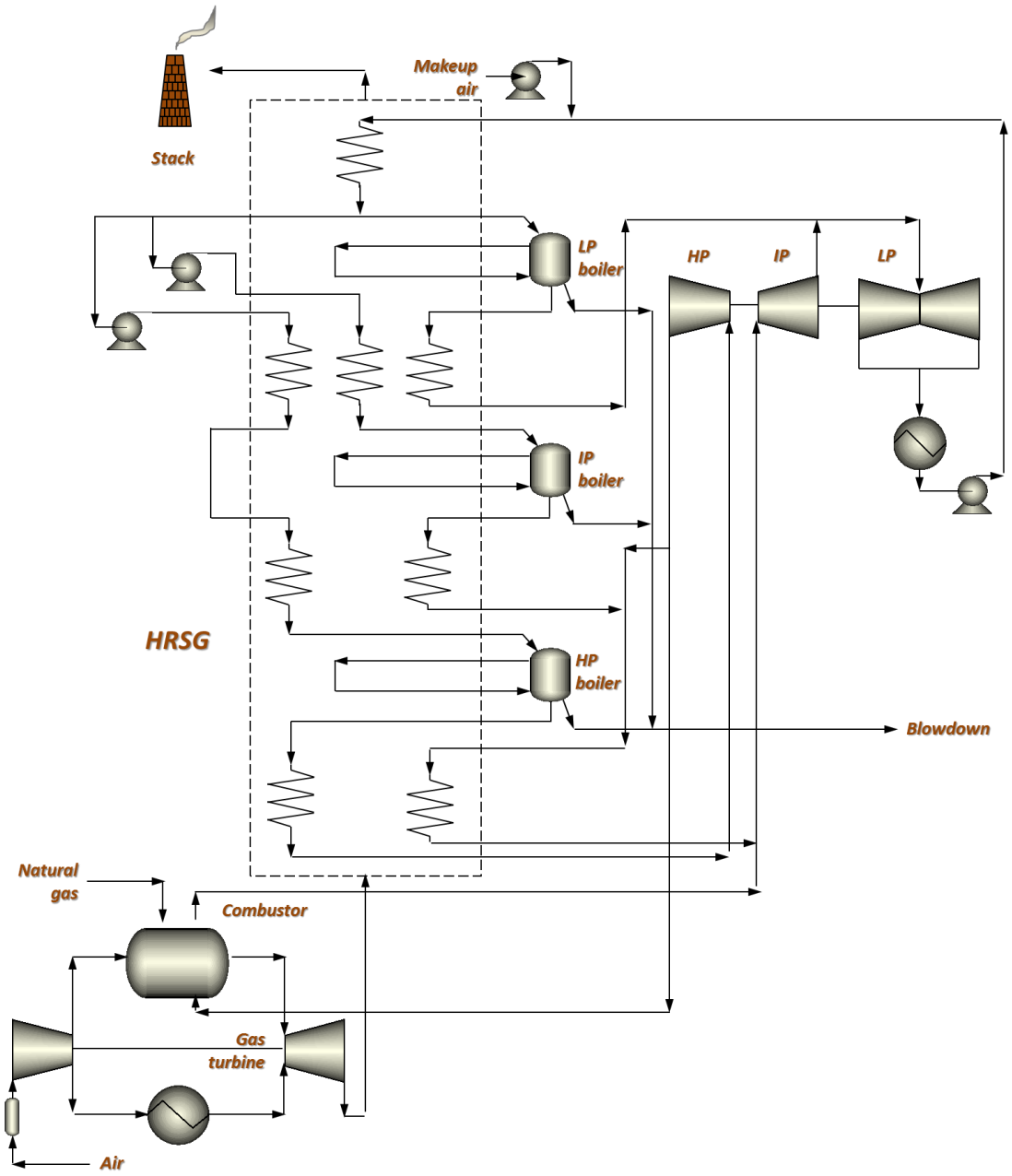

Figure 1-4 A typical flow diagram of Natural Gas Combined Cycle (NGCC) power plant (Parsons et al., 2002)

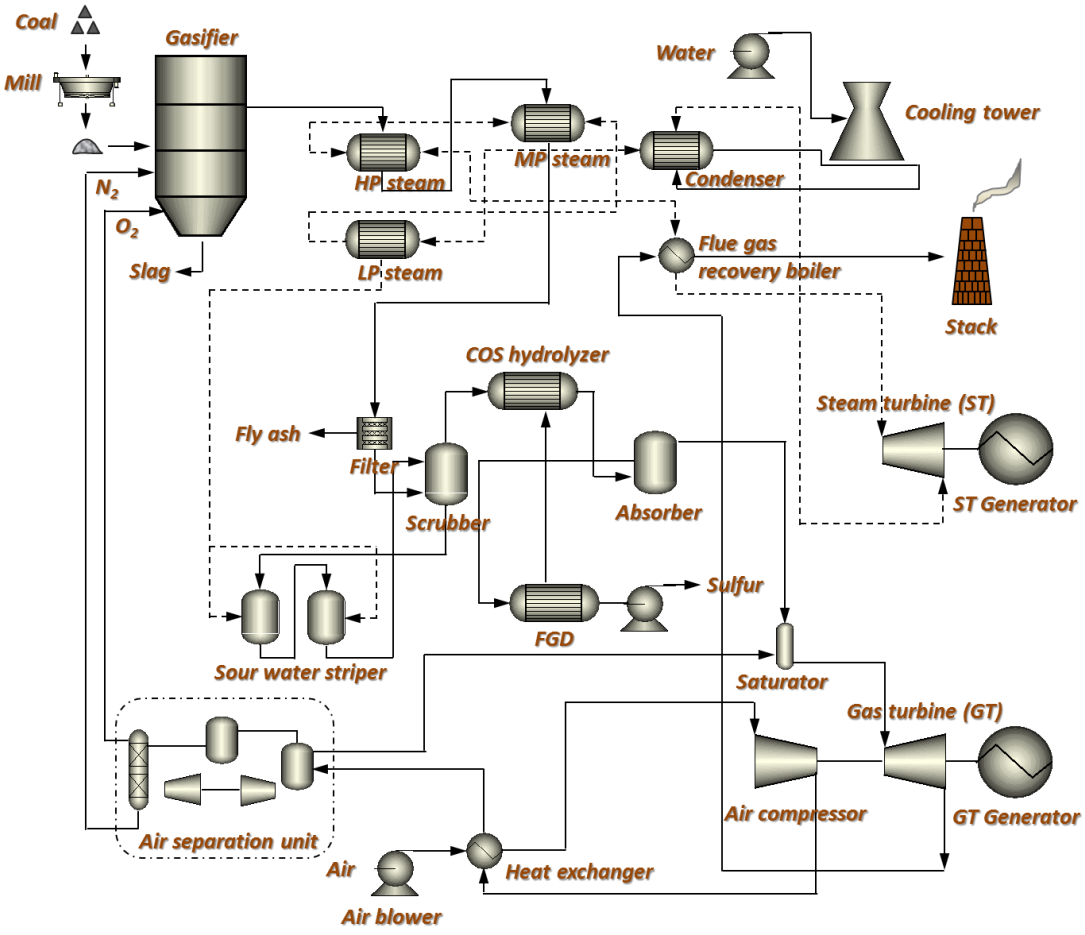

Figure 1-5 A typical flow diagram of Integrated Gasification Combined Cycle (IGCC) power plant (Perez-Fortes et al., 2009).

2.4 Other emissions

Besides the power plants, industrial processes (i.e. iron and steel sector, cement sector, petroleum refineries and chemical sector) account for nearly 30% of total global CO_2 emissions (Olajire, 2010). The iron and steel sector is one of the largest energy-consuming manufacturing sectors in the world. The iron and steel sector alone emitted 2.3 Gt CO_2 worldwide in 2007, accounting for 30% of total direct industrial CO_2 emissions and nearly 10% of global total CO_2 emissions. Cement production is the second most CO_2 intensive industrial process, accounting for 2 Gt CO_2/year worldwide in 2007. CO_2 emissions from petroleum refineries are close to 1 Gt/year worldwide, or about 4% of global total emissions. The chemical and petrochemical emitted nearly 1.3 Gt CO_2 in 2007 (IEA, 2009).

3. PREDOMINANT CO_2 CAPTURE AND STORAGE STRATEGIES

There are three CO_2 capture strategies for CO_2 mitigation from power generation: post combustion, pre-combustion and oxy-fuel combustion. The concentration of CO_2 in the gas stream, the pressure of the gas stream and the fuel type (solid or gas) are important factors in selecting the capture strategy.

3.1 Post combustion

The process flow diagram of post combustion CO_2 capture is described in Figure 1-6. In this strategy, fuel is combusted in the air and as a conventional combustion process, the concentration of CO_2 in the flue gas is low (typically 4~14%) (Olajire, 2010). For this reason, there is a high demand for equipment and energy to separation

CO_2 from other flue gas (i.e. sulphide and nitride). Among the three CO_2 mitigation strategies, post combustion is the easiest to be retrofitted into the existing power stations (Mondal et al., 2012).

3.2 Pre-combustion

In the pre-combustion capture process, fuel is reacted with oxygen and water, in the reaction, the carbon in the fuel is changed into carbon dioxide and carbon monoxide, simultaneously hydrogen is produced (as shown in Figure 1-7). This capture method is mainly used for coal gasification in Integrated Gasification Combined Cycle (IGCC) (Olajire, 2010). The main advantage of the pre-combustion technology is that the CO_2 concentration and partial pressure are both higher than post combustion. Thus the energy penalty can be reduced and capture efficiency can be improved. However, its disadvantage is that the total capital costs of the generating facility are very high.

3.3 Oxy-fuel combustion

Figure 1-8 introduces the detailed oxy-fuel combustion CO_2 capture process. In the process, fuel is combusted in the pure oxygen, causing the concentration of CO_2 is high (over 80%) and so the purification of CO_2 in this process is easy. Moreover, due to combusting in pure oxygen, the temperature of flue gas is high and the flue gas is often recycled to combustor to provide heat. The main disadvantage of oxy-fuel combustion is that a large quantity of oxygen is required. Therefore, an air separation unit (ASU) is required to product the pure O_2 for the combustion process, and which is expensive, both in terms of capital cost and energy consumption.

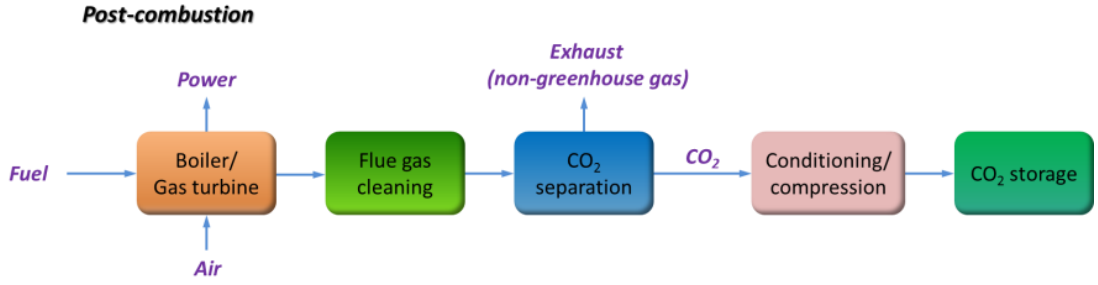

Figure 1-6 Flow diagram of the typical post-combustion CO_2 capture process

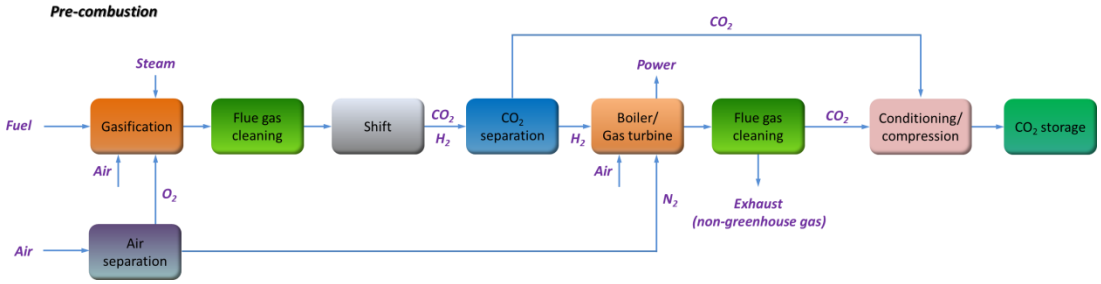

Figure 1-7 Flow diagram of the typical pre-combustion CO_2 capture process

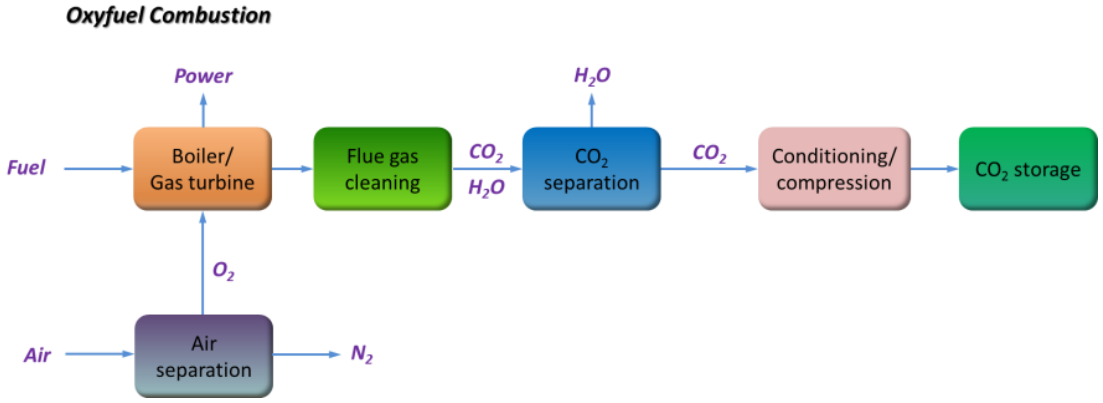

Figure 1-8 Flow diagram of the typical oxy-fuel combustion CO_2 capture process

4. MAIN CO_2 CAPTURE TECHNOLOGIES

The main CO_2 capture technologies are summarized in Figure 1-9. The choice of technology is dependent on the requirements for product purity and on the conditions of the gas stream being treated (such as its temperature, pressure CO_2, concentration and the type and level of trace species or impurities). In most cases, the captured CO_2 stream is simply vented to the atmosphere. Other common applications for CO_2 capture systems include the removal of CO_2 impurities in natural gas treatment and the production of hydrogen, ammonia and other industrial chemicals.

4.1 Chemical absorption

The typical absorption process by chemical solutions is described in Figure 1-10. The flue gas entering the absorption column flows up through the vessel, countercurrent to the aqueous solution. The CO_2 in the flue gas reacts chemically with the solvent, while the purified gas is vented to the atmosphere, and the solvent enriched by CO_2 (referred to as rich solvent) is pumped from the contact tower to a heat exchanger. The rich solvent solution enters the top of the regenerator, where it flows down through the vessel countercurrent to the stripping steam generated in the solution reboiler. Steam and solvent vapors move up the regenerator column, condensing as CO_2 is liberated and the solvent solution is heated. Uncondensed steam and CO_2 leave the top of the regenerator and then enter the re flux condenser. The condensate is recycled through the system while the CO_2 is removed for further processing.

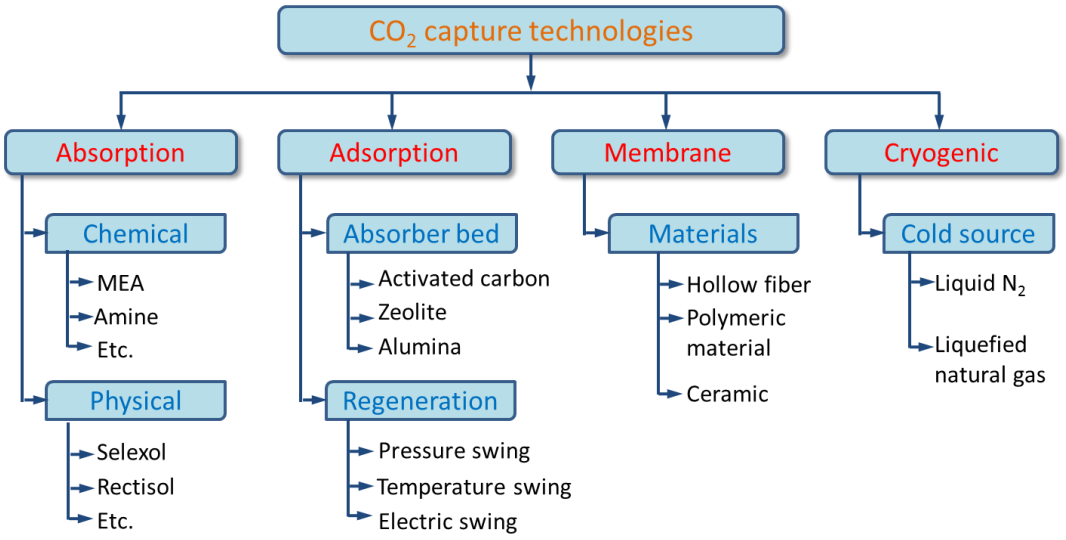

Figure 1-9 The main CO_2 capture technologies.

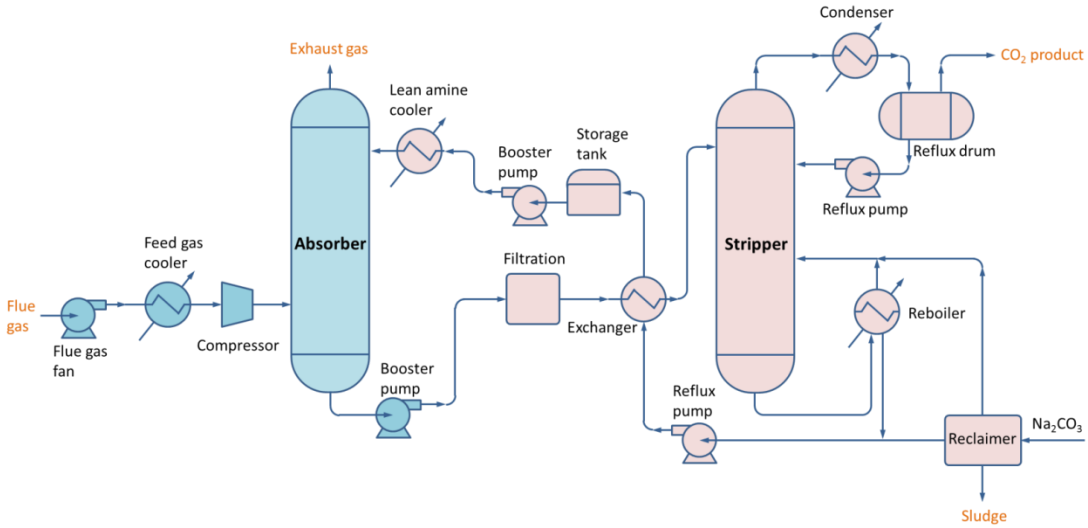

Figure 1-10 Process flow diagram of a typical chemical absorption system for CO_2 recovery from flue gas (White et al., 2003).

4.2 Physical adsorption

Figure 1-11 illustrates a typical configuration of a CO_2 capture process for the flue gas of fossil fuel-fired stationary stations by physical adsorption. As shown in the figure, the system comprises a flue gas feed to a pre-treatment stage if necessary prior to its flowing to one of the adsorption chambers for the capture of CO_2 by adsorption. Each of the adsorption chambers contains solid adsorbent. There are three adsorption chambers in the whole process. So that, at any time during operation of the system one chamber is receiving the feed for adsorption, a second chamber is desorbing the captured component and the third chamber is on stand-by to receive the feed. The system can thus operate continuously.

4.3 Membrane separation

Strategy using part of permeate as sweep is separately investigated in the process design depicted in Figure 1-12, where 70% of permeate from the first membrane stage is fed to the second membrane stage as feed and the remaining 30% of permeate is re-circulated as sweep to the first membrane stage whereas 5% of the permeate from the second membrane stage is re-circulated as sweep to second membrane stage. This distribution of sweep corresponds to roughly 5% of feed flow rate in the respective membrane stage.

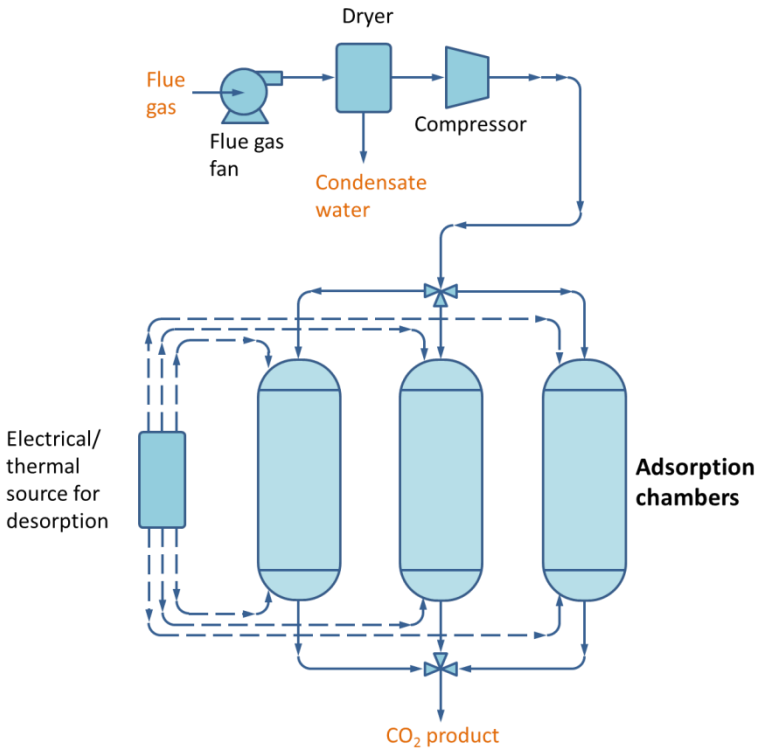

Figure 1-11 Process flow diagram for the CO_2 capture from flue gas by adsorption process (Thiruvenkatachari et al., 2009).

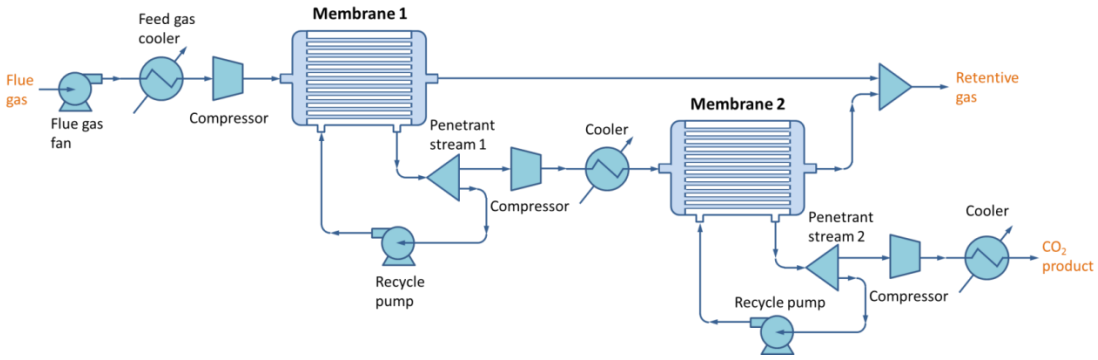

Figure 1-12 Process flow diagram for the CO_2 capture from flue gas by membranes (recycled permeate as sweep gas) (Hussain and Hägg, 2010).

4.4 Cryogenic distillation

The cryogenic CO_2 capture (CCC) process (as shown in Figure 1-13) dries and cools flue gas from existing systems, modestly compresses it, cools it to a temperature slightly above the point where CO_2 forms a solid, expands the gas to further cool it, precipitating an amount of CO_2 as a solid that depends on the final temperature, pressurizes the CO_2, and reheats the CO_2 and the remaining flue gas by cooling the incoming gases. The final result is the CO_2 in a liquid phase and a gaseous nitrogen stream.

4.5 Other technologies

4.5.1 Microalgae

Currently, culturing of microalgae for CO_2 bio-fixation has gained a huge momentum due to their high photosynthetic rate that allows bio-fixation of CO_2 more efficient than terrestrial plants. Moreover, the capture process using microalgae has the following advantages (Pires et al., 2012): 1) being an environmental sustainable method; 2) using directly the solar energy; 3) co-producing high added value materials based on biomass, such as human food, animal feed mainly for aquaculture, cosmetics, medical drugs, fertilizers, biomolecules for specific applications and biofuels. The brief microalgae CO_2 fixation process is introduced in Figure 1-14.

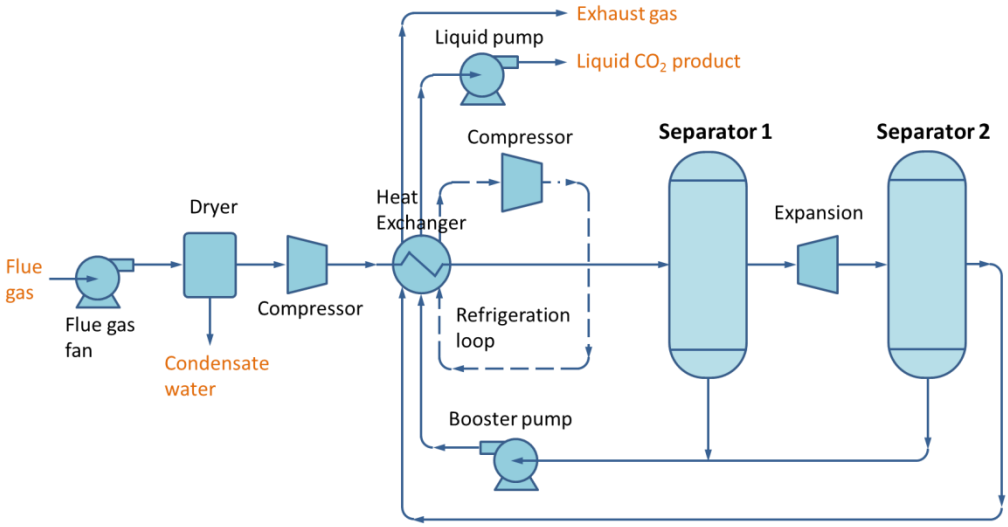

Figure 1-13 Process flow diagram for the CO_2 capture from flue gas by cryogenic process (Burt et al., 2009).

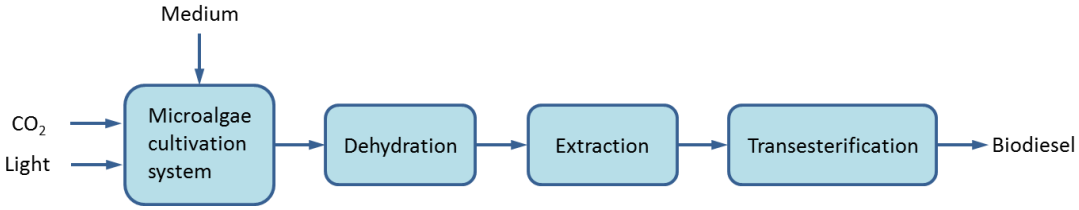

Figure 1-14 Process flow diagram for the CO_2 capture from flue gas by microalgae fixation process (Zeng et al., 2011).

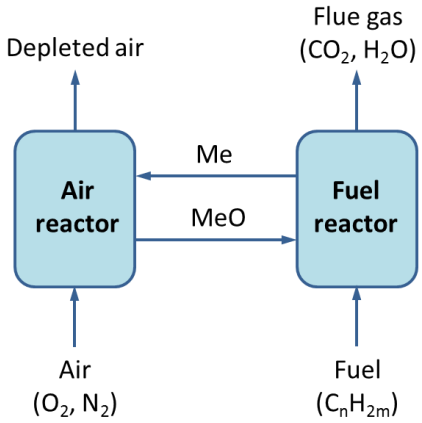

Figure 1-15 Process flow diagram for the CO_2 capture from flue gas by chemical-looping combustion process (Adanez et al., 2012).

4.5.2 Chemical-looping combustion

Chemical-looping combustion (CLC), proposed by Richter and Knoche in 1983, divides combustion into intermediate oxidation and reduction reactions that are performed separately with a solid oxygen carrier circulating between the separated sections. Suitable oxygen carriers are small particles of metal oxide such as Fe_2O_3, NiO, CuO or Mn_2O_3. A basic CLC system is shown in Figure 1-15. The CLC has two reactors, one each for air and fuel. The oxygen carrier circulates between the reactors. In the air reactor, the carrier is oxidized by oxygen. In the fuel reactor, the metal oxide is reduced by the fuel, which is oxidized to CO_2 and H_2O. The main advantages of CLC can be summarized as (Olajire, 2010): 1) the exhaust gas from air reactor is mainly N_2, and thus is harmless. 2) The exhaust gas stream from fuel reactor is composed of CO_2 and H_2O. Therefore, the CO_2 can be separated by a condenser, and which avoids the energy penalty in the conventional absorption process and reduces the capital cost.

5. LIMITATIONS OF THE EXISTING CAPTURE TECHNOLOGIES

5.1 Chemical absorption

Undoubtedly, Post-combustion CO_2 capture based on chemical solutions (such as aqueous amine solutions and MEA) has been considered as the most mature gas separation technology. However, there are still several limitations that remain to be solved (such as, solvent degradation, corrosion, solvent regeneration efficiency). According to the work of Rao and Rubin in 2002, solvent degradation is around 10% of total cost of CO_2 capture. The degradation mainly contains two types: 1) thermal

degradation. It occurs at the high temperature and high CO_2 partial pressure condition. 2) Oxidative degradation. It is mainly due to the presence of a large amount of O_2 in the flue gas. Meanwhile, some impurity gas (e.g. SOx and NOx) can also result in the solvent degradation. In addition, the volatile components could be emitted into atmosphere and which are unfriendly for the environment.

5.2 Physical adsorption

At present, most of the CO_2 adsorption technologies from a gas stream are assumed as a dry process. Furthermore, some other limitations that also make this process less effective such as: 1) low selectivity and capacity of available adsorbent for CO_2. 2) lower removal efficiency as compared to other technologies such as absorption and cryogenic. 3) regeneration and reusability of adsorbent.

5.3 Membrane separation

As a promising alternative, membrane-based technology has become a competitive CO_2 capture process. However, it is worthwhile to note that it is difficult to maintain the membrane performance in long-term operation. Most membranes do not have the resilience in practical industry conditions and quickly fail, which is one of the biggest challenges for their potential applications in industrial practice (Zhang et al., 2013). Additionally, when the concentration of CO_2 in feed stream is diluted (below 20%), multiple stages and/or recycle of one of the streams are necessary. For most of the current membrane process, the influence of the oxide components (such as SOx, NOx and H_2S) is not considered. Thus much attention is necessary for the investigation of this influence.

5.4 Cryogenic distillation

Cryogenic CO_2 capture technologies are not widely researched, due to the expected excessive cooling costs. The main disadvantage of using direct heat exchange between the flue gas and a refrigerant in heat exchangers is that no H_2O can be tolerated in the inlet stream in order to prevent plugging by ice during operation. In addition the built up of solid CO_2 onto heat exchanging surfaces causes a decrease in the heat transfer rate and thus a decrease in process efficiency. Furthermore, large spatial and temporal temperature gradients may result in undesired mechanical stresses in the expensive cryogenic heat exchangers (Tuinier et al., 2011).

5.5 Other technologies

5.5.1 Microalgae

For the microalgae CO_2 fixation process, due to the lack of understanding on this technology, several issues and problems are normally ignored (such as heavy requirement of inorganic nutrients source and intensive energy in cultivating, harvesting and drying of microalgae biomass). The consequence of these limitations may lead to serious negative CO_2 and energy balance for the life cycle microalgae biodiesel production. Apart from that, low solubility of CO_2 in water is another problem that needs further attention.

5.5.2 Chemical-looping combustion

At present, most of the CLC processes have only been tested at lab-scale, and there is no large-scale demonstration so far has been performed. Meanwhile, several significant problems still remain in the existing processes (such as insufficient stability of the oxygen carrier and slow redox kinetics) (Solunke and Veser, 2011). In addition,

the desulfurization of the fuel is also necessary to avoid the sulfidation phenomenon of the carrier.

6. COMPOSITION OF THE THESIS

The aim of this thesis is to develop a novel cryogenic CO_2 capture process based on Stirling cooler (SC) system. Meanwhile, a feasibility investigation on the novel system is implemented.

In Chapter 1, the background of our research is introduced. The main CO_2 emission and mitigation technologies are summarized. Furthermore, the advantages and disadvantages of these technologies are illustrated in detail.

In Chapter 2, the developed cryogenic CO_2 capture system based on Stirling coolers is introduced in detail. The cryogenic principle of the system is illustrated. The properties of the novel process are investigated and capture performance of the system is evaluated. Finally, a brief comparison with other dominant technologies (i.e. chemical absorption and membrane) is carried out.

In Chapter 3, the characteristic of Stirling cooler is investigated in detail and its working principle is theoretically analyzed. The energy efficiency of the cryogenic system is evaluated by the parameter of coefficient of performance (COP). Meanwhile, the influence of capture conditions (e.g. flow rate and temperature) on the COP is also studied.

In Chapter 4, the key parameters (such as the flow rate of gas stream, the temperature of Stirling coolers, the operating time of the system, the vacuum degree of the interlayer, the ambient temperature and humidity) that influence the performance of the system are investigated. The detailed CO_2 capture performance of the system is investigated.

In Chapter 5, as the most critical stage, the characteristic of CO_2 frost process is numerically analyzed. The growth of the frost layer is simulated. For the detail, the variation of the thickness and thermal conductivity of the frost CO_2 is investigated.

In Chapter 6, the energy analysis of the cryogenic system is implemented to improve the efficiency of the whole process. The energy requirement of the main stage (e.g. pre-chilling column, main freezing column and storage column) is analyzed in detail.

In Chapter 7, the outlook of CO_2 capture technologies is put forward. In particular, the future direction of the SC based cryogenic CO_2 capture system is forecasted. A hybrid CO_2 capture system is conceived by combing a membrane module with the cryogenic system. In order to reduce the energy penalty and improve the capture performance of the system, a membrane module is used after the pre-chilling process to pre-concentrate the CO_2 in the flue gas.

In Chapter 8, the conclusion of my research is summarized.

REFERENCES

Inventory of U.S. Greenhouse Gas Emissions and Sinks, 2008. EPA.

R. Thiruvenkatachari, S. Su, H. An, X.X. Yu, 2009. Post combustion CO_2 capture by carbon fibre monolithic adsorbents. Progress in Energy and Combustion Science 35, 438–455.

IEA (International Energy Agency), 2007. Tracking Industrial Energy Efficiency and CO_2 Emissions. Stedi Media, France.

R. Khalilpour, A. Abbas, 2011. HEN optimization for efficient retrofitting of coal-fired power plants with post-combustion carbon capture. International Journal of Greenhouse Gas Control 5, 189-199.

N. Sipöcz, F. A. Tobiesen, 2012. Natural gas combined cycle power plants with CO_2 capture – Opportunities to reduce cost. International Journal of Greenhouse Gas Control 7, 98-106.

E.L. Parsons, W.W. Shelton, J.L. Lyons, 2002. Advanced fossil power systems comparison study. Morgantown: National Energy Technology Laboratory.

M. Perez-Fortes, A.D. Bojarski, E. Velo, J.M. Nougues, L. Puigjaner. 2009. Conceptual model and evaluation of generated power and emissions in an IGCC plant. Energy 34, 1721–1732.

A.A. Olajire. 2010. CO_2 capture and separation technologies for end-of-pipe applications-A review. Energy 35, 2610-2628.

M.K. Mondal, H. K. Balsora, P. Varshney, 2012. Progress and trends in CO_2 capture/separation technologies: A review. Energy 46, 431-441.

C.M. White, B.R. Strazisar, E.J. Granite, J.S. Hoffman, 2003. Separation and capture of CO_2 from large stationary sources and sequestration in geologic formations-coalbeds and deep saline aquifers. Journal of the Air & Waste Management Association 53, 645-715.

A. Hussain, M.B. Hägg, 2010. A feasibility study of CO_2 capture from flue gas by a facilitated transport membrane. Journal of Membrane Science 359, 140-148.

S. Burt, A. Baxter, L. Baxter. Cryogenic CO_2 capture to control climate change emissions. 34th International Technical Conference on Clean Coal and Fuel Systems (2009).

J.C.M. Pires, M.C.M. Alvim-Ferraz, F.G. Martins, M. Simões, 2012. Carbon dioxide capture from flue gases using microalgae: Engineering aspects and biorefinery concept. Renewable and Sustainable Energy Reviews 16, 3043-3053.

X. Zeng, M.K. Danquah, X.D. Chen, Y. Lu. Microalgae bioengineering: From CO_2 fixation to biofuel production.

H. Richter, K. Knoche, 1983. Reversibility of combustion processes. ACS Symposium Series, 235, 71–86.

J. Adanez, A. Abad, F. Garcia-Labiano, P. Gayan, L. F. de Diego. 2012. Progress in Chemical-Looping Combustion and Reforming technologies. Progress in Energy and Combustion Science 38, 215-282.

A.B. Rao, E.S. Rubin, 2002. A technical, economic, and environmental assessment of amine-based CO_2 capture technology for power plant greenhouse gas control. Environmental Science & Technology 36, 4467-4475.

Y. Zhang, J. Sunarso, S. Liu, R. Wang, 2013. Current status and development of membranes for

CO_2 /CH_4 separation: A review. International Journal of Greenhouse Gas Control 12, 84–107.

M.J. Tuinier, M. van Sint Annaland, J.A.M. Kuipers, 2011. A novel process for cryogenic CO_2 capture using dynamically operated packed beds—An experimental and numerical study. International Journal of Greenhouse Gas Control 5, 694-701.

R.D. Solunke, G. Veser, 2011. Integrating desulfurization with CO_2-capture in chemical-looping combustion. Fuel 90, 608-617.

CHAPTER 2

CRYOGENIC CO_2 CAPTURE PROCESS BASED ON STIRLING COOLER SYSTEM

In the present chapter, a novel cryogenic CO_2 capture system based on Stirling coolers has been developed. By the capture system designed, an effective separation can be achieved according to differences in condensation and anti-sublimation. From the capture process, H_2O and CO_2 can condense and anti-sublimate at different parts of the capture system, while residual gas flows out without properties change. It is noteworthy that in the process, CO_2 can be captured in a solid form, thus avoiding the use of the solvents and consideration of pressure in other methods. Furthermore, two significant parameters (the temperature of Stirling coolers and the flow rate of the gas stream) were investigated in detail. The results showed that under the optimal temperature and flow rate, CO_2 recovery of the cryogenic process can reach 96%, which demonstrated that the system can capture CO_2 gas effectively.

1. INTRODUCTION

Climate change caused by greenhouse gas has become a critical issue of worldwide concern. Among greenhouse gas, CO_2 makes up a high proportion of the amount in the atmosphere and is responsible for 70% of global warming effect (U.S. Department of Energy, 2007). Although new renewable resources of energy production have been exploited (such as wind, solar, and biomass energy), the world will remain largely dependent on fossil fuels for the next decades. Thus, the capture and separation of CO_2 are significant for greenhouse effect control, and it is a serious global priority. In this case, CO_2 capture and storage (CCS) has been proposed as a sustainable technology to mitigate greenhouse gas by the Intergovernmental Panel on Climate Change (IPCC) (Metz et al., 2005).

In recent years, the focus of the researchers fastens on the fossil fueled power plants, which are the main emissions of CO_2. There are three ways to capture CO_2 from coal-fired plants: post-combustion, pre-combustion and oxy-fuel combustion (Irons et al., 2007). Although capture of CO_2 contributes 75% to the overall CCS costs, the separation of CO_2 is also a crucial part of CCS. Nowadays, the technologies of CO_2 separation mainly contain absorption, adsorption, cryogenics and membranes (Jeremy, 2000; Audus, 2000). Among these technologies, chemical solvents absorption processes are considered to be the most feasible method and already at an advanced stage of development, but they still have several areas that need to be improved, such as energy penalty caused by solvents regeneration. In order to achieve the aim of reducing energy consumption, the improvement of existing technologies and exploitation of novel capture processes have been paid an increasing attention.

As an available approach for CO_2 capture, the cryogenic separation technology has

been researched for several decades. However, for the past years, this technology was not extensively studied due to the high expected cooling cost. In fact, by the application of cryogenic separation, no absorbents are required and CO_2 can be captured at atmospheric pressure. With these advantages, the research of cryogenic CO_2 capture technologies has made significant progress. In 2002, Clodic and Younes developed a cryogenic CO_2 capture process, in their process CO_2 could be anti-sublimated as a solid onto the surfaces of heat exchangers, which were cooled by evaporating a refrigerants blend. The energy requirement of the whole process was in the range of 541 to 1119 kJ/kg CO_2 (Clodic et al., 2004a). In 2010, Tuinier et al. exploited a novel cryogenic CO_2 capture process using dynamically operated packed beds. By the developed process above 99% CO_2 could be recovered from a flue gas containing 10 vol. % CO_2 and 1vol. % H_2O with1.8 MJ/kg CO_2 energy consumption.

In addition, as the most important part of the cryogenic system, Stirling cooler (SC) gets interest of researchers because of its significant advantages, such as high efficiency, high reliability and small size (Hu et al., 2010). The operation of SC contains four processes: expansion under an isothermal condition, refrigeration under a constant volume condition, compression under an isothermal condition, and heating under a constant volume condition (Sun et al., 2008). As a typical mechanical cooler, Stirling cycle coolers have been widely applied to the area of infrared detectors, superconductor filters, space exploration and cryopumps (Park et al., 2002; Chen et al., 2009). Nevertheless, the application of Stirling cooler on greenhouse gas control is novel. Compared to current technologies, its advantage is low energy consumption. Furthermore, this method is mainly based on a thermal process for CO_2 capture and separation, thereby avoiding the use of any chemical solvents that can lead to increasing operating costs and environmental impact (Metz et al., 2005).

Based on the above discussion, it is significant to develop an efficient and convenient method of CO_2 capture. In this chapter, a completely different system of cryogenic CO_2 capture is developed according to the invention patent of Kitamura in 2006. The effect of temperature and flow rate on CO_2 recovery and process performance is researched, and the result of experiments showed that the SC-based CO_2 capture system can capture CO_2 gas effectively.

The structure of this chapter is as follows. Section 2 introduces the developed cryogenic CO_2 capture process in details. Section 3 describes the detailed structure of FPSC and experimental conditions. Section 4 investigates the temperature variation and capture performance of the system. Finally, a brief comparison with chemical, membrane and other cryogenic processes is carried out. Section 5 summarizes the main conclusions of this chapter.

2. CRYOGENIC CO_2 CAPTURE PROCESS

The schematic of the cryogenic capture process is shown in Figure 2-1. The main parts contain SCs, vacuum pump, freezing tower, camera and control panel. The whole process is composed of three stages: refrigeration, capture and storage.

2.1 Refrigeration by SC-1

Firstly, feed gas is cooled from 25 ℃ to 0 ℃ by SC-1 in the pre-freezing tower. At the pre-freezing tower, the moisture in feed gas condenses into water by SC-1 and then moves through the condenser pipe to the outlet to avoid plugging the vessel, which is the key issue of cryogenic separation technology. Meanwhile, the other gas flows into the main-freezing tower.

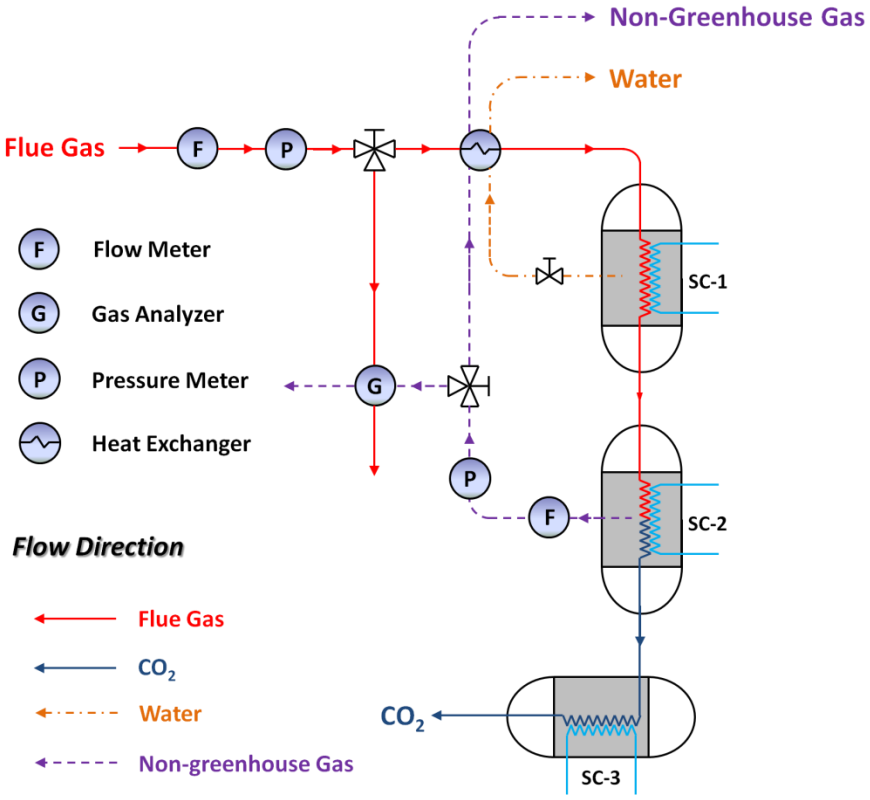

Figure 2-1 The developed novel cryogenic CO_2 capture process based on Stirling coolers

2.2 Capture by SC-2

According to the work of Clodic et al. in 2004, the freezing point of CO_2 is related to its partial pressure in the gas mixture. Figure 2-2(a) shows the relationship between freezing point and CO_2 concentration. Typically for flue gas in Figure 2-2(b), the freezing point of CO_2 varies between -112 ~ -97 ℃. In our research, the percentage of CO_2 in flue gases is 13 vol.%, and consequently has a frost point of around -100 ℃. In the main-freezing tower, SC-2 provides a cryogenic condition (approximately -100 ~ -105 ℃), and the flue gas after water removed is cooled down to about -100 ℃. In this condition, CO_2 in flue gas (about 15 vol.%) anti-sublimates into the solid form, which has a frost point of -100 ℃. Afterwards, the dry ice frosts onto the heat exchanger of SC-2 immediately. In this way, the capture of CO_2 from feed gas is realized. The detailed connection of nozzle, heat exchanger and scraper in the main freezing tower is shown in Figure 2-3.

2.3 Storage by SC-3

The last step is to store the solid CO_2 by SC-3. In this section, by spinning the scraping rod on the cooling fin of SC-2 heat exchanger, dry ice falls down to the storage tank, where SC-3 provides a cryogenic condition (below -78.5 ℃) to prevent it gasifying. On the other hand, residual gas exhausts from gas outlet.

3. EXPERIMENTAL SECTION

3.1 Apparatus

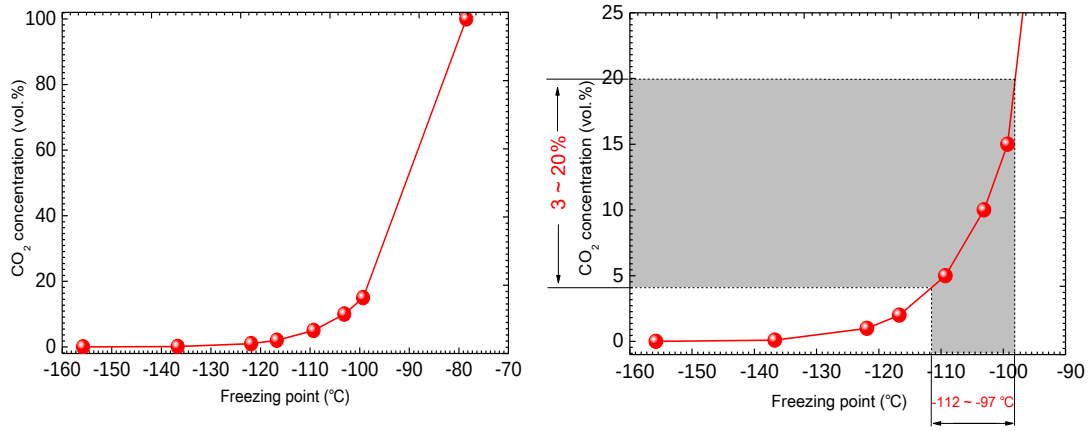

(a) (b)

Figure 2-2 The relationship between freezing point (℃) and CO_2 concentration (vol.%) (a); typically in flue gas (b). (Clodic et al., 2004)

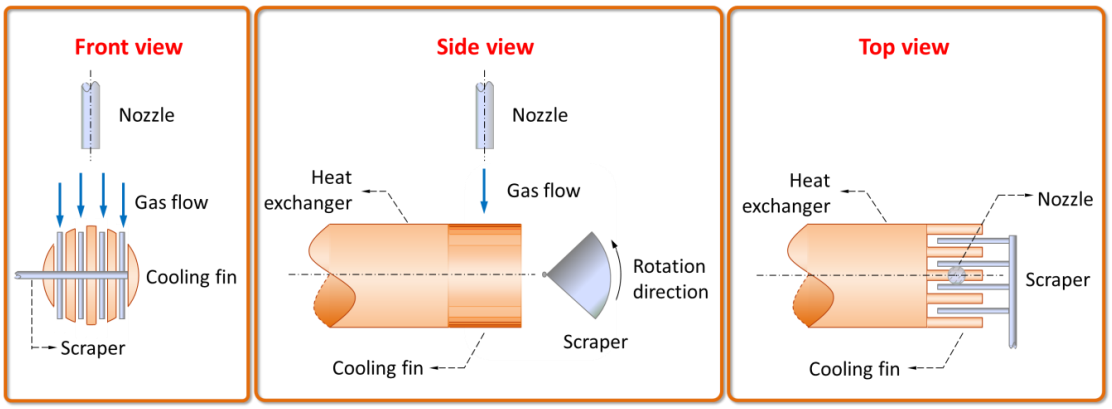

Figure 2-3 The detailed connection of nozzle, heat exchanger and scraper in the main freezing tower

The detail structure of the exploited system is shown in Figure 2-4 and 2-5. The materials of the structure should be selected considering their influence on cryogenic performance. First of all, the materials used as the structure of experimental setup are stainless steel. Then as the key part, copper is used as the cold head of heat exchangers, since it has a well coefficient of heat transfer. The junctions between the cold head of the SCs and freezing tower are wrapped up by thermal insulating materials to reduce the heat loss. For some synthetic materials may become ineffective at low temperature (approximately -120 ℃), specific sealing materials and gaskets are typically required for the pipe fittings to avoid air leakage of the system.

The flow rate and pressure of the gas stream at the inlet and outlet are controlled by a flow controller (Bronkhorst El-flow) and analogue pressure controller. The temperature of the main parts of the cryogenic system is measured with thermocouples (Thermo-Electric K-type) every 0.1 seconds. The heat transfer parts are maintained under a vacuum condition and recorded by vacuum pump (Nakamura Seisakusho Co., Ltd.) and indicator (NVC-1100, Tokyo Rikakikai Co., Ltd.), respectively. The process of anti-sublimation is monitored by a camera in the main freezing tower.

3.2 Experiments

There are three SCs in the system and their features are summarized in Table 2-1. The flue gas of post-combustion was simulated by N_2, H_2O and CO_2. The composition and condition of feed gas for the experiment are presented in Table 2-2. It is noted that the process of pollutant separation from flue gas (such as SO_x and NO_x) is not taken into account. The capture performance of the system is investigated under 5 different flow rates (from 2 to 6 L/min).

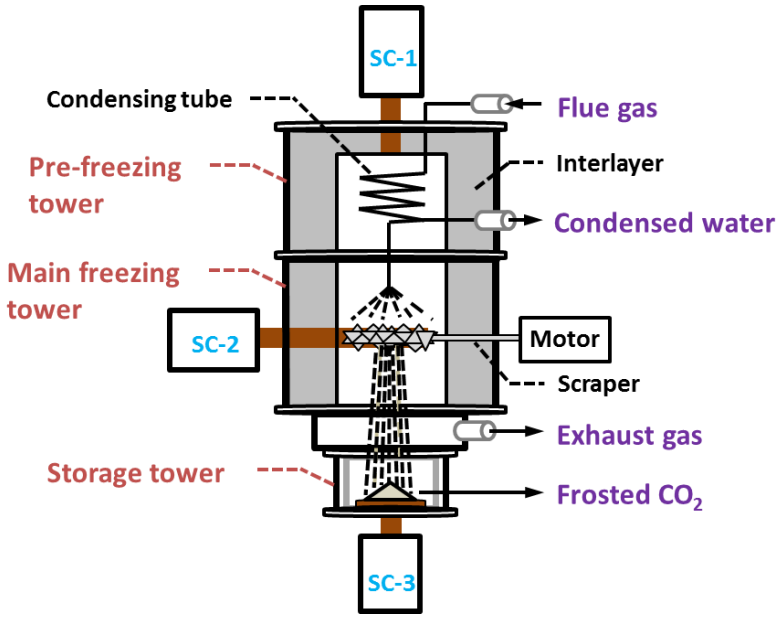

Figure 2-4 The structure of the Stirling cooler system

Figure 2-5 The Stirling cooler system

Table 2-1 Properties of SCs in the system.

SCs	Properties		
	Temperature range (℃)	Power (W)	Cooling capacity
1	-90 ~ +20	90 ± 20	More than 25 W (at an ambient temperature of 25 ℃ and cold side temperature of -80 ℃)
2 , 3	-120 ~ +70	≤200	Approx. 50 W (at the cold side temperature of -80 ℃)

Table 2-2 Composition and condition of feed gas.

N_2 (vol. %)	82
CO_2 (vol. %)	13
H_2O (vol. %)	5
Gas flow rates (L/min)	2~6
Gas temperature (℃)	24~25
Ambient temperature (℃)	24~26
Ambient humidity (%)	30~50
Ambient pressure (Pa)	1.01×10^5

4. RESULTS AND DISCUSSION

4.1 Temperature variation of the system

The details in Figure 2-6 show that when the temperature threshold of SC-1 changed from -60 ℃ to -30 ℃ before gas mixture flowed into the system, the temperature of SC-1 heat exchanger, pre-cooling tube and water condensate tube increased obviously; the temperatures of SC-2 heat exchanger and dry ice storage tank were consistent. Nevertheless, when the temperature threshold of SC-1 exceeded -30 ℃, the system was not able to maintain a cryogenic condition. Although the temperature of SC-2 heat exchanger could also reach -90 ℃, the gas stream could not be precooled adequately, and the temperature in the CO_2 storage tank was far above the condition of cryopreservation. This led to a decline of capture efficiency.

It was obvious that in order to maintain high purity of frosted CO_2, the water in the gas stream should be separated as much as possible. According to the tests, an effective separation between CO_2 and H_2O was obtained and the problem of plugging was intrinsically avoided by keeping the temperature threshold of SC-1 under -30 ℃. With the range of -60 ℃ to -30 ℃, the lower the temperature threshold of SC-1 was, the better efficiency of the capture system performed. However, when the temperature threshold of SC-1 was set at above -30 ℃ (e.g., -20 ℃ in Figure 2-8), the system could not separate H_2O from the gas stream effectively. Consequently, the upper limit of the temperature of SC-1 should be controlled below -30 ℃.

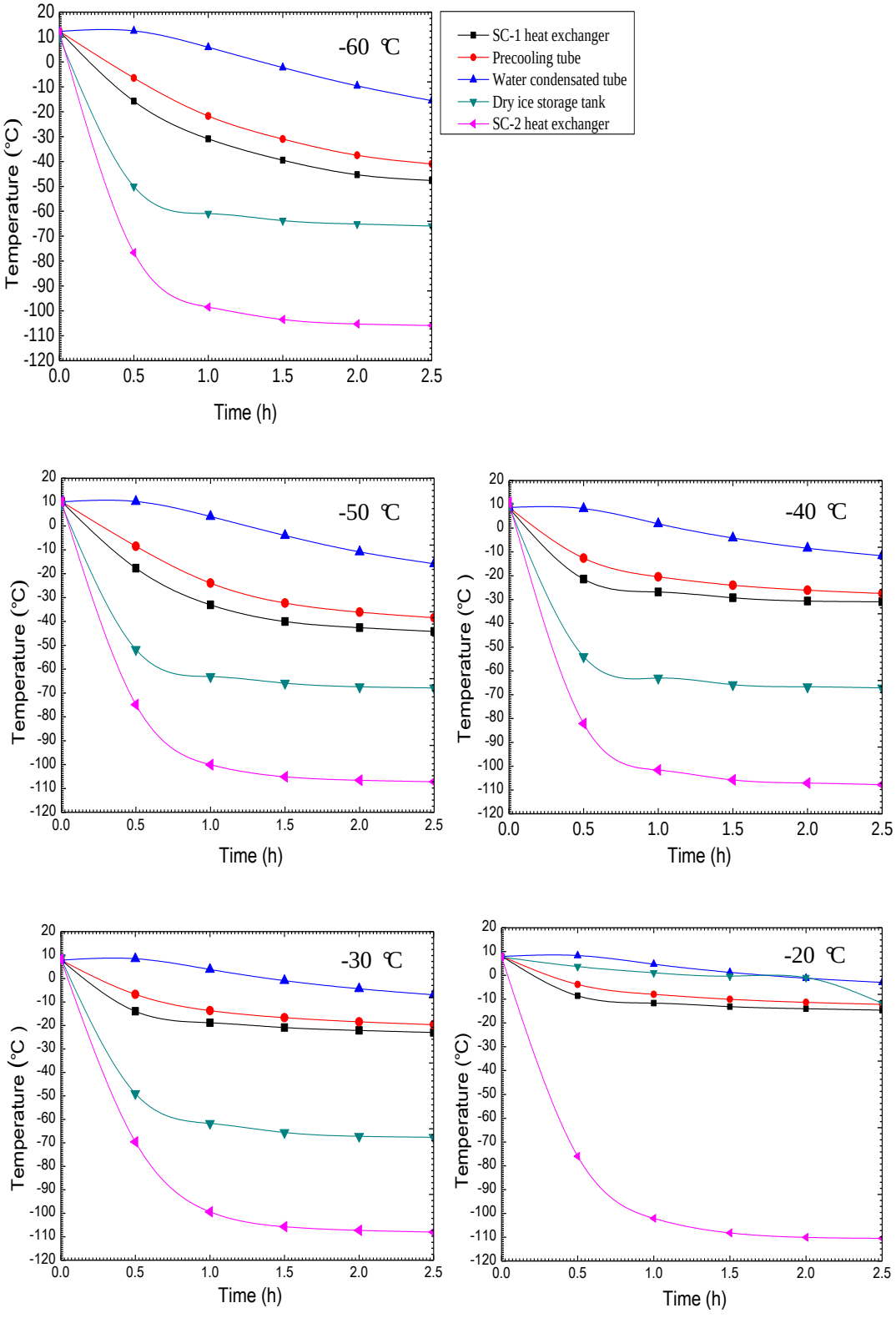

Figure 2-6 Effect of SC-1 on the tendency of temperature variation of system (before gas mixture inflow).

4.2 Cryogenic performance

In the cryogenic process, there was some ice crystal generated on the joints between the heat exchangers and freezing towers. This phenomenon indicated that the effect of heat insulation jacket was not optimal. In addition, the frost layer of CO_2 onto the cooling fin of the heat exchanger of SC-2 is shown in Figure 2-7(a); the deposition of captured CO_2 in the storage column is shown in Figure 2-7(b). It is observed that the increasing layer of solid CO_2 onto the heat exchanger surfaces during the capture cycle would adversely affect the heat transfer and reduce the process efficiency. Figure 2-8 shows the temperature of the main parts of the cryogenic system during capture process.

4.3 CO_2 capture efficiency

The energy consumption (EC) of the cryogenic system for per unit mass CO_2 captured is defined as following:

$$\mathrm{EC} = \frac{UIt}{(v_{in}\omega_{CO_2,in} - v_{out}\omega_{CO_2,out})\rho_{CO_2}} \tag{2-1}$$

where U and I are voltage and current in the system, respectively. v_{in} and v_{out} are the volume flow rate of gas mixture at the inlet and outlet. t is the run time of the cryogenic system, and ρ_{CO_2} is the density of CO_2 gas.

(a) (b)

Figure 2-7 The frost layer of CO_2 onto the cooling fin of SC-2's heat exchanger (a) and deposition in the storage column (b)

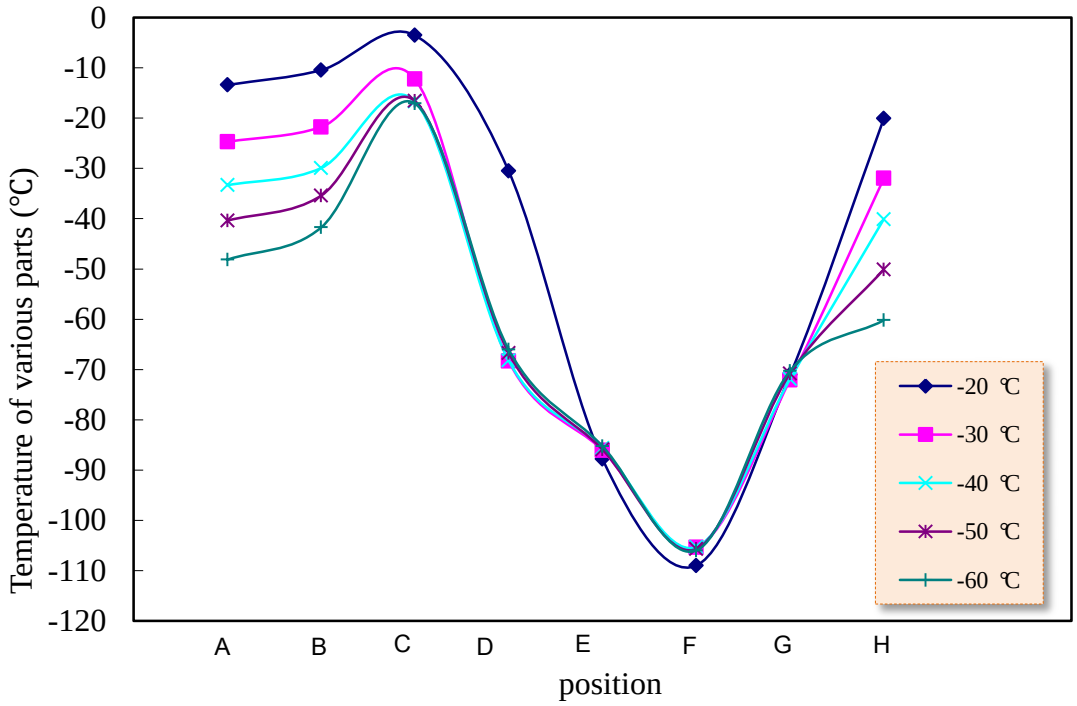

A SC-1 heat exchanger B Precooling tube C Water condensate tube

D Dry ice storage tank E SC-2 heat exchanger F SC-2 G SC-3 H SC-1

Figure 2-8 Temperature variation of key parts in cryogenic capture system (under different temperature threshold of SC-1)

In addition, the capture performance of the exploited system was undertaken using different flow rates of the influent gas. From the results in Figure 2-9 it can be concluded that when the flow rate of the gas stream was below 4 L/min, the CO_2 recovery of the system could reach 100%. This indicates the all of the CO_2 in the flue gas can be effectively captured. It needs to be pointed out that this result is based on some assumptions and is as a result of experiments in the laboratory scale. Therefore, it can not be achieved in a real coal-fired power station. As the flow rate was set at 5 L/min, the average CO_2 recovery decreased slightly (around 95%) but the energy consumption could be reduced significantly (about 0.55 MJ/kg CO_2). When the flow rate continually increased to 6 L/min, the CO_2 recovery decreased rapidly (below 80%). This can be explained by the fact that the surface of the cold head to capture CO_2 is limited. When the flow rate is low, most of flue gas can pass through the cooling fin of the cold head. By contrast, the gas stream slops over the cold head briefly without sufficient deposition occurring under a high flow rate (6 L/min). In addition, along with the growth of the frost layer, the influence of insulation will become increasingly obvious. Although there is a scraper to separate the frosted CO_2 down to the storage column, its function will become weak with the increase of the flow rate. When the flow rate was set at 6 L/min, the energy consumption to capture per kg of CO_2 increased rapidly (approximately 0.71 MJ/kg CO_2 after 60 min). Meanwhile, the CO_2 recovery decreased from 92% at 10 min to 61% at 60 min.

4.4 Comparison with the existing CO_2 capture technologies

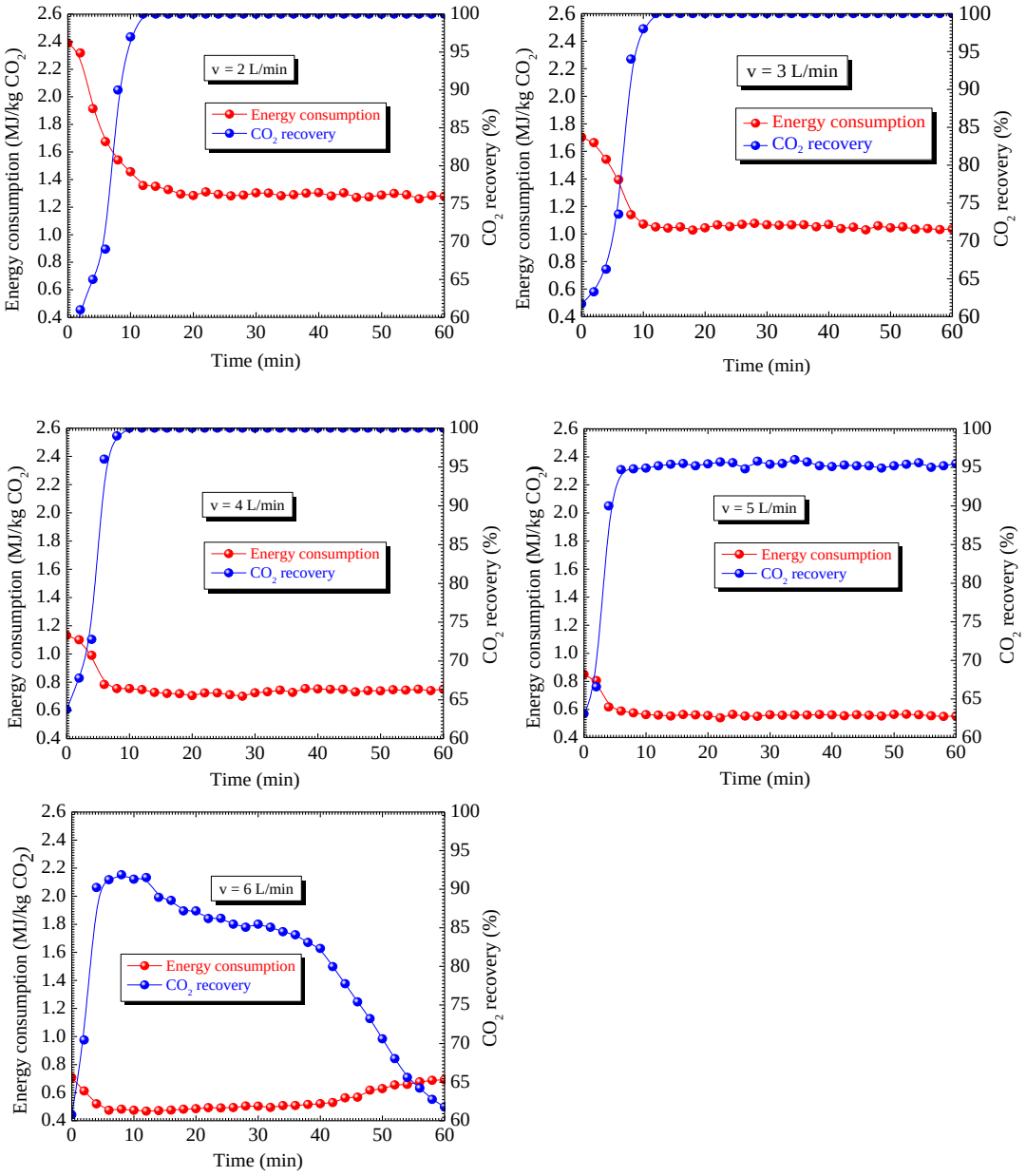

Figure 2-9 Performance of the cryogenic CO_2 capture system under different flow rates of influent gas (The flow rate is set at 2 L/min, 3 L/min, 4 L/min, 5 L/min and 6 L/min).

At present, the main CO_2 capture technologies are chemical absorption and membrane separation. For the two technologies, solvent regeneration and pressure difference as driving force lead to capital penalties, respectively. With respect to the capture efficiency, the comparison of these major technologies cannot be neglected. In previous studies, some researchers have attempted to make a quantitative comparison between each two methods, e.g. MEA and membranes by Favre in 2011, MEA and cryogenic by Clodic et al. in 2005. In our work, a brief comparison among the three processes has been made. Ahead of comparison, it is should be pointed out that for different technologies the types of requirement energy are also different. 1) For the MEA methods, there are two parts of the energy that should be considered. One is the thermal energy used for regenerating the solvent and extracting steam from the steam turbine, which dominates the energy consumption of the whole capture process. The other small part is electrical energy for the operation of the machines. 2) For the membrane methods, all the energy required is electrical energy to generate the partial pressure difference. 3) For the cryogenic separation process in this research, the cryogenic condition and operation of the system are both based on the electrical energy consumption. In addition, for these technologies, the compression energy of CO_2 to transport and storage pressure should also be considered as an important part. It is therefore not correct to make a direct comparison of the energy consumption between these methods without any calculation exchange. In order to obtain meaningful results, the condition of each technology should be stated accompanying with the comparison. The comparison results are presented in Table 2-3. The results indicate that the energy consumption for membrane process is substantially higher than that for MEA and cryogenic processes, which is due to its capital requirement for permeation under the flue gas condition.

Table 2-3 Comparison among the different CO_2 capture technologies.

Technologies	MEA (Ho et al., 2011)	Membrane (Hussain and Hägg, 2010)	Cryogenic (The present work)
Power output (MWe)	500	–	5×10^{-4}
Total efficiency (%LHV)	39	–	–
Flue gases mass flow (kg/s)	630	284	4.95×10^{-5}
Temperature (℃)	110	40	30
Pressure (Pa)	1.01×10^{5}	1.01×10^{5}	1.01×10^{5}
Flue gases composition			
N_2	75 (mol.%)	80 (vol.%)	82 (vol.%)
CO_2	13	10	13
O_2	5	5	–
H_2O	7	5	5
CO_2 capture efficiency (%)	>85	>90	96
Energy penalty (MJ power /kg CO_2)	1.6	3~4	0.5

Table 2-4 Comparison among the mentioned cryogenic capture processes.

Cryogenic processes	Advantages	Disadvantages
Clodic et al., 2004b	The fusion latent heat of CO_2 defrosting is recovered.	1) The water content in the flue gas should be removed before capture process, which step would increase the capital cost or energy consumption; 2) The frost layer of solid CO_2 onto the cold head surface will adversely affect the heat transfer and reduce the overall efficiency; 3) The costly heat exchangers have to be used for resisting the impact of temperature and mechanical stress.
Tuinier et al., 2011	The CO_2, N_2 and H_2O can be separated in different parts of the process, avoiding the phenomenon of plugging and pressure drop.	Due to the low coefficient of performance (COP) of the refrigerator (about 0.5 at -140 ℃), above 3.6 MJ electric energy was required for per unit CO_2 capture.
The present work	The separation among CO_2, N_2 and H_2O can be achieved.	1) It takes a long time for the whole system to reach the required cryogenic condition; 2) There is some heat loss in the capture at the junction of heat exchangers and tower; 3) The frost layer of solid CO_2 onto the heat exchanger surface will adversely affect the heat transfer and reduce the overall efficiency; 4) The costly heat exchangers have to be used for resisting the impact of temperature variation; 5) The oscillation of Stirling coolers would lead to a certain amount of energy loss.

In addition, the common characteristic of the present work and the other cryogenic

processes described in section 1 (*i.e.* the outcomes of Clodic and Tuinier) are that no chemical absorbent is required, and the capture of CO_2 can be realized at atmospheric pressure. Meanwhile, each of these methods has their own features, and a comparison is shown in Table 2-4. From the comparison, it is observed that further investigation on this process is significant and promising.

5. CONCLUSION

In this chapter, a novel cryogenic CO_2 capture system based on the commercial SC has been designed. The principle of operation and advantages of the system were demonstrated and verified in detail. According to the experimental results, an effective separation on the basis of differences in frost points can be achieved without increasing pressure drops and plugging problems. From the performance of system, it demonstrated that the system can separate CO_2 efficiently. Furthermore, the influence of flow rate of gas stream and temperature of SC-1 on the performance of system was investigated. Based on the designed cryogenic system, the recovery of CO_2 can achieve 96% with 0.5 MJ/kg CO_2 energy consumption, which demonstrated that the research of the CO_2 capture process based on Stirling coolers is promising. Meanwhile, further testing has been planned to determine the range and overall performance of the system and solve the problem of heat loss. Besides, the test of CO_2 capture from flue gas and biogas will be carried out.

REFERENCES

U.S. Department of Energy., 2007. Energy Information Administration (EIA). International energy outlook. U.S. Government. 61-71.

B. Metz, O. Davidson, H. Coninck, M. Loos, L. Meyer, 2005. IPCC Special Report on Carbon

Dioxide Capture and Storage. Prepared by Working Group III of the Intergovernmental Panel on Climate Change. Cambridge University Press, Cambridge, UK, New York, NY.

R. Irons, G. Sekkapan, R. Panesar, J. Gibbins, M. Lucqiuaud, 2007. CO_2 capture ready plants. IEA Greenhouse Gas R & D Programme, http: //www.ieagreen.org.uk.

D. Jeremy, 2000. Economic evaluation of leading technology options for sequestration of carbon dioxide. M.S thesis, MIT, Cambridge, MA.

H. Audus, 2000. Leading options for the capture of CO_2 at power stations. Presented at the 5th international conference on greenhouse gas control technologies, Cairns, Australia. 13-16 August.

D. Clodic, M. Younes, 2002. A new method for CO_2 capture: frosting CO_2 at atmospheric pressure. Sixth International Conference on Greenhouse Gas Control Technologies, GHGT6, Kyoto, Japan, 1-4 October, pp.155–160, [CD ROM].

D. Clodic, M. Younes, A. Bill, 2004a. Test result of CO_2 capture by anti-sublimation capture efficiency and energy consumption for boiler plants. Seventh International Conference on Greenhouse Gas Control Technologies, GHGT7, Vancouver, Canada, 6-9 September.

M.J. Tuinier, M. van Sint Annaland, G.J. Kramer, J.A.M. Kuipers, 2010. Cryogenic CO_2 capture using dynamically operated packed beds. Chemical Engineering Science. 65, 114-119.

J.Y. Hu, W. Dai, E.C. Luo, X.T. Wang, Y. Huang, 2010. Development of high efficiency Stirling-type pulse tube cryocoolers. Cryogenics. 50, 603-607.

J.F. Sun, Y. Kitamura, T. Satake, 2008. Application of Stirling cooler to food processing: Feasibility study on butter churning. Journal of Food Engineering 84, 21-27.

S.J. Park, Y.J. Hong, H.B. Kim, D.Y. Koh, J.H. Kim, B.K. Yu, K.B. Lee, 2002. The effect of operating parameters in the Stirling cryocooler. Cryogenics 42, 419-425.

X. Chen, Y.N. Wu, H. Zhang, N. Chen, 2009. Study on the phase shift characteristic of the pneumatic Stirling cryocooler. Cryogenics 49, 120-132.

D. Clodic, M. Younes, R. EL Hitti, E. Boulawz Ksayer, F. Casier, A. Bill, 2004b. Feasibility study of CO_2 and water capture by anti-sublimation for power station units. Report for the French Agency for Environment and Energy Management (ADEME), confidential.

O. Ercan Ataera, H., Karabulut, 2005. Thermodynamic analysis of the V-type Stirling-cycle refrigerator. International Journal of Refrigeration 28, 183-189.

D.M. Berchowitz. Free-Piston Stirling Coolers. International Refrigeration Conference Energy Efficiency and New Refrigerants, July 1992, Purdue University.

H. Karabulut, 2011. Dynamic analysis of a free piston Stirling engine working with closed and open thermodynamic cycles. Renew Energy 36, 1704-1709.

E. Favre, 2011. Membrane processes and post combustion carbon dioxide capture: Challenges and prospects. Chemical Engineering Journal 171, 782-793.

D. Clodic, E.R. Hitti, , Younes, M., Bill, A., 2005. CO_2 capture by anti-sublimation thermo-economic process evaluation. 4th Annual Conference on Carbon Capture & Sequestration, May 2-5, Alexandria (VA), USA.

M.T. Ho, G.W. Allinson, D.E. Wiley, 2011. Comparison of MEA capture cost for low CO_2 emissions sources in Australia. International Journal of Greenhouse Gas Control 5, 49-60.

A. Hussain, M.B. Hägg, 2010. A feasibility study of CO_2 capture from flue gas by a facilitated transport. Journal of Membrane Science 359, 140-148.

M.J. Tuinier, M. van Sint Annaland, J.A.M. Kuipers, 2011. A novel process for cryogenic CO_2 capture using dynamically operated packed beds—An experimental and numerical study. International Journal of Greenhouse Gas Control 5, 694-701.

CHAPTER 3

FREE PISTON STIRLING COOLER

Free piston Stirling cooler (FPSC) is a promising alternative for conventional coolers and has been applied to various fields. In the previous research, a novel cryogenic CO_2 capture system based on FPSCs has been exploited. Nevertheless, it is noteworthy that the original cold range of FPSC is limit. In order to enhance the cryogenic capture efficiency, the investigation on the coefficient of performance (COP) of the FPSC is significant. In this chapter, the theoretical analysis of the COP of FPSC was studied systematically. Meanwhile, the COP and cryogenic temperature of FPSC were investigated under different materials (aluminium and copper), size of cold head (length and diameter), as well as ambient conditions (humidity and temperature). From the experimental results, it can be concluded that when the temperature of the cold head reached -140 ℃ (material was copper, length and diameter were 180 and 40 mm, respectively), the COP of the FPSC was 0.82. Furthermore, the COP of the cryogenic CO_2 system was 0.7.

1. INTRODUCTION

According to the prediction of Intergovernmental Panel on Climate Change (IPCC), by the year 2100, the atmosphere may contain up to 570 ppmv of CO_2, causing a rise of mean global temperature of around 1.9 ℃ and an increase in mean sea level of 3.8 m (IPCC, 2007). As an effective strategy to mitigating CO_2 emissions, much attention has been paid on post combustion CO_2 capture (PCC) strategies. Nowadays, the most mature post-combustion CO_2 capture technology is based on CO_2 absorption by aqueous amine solutions and has been commercially utilized on the large CO_2 emission sources (i.e. coal-fired power plants, cement plant and steel plant) (Abu-Zahra et al., 2007; Versteeg and Rubin, 2011). CO_2 reacts reversibly in an absorber with amines which are regenerated by heating the solution in a stripper column (Gouedard et al., 2012). The biggest bottleneck for chemical adsorption processes is that the regeneration of solvents is energy penalty (Luis et al., 2012; Lee et al., 2012). Meanwhile, the degradation of aqueous amine solvents also causes increasing cost (Dumée et al., 2012). Compared to other CO_2 capture technologies, cryogenic CO_2 capture approach can achieve a high CO_2 purity (above 99%) and that can minimize the compression and transport costs significantly (Belaissaoui et al., 2012). Consequently, a number of researches have been driven toward cryogenic CO_2 capture process.

Several low temperature sources have been investigated for utilization on cryogenic CO_2 capture technique. In 2002, Clodic et al. developed a novel cryogenic CO_2 capture process by using the cold duty from liquid nitrogen (LN_2). The CO_2 in the flue gas can be recovered in liquid form and that is beneficial to the further compression and transport. The main disadvantage of the process is that the deposited CO_2 on the

cold head will adversely affect the heat transfer. Moreover, the moisture in the flue gas has to be separated beforehand to avoid the plugging by ice during operation. In 2011, Tuinier et al. exploited a cryogenic packed bed taking advantage of the cold energy from liquefied natural gas (LNG) regasification terminal. The moisture and CO_2 can be collected at different locations in the process. However, the coefficient of performance (COP) of the system is typically 0.5, about 3.6 MJ electric energy is required and resulting in even higher thermal energy to capture per kg CO_2.

Free piston Stirling cooler (FPSC) is a new type cryogenic cooler attracting interest as low temperature source (Berchowitz et al., 1995). Compared to conventional coolers, FPSC can use helium as regenerator, and avoid increasing environmental issues (such as ozone depletion) caused by CFCs, HCFCs and HFCs (Mennink and Goossen, 1995). Meanwhile, high energy efficiency and reliability is another advantage of FPSC (Song et al., 2012). For these reasons, FPSC has been utilized in cryogenic CO_2 capture process. However, it needs to point out that the original cooling region of FPSC is limit duo to the size of itself. During the application process, it often needs to extend the cold head for further refrigeration. Therefore, the investigation on the COP and cryogenic temperature of FPSC is significant for improving the CO_2 capture efficiency.

The objective of this chapter is to investigate the characteristic of FPSC and theoretically analyze the COP of the FPSC. The research also focuses on the influence of the key parameters on the COP of FPSC, such as material (aluminium and copper) of the cold head, size (length and diameter) of the cold head and ambient conditions (temperature and humidity).

The structure of this chapter is as follows. Section 2 describes the base case of cryogenic CO_2 capture process in brief. Section 3 introduces the detailed configuration

of FPSC and studies its working mechanism, and then theoretically deduces the COP of FPSC. Section 4 shows the detailed experimental conditions. Section 5 investigates the key parameters that influence the COP and cryogenic temperature of FPSC. Section 6 summarizes the main conclusions of this research.

2. BASE CASE

The base case of the exploited cryogenic CO_2 capture process is described in Figure 3-1. The three Stirling coolers used in the system are named as FPSC-1, FPSC-2 and FPSC-3, respectively. First, the flue gas is introduced into pre-freezing tower. Under the low temperature, the moisture in the gas stream can condense and be separated. Then the dry flue gas (around -20 ℃) flows into main freezing tower. Under the cryogenic condition (approximately -105 ℃), the CO_2 in the gas stream frosts on the surface on the cold head of FPSC-2, and simultaneously the other gas (such as N_2) is exhausted. Finally, the captured CO_2 is gathered in the storage column to further compress for transport. In the flow diagram, it has been shown that the low temperature conditions in the pre-freezing tower, main freezing tower and storage column are provided by FPSC-1, 2 and 3, respectively. Q_{C1}, Q_{C2} and Q_{C3} represent the required cold energy. The detail capture process is introduced in the previous work (Song et al., 2012a, b).

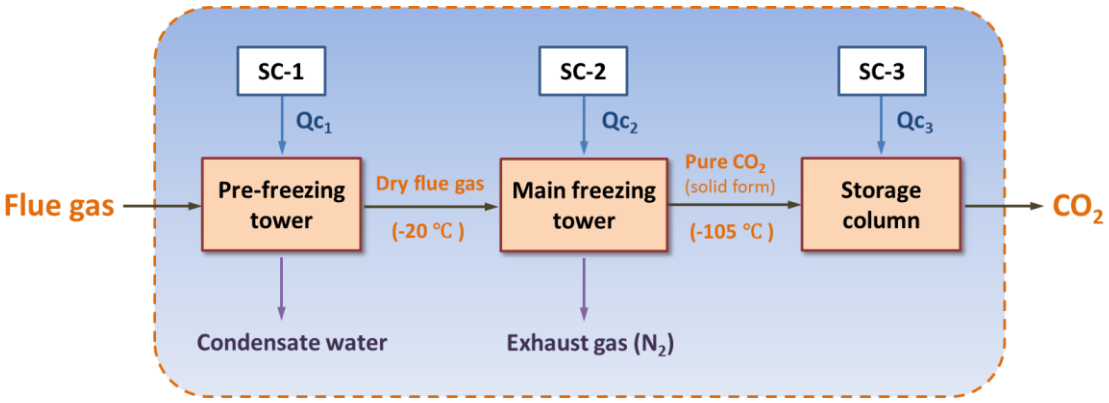

Figure 3-1 The cryogenic CO_2 capture process based on the exploited FPSC system

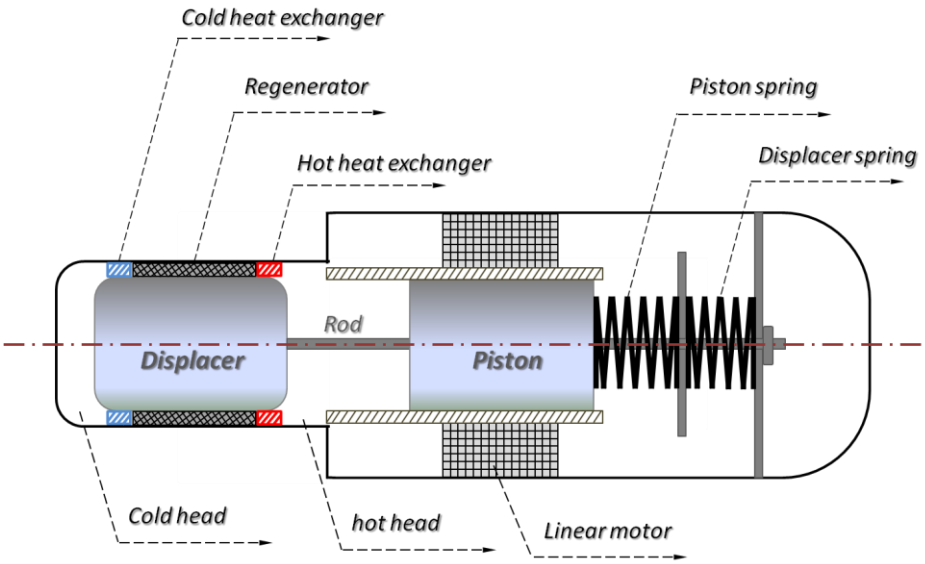

Figure 3-2 The detailed configuration of FPSC

3. FREE PISTON STIRLING COOLER

3.1 Configuration

A schematic diagram of the free piston Stirling cooler is shown in Figure 3-2. The FPSC may be defined as a pressure vessel which operates by shuttling approximately 1 gram of Helium back and forth by the combined movements of two parts, namely the piston and the displacer. While the piston that compresses the gas is driven by a linear motor, the displacer is moved by the pressure difference. Heat exchanger and regenerator are assembled to separate the compression and expansion spaces for the creation of a thermal gradient which allows the FPSC to extract heat from the cold head and reject heat to the region around hot head. This process is repeated many times per second and can ultimately produce temperature differences between the cold and hot head. During the whole process, heat can be moved from a remote location to the FPSC and then rejected to the environment.

3.2 Theoretical analysis

3.2.1 Mechanism

In theory, Stirling cooler consists of two isothermal and two isovolumetric heat transfer processes. The isovolumetric heat transfer takes place in a regenerative manner. While rejecting thermal energy to the environment during the isothermal compression process, the gas absorbs thermal energy from the environment during the isothermal expansion. Therefore, a Stirling cooler may be determined by a high and a low temperature which are generally named warm and cold head temperatures. The detailed working mechanism of FPSC is demonstrated in Figure 3-3.

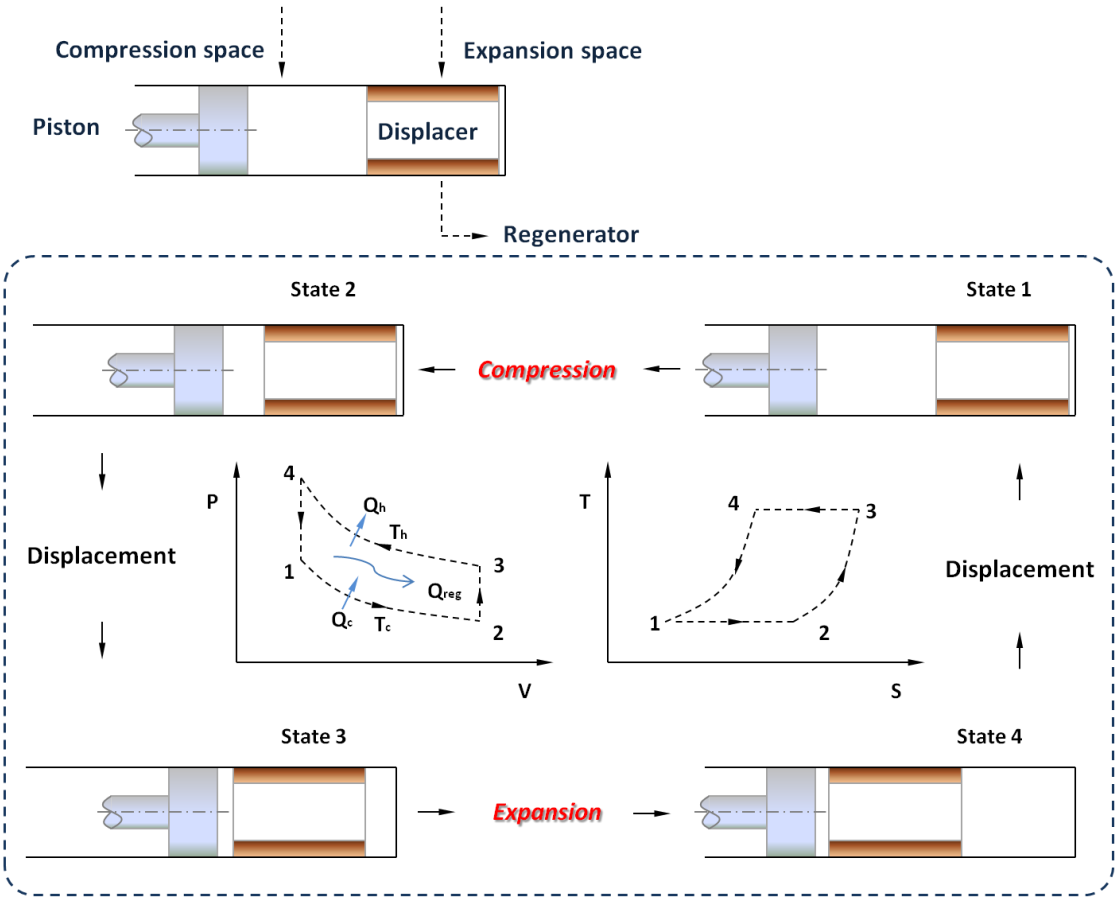

Figure. 3-3 The working mechanism of FPSC

The variation of expansion (V_e) and compression (V_c) volumes of Stirling cooler can be expressed as follows (Ercan Ataer and Karabulut, 2005):

$$V_e = V_{e,d} + \frac{1}{2}V_s(1+cos\theta) \tag{3-1}$$

$$V_c = V_{c,d} + \frac{1}{2}V_s\left[1+cos(\theta-\varphi)\right] \tag{3-2}$$

where $V_{e,d}$ and $V_{c,d}$ are the dead volumes of expansion and compression. V_s is the swept volumes, respectively. θ is the crank angle. φ is the phase angle of the displace relative to the piston and can be calculated by (Berchowitz, 1992):

$$\varphi = \tan^{-1}\left\{\frac{\frac{\omega_0}{\omega_d}\cdot\frac{1}{2\pi Q_d} - \frac{\omega_0 C_{dp}}{\alpha_p}\left[1-\left(\frac{\omega_0}{\omega_d}\right)^2\right]}{-\left[1-\left(\frac{\omega_0}{\omega_d}\right)^2\right] - \frac{\omega_0}{\omega_d}\cdot\frac{\omega_0 C_{dp}}{\alpha_p}\frac{1}{2\pi Q_d}}\right\} \tag{3-3}$$

where ω_0 and ω_d are radial and undamped natural frequency. C_{dp} is relative damping coefficient between displacer and piston. α_p is piston coupling. Q_d is defined as the ratio of stored energy and energy loss per cycle at ω_d. The specific definitions of α_p and Q_d are shown as follows:

$$\alpha_P = A_R\left(\frac{\partial P_c}{\partial x_P} - \frac{m_P}{m_c}\cdot\frac{\partial P_c}{\partial x_c}\right) + K_{ext}\frac{m_P}{m_c} \tag{3-4}$$

$$Q_d = \left(\frac{\omega_d m_d}{2\pi C_d}\right) \tag{3-5}$$

where A_R is the crosscut area of the displacer rod. K_{ext} is displacer external spring. m_c, m_d and m_p are the mass of cylinder, displacer and piston, respectively. P_c is the cylinder pressure. C_d is the damping coefficient of displacer. x_c and x_p are the displacements of cylinder and piston.

The momentum equation of the displacer and piston may be written as follows: (Karabulut, 2011):

$$\frac{d^2y}{dt^2} = -\frac{C_d}{m_d}\frac{dy}{dt} - \frac{k_d}{m_d}(y - y_e) + \frac{A_R}{m_d}(P_\omega - P_b) \tag{3-6}$$

$$\frac{d^2x}{dt^2} = -\frac{C_P}{m_P}\frac{dx}{dt} - \frac{k_P}{m_P}(x - x_e) + \frac{(A_P - A_R)}{m_P}(P_\omega - P_b) \tag{3-7}$$

here C_P is the damping coefficient of the piston. k_d is the stiffness of the displacer spring. k_p is the stiffness of the piston spring. A_p is the crosscut area of the piston. P_b is the block pressure. P_ω is the working volume pressure. x is the distance indicating the position of the piston top. x_e is the static position of the piston top. y is the distance indicating the position of the displacer bottom. y_e is the static position of the displacer bottom.

3.2.2 COP of free piston Stirling cooler

As an important quality to evaluate the performance of FPSC, the investigation on the COP is significant. The COP is defined as the ratio of the cooling capacity (Q_e) and the input power (W) of the system, and can be expressed as follows:

$$COP = \frac{Q_e}{W} \tag{3-8}$$

where the input power (W) can be obtained from:

$$W = \frac{\omega_0}{2\pi}\int_0^{2\pi} P_c dV \tag{3-9}$$

here P_c and V are the pressure and volume of cylinder, and can be given by the following equations (Berchowitz, 1992):

$$P_c = \langle P \rangle + |P_c| \sin\phi \tag{3-10}$$

$$V = V_0 - A_P X_P \sin\phi \tag{3-11}$$

Taking equation (3-10) and (3-11) into equation (3-9), the input power (W) can be expressed as:

$$W = -\frac{\omega_0}{2}\alpha_T X_p X_d sin_\phi \tag{3-12}$$

where, X_d and X_p are the amplitude of the displacer and piston. α_T is the thermal coupling between the displacer motion and piston force.

$$\alpha_T = A_p \frac{\partial P_c}{\partial x_d} \tag{3-13}$$

In addition, the heat lift (Q_e) is described as follows:

$$Q_e = -\frac{\omega_0}{2}\left\{\alpha_p X_p \left(\frac{A}{A_R} - 1\right) sin_\phi - K_{ext_d} X_p \frac{A}{A_R}\frac{m_p}{m_c} sin_\phi + C_{ext}\omega_0 X_d\right\} X_d \tag{3-14}$$

where A is the crosscut area of the cylinder. C_{ext} is incidental damping. It should be noted that heat transfer losses (Q_L) is inevitable. Among the heat losses, conduction (Q_{cond}) and regenerator (H) losses are the most significant.

$$Q_L = Q_{cond} + H \tag{3-15}$$

In conclusion, the COP of the FPSC can be expressed as the following equation:

$$COP = \frac{\alpha_P}{\alpha_T}\left(\frac{A}{A_R} - 1\right) - \frac{A}{A_R}\frac{K_{ext}}{\alpha_T}\frac{m_P}{m_c} + \frac{C_{ext}}{\alpha_T}\frac{\omega_0}{sin_\phi}\frac{X_d}{X_P} \tag{3-16}$$

4. EXPERIMENTAL SECTION

The detailed experimental conditions are introduced in this section. First, the cold head of FPSC is tested with different materials (aluminium and copper). Second, the size (length and diameter) of the cold head is investigated. The length (L) of cold head is set at (180 mm and 270 mm), respectively. The diameter (D) of the cold head is investigated under 30 mm and 40 mm. It needs to point out that the selection of length and diameter is just depending on the configuration of the system, and there is no special representation. Additionally, during the operating process, the FPSC needs to

intake the air from ambient and exhaust the hot air simultaneously. Therefore, the influence of ambient humidity (h_a) and temperature (T_a) on the COP of FPSC is also investigated. As mentioned above, at present one of the main tasks for CO_2 capture technologies is to reduce the energy consumption and optimize the capture efficiency. It shows that the investigation on the coefficient of performance for the whole system (COPS) is also necessary. The COPS of the system can be calculated as follows:

$$COPS = \frac{Q_{C1} + Q_{C2} + Q_{C3}}{W_s} \tag{3-17}$$

here Q_{C1}, Q_{C2} and Q_{C3} are the cooling capacity of FPSC-1, 2 and 3, respectively. W_s is the input energy of the system.

5. RESULTS AND DISCUSSION

5.1 Effect of cold head on the COP

5.1.1 Material

The influence of the material of cold head on the COP of FPSC is investigated in this section. The structure of the cold head with different materials (aluminium and copper) is shown in Figure 3-4. The advantages and disadvantages of aluminium and copper are listed in Table 3-1. The influence of the material of the cold head on the COP of FPSC is shown in Figure 3-5. With the temperature reduction of the cold head, the cooling capacity of FPSC decreased, and which led to the fall of COP. However, the aluminium cold head has a relative higher COP decreasing rate compared to the copper one. It results that the FPSC with an aluminium cold head has a lower COP than the copper one in the whole temperature drop process. When the root temperature of the cold head dropped to -140 ℃, the COP of FPSC with the aluminium and copper

cold head are 0.61 and 0.82 respectively. It can be deduced that although the oscillation of system with copper cold head is serious and the capital cost is also expensive compared to aluminium, its COP is high which means a large cooling capacity can be obtained. Therefore, copper should be selected as the material of the cold head.

The effect of the material of cold head on the cryogenic temperature is depicted in Figure 3-6. From the results, it can be concluded that the cold head made by copper has a lower temperature than aluminium. After 240 min, the root temperatures are -111.2 ℃ for the aluminium cold head and -111.3 ℃ for the copper. Meanwhile, the front temperatures of the aluminium and copper cold head are -78.09 ℃ and -97.82 ℃. In addition, the temperature decreasing rate for the copper cold head is higher than the aluminium. For copper, the temperature drop from the root of the cold head to the front is 13.38 ℃. By contrast, although the mass of the cold head by aluminium is light, the thermal loss is great (with a temperature drop of 33.31 ℃).

Table 3-1 The advantages and disadvantages of different materials for the cold head of FPSC.

Material of the cold head	Advantages	Disadvantages
Aluminium	• Light weight • Low capital cost	• Low thermal conductivity • Easy to distortion
Copper	• High thermal conductivity • Hard to distortion	• High capital cost • Serious oscillation • Easy to be corroded

Figure 3-4 The cold head of FPSC with different materials (aluminium and copper)

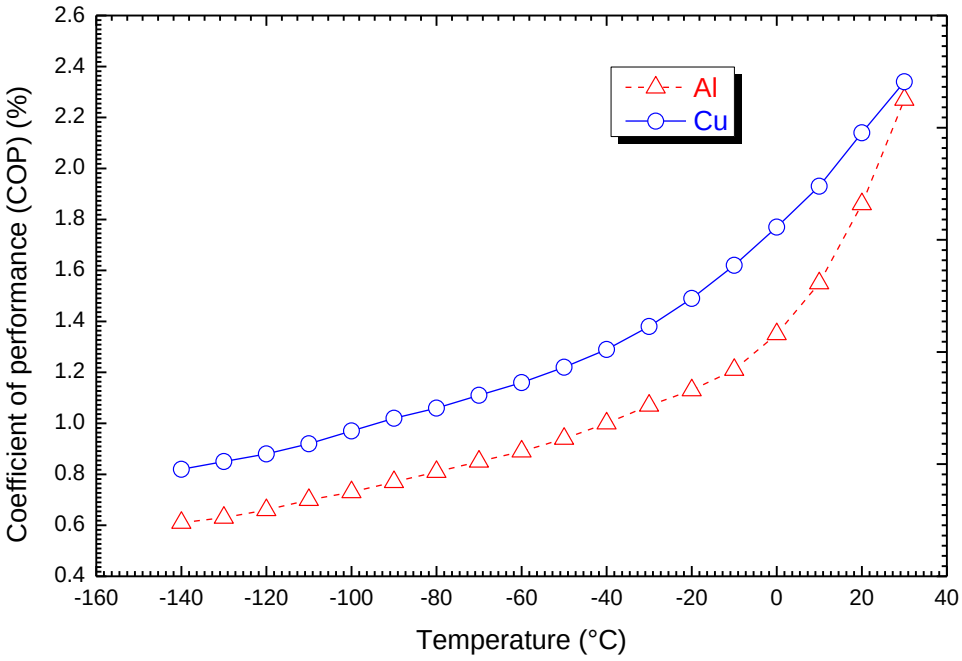

Figure 3-5 COP variation of FPSC with the root temperature of the cold head under different material (L=180 mm; D=40 mm)

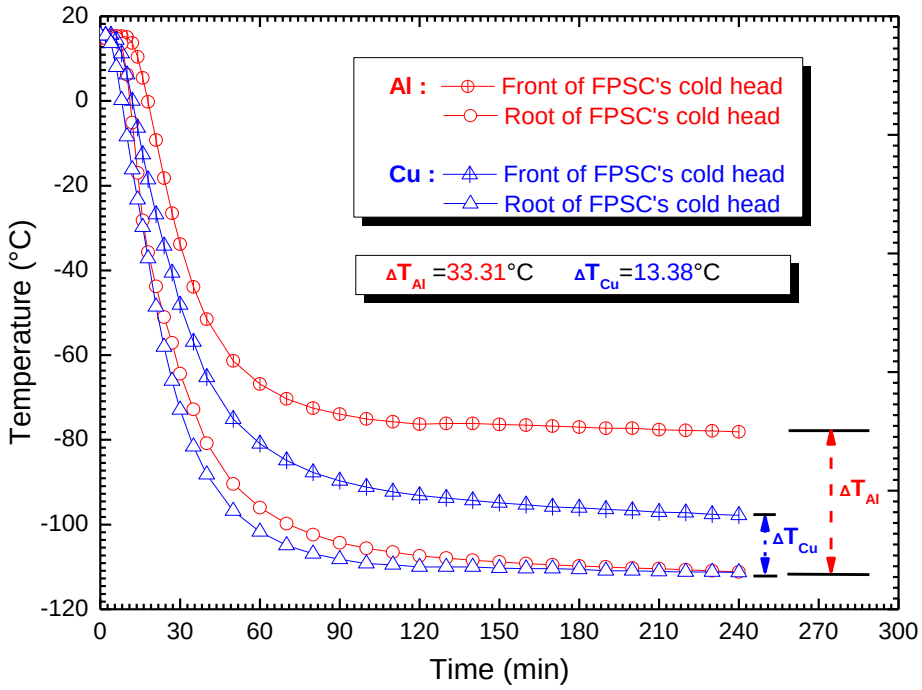

Figure 3-6 The effect of the material of cold head on the cryogenic temperature (L=180 mm; D=40 mm)

5.1.2 Length

The results in Figure 3-7 show that the influence of the length of cold head on the COP of FPSC. It can be observed that with the increase of the length, the COP of FPSC decreased obviously. However, for the aluminium cold head, the decreasing rate of COP is higher than the copper one. When the length is extended from 180 mm to 270 mm, the COP dropped from 0.82 down to 0.59 (the root temperature of the cold head was -140 ℃). It can be explained by the fact that along with the increasing of the length of the cold head, the heat loss also increase and the cooling capacity of the cold head reduced accordingly. Therefore, the COP of FPSC also dropped.

As the results in Figure 3-8, the cryogenic temperature of the cold head decreases with the extension of the length. When the length of the cold head is set at 180 mm, the temperature drop from the root to the front is 9.92 ℃. However, with the length extending to 270 mm, the temperature drop rose up to 15.73 ℃. Furthermore, after 240 min, the front temperature of the cold head for 180 mm and 270 mm are -84.08 ℃ and -73.17 ℃. That is because that along with the extension of the length, the temperature loss of the cold head also increases. Therefore, it can be concluded that to reduce heat loss and enhance the thermal transfer efficiency, the length of the cold head should be shortened as much as possible.

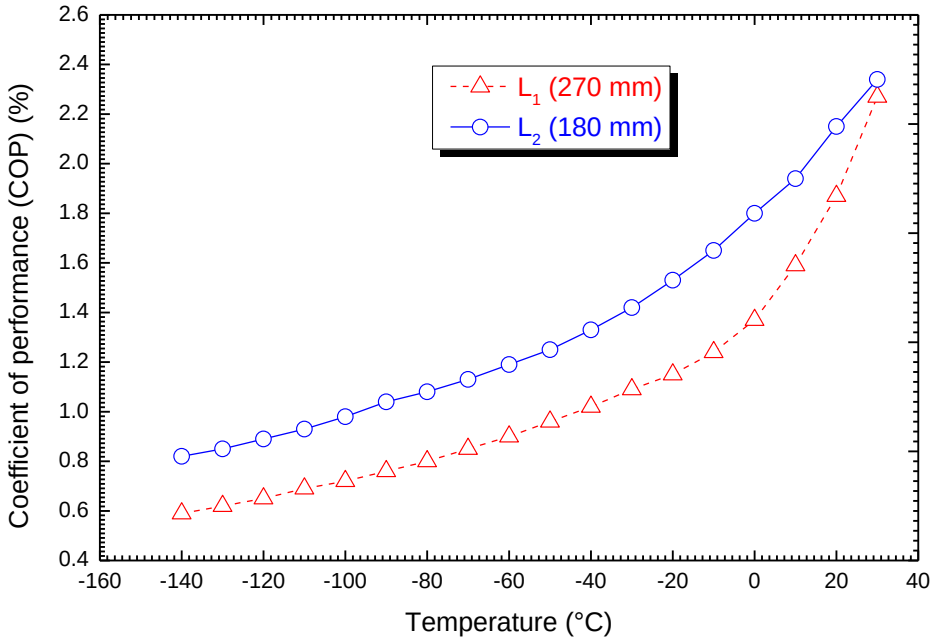

Figure 3-7 COP variation of FPSC with the root temperature of cold head under different length (*L*) (material of cold head is copper; *D*=40 mm)

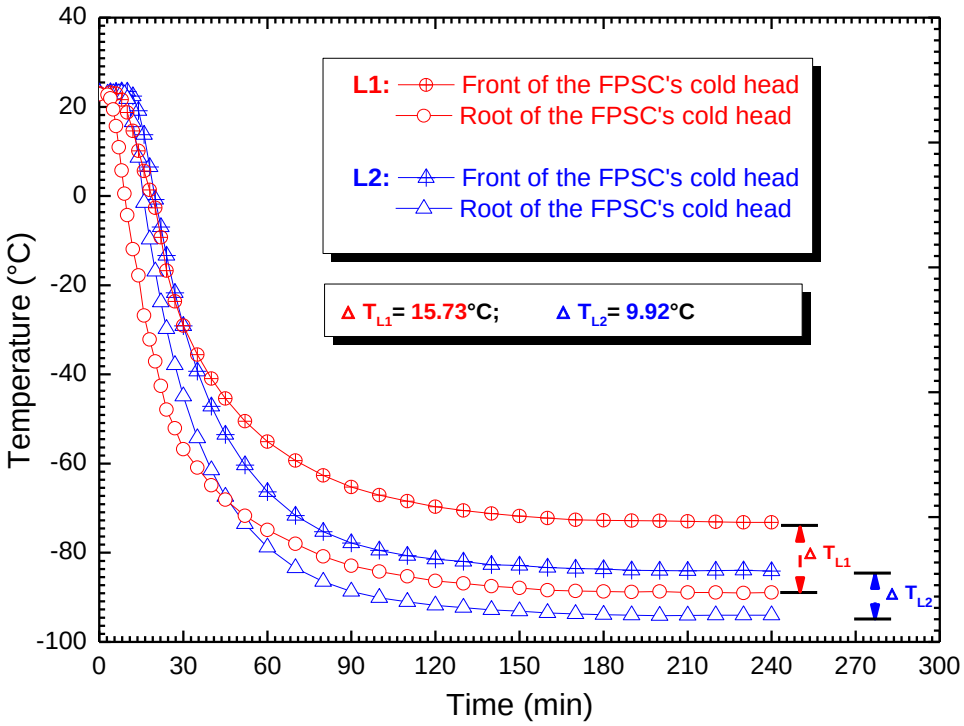

Figure 3-8 The relationship of length (L) and cryogenic temperature (T_c) of the cold head (material of cold head is copper; D=40 mm)

5.1.3 Diameter

As presented in Figure 3-9, the COP variation process with different diameters was investigated. The COP of FPSC reduced according with the temperature drop of the cold head. With the expanding of the diameter of the cold head (from 30 mm to 40 mm), the COP of FPSC increased obviously. Meanwhile, the decreasing rate of the COP was decelerated. When the root temperature of the cold head decreased to -140 ℃, the COP was 0.52 (diameter of 30mm) and 0.59 (diameter of 40 mm), respectively.

In addition, the relationship between the diameter and cryogenic temperature of the cold head was depicted in Figure 3-10. From the results, it can be concluded that a large diameter is beneficial to reduce temperature loss. When the diameter of the cold head is set at 30 mm, the lowest temperature for the root and front of the cold head is -85 ℃ and -64.72 ℃. The temperature drop is 20.28 ℃ from the root to the front side. By contrast, when the diameter is set at 40 mm, the lowest temperature for the root and front sides is -88.9 ℃ and -73.17 ℃ respectively. The temperature drop can be reduced to 15.73 ℃. For the larger diameter (40 mm), both of the root and front temperature are lower than the smaller one (30 mm). It indicated that expanding the diameter of the cold head is beneficial to improve heat transfer efficiency and the COP of FPSC.

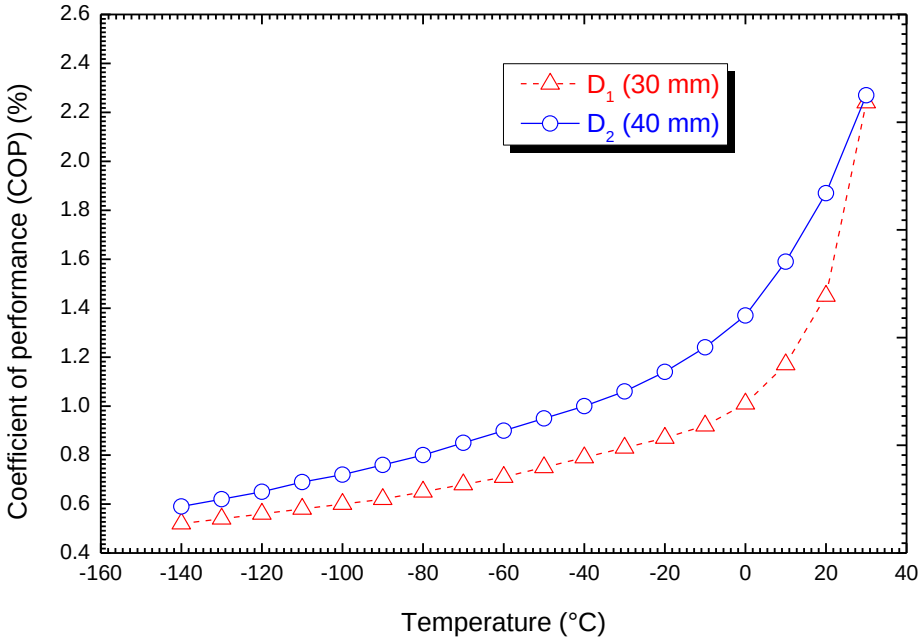

Figure 3-9 COP variation of FPSC with the root temperature of cold head under different diameter (*D*) (material of cold head is copper; *L*=270 mm)

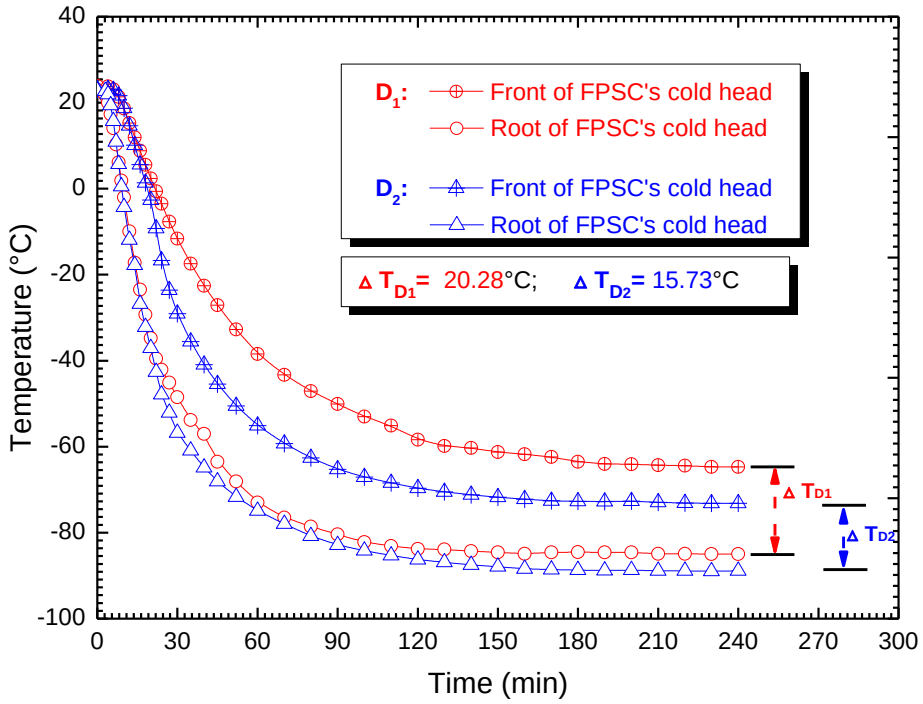

Figure 3-10 The relationship of diameter (D) and cryogenic temperature (T_c) of the cold head (material of cold head is copper; L=270 mm)

5.2 Effect of the ambient conditions on the COP

The effect of ambient temperature on the COP of FPSC is summarized in Figure 3-11. From the result, it can be observed that the COP of FPSC increased with the decreasing of ambient temperature. When the ambient temperature varied from 8 ℃ to 28 ℃, the COP of FPSC reduced from 0.7 to 0.6. That is for the reason that during the refrigeration process of FPSC, it absorbs cool air from surrounding and simultaneously exhausts warm air. A low ambient temperature is favor of increasing temperature difference from the cold head of FPSC to the warm side. Thus, in order to improve the performance of FPSC, the ambient temperature should be dropped as low as possible. The influence of ambient humidity on the COP of FPSC is shown in Figure 3-12. From the results in the figure, it shows that with the ambient humidity increasing from 20% to 75%, the COP of FPSC varied in the range of 0.62 to 0.68. It indicated that the influence of ambient humidity on the COP of FPSC is not significant.

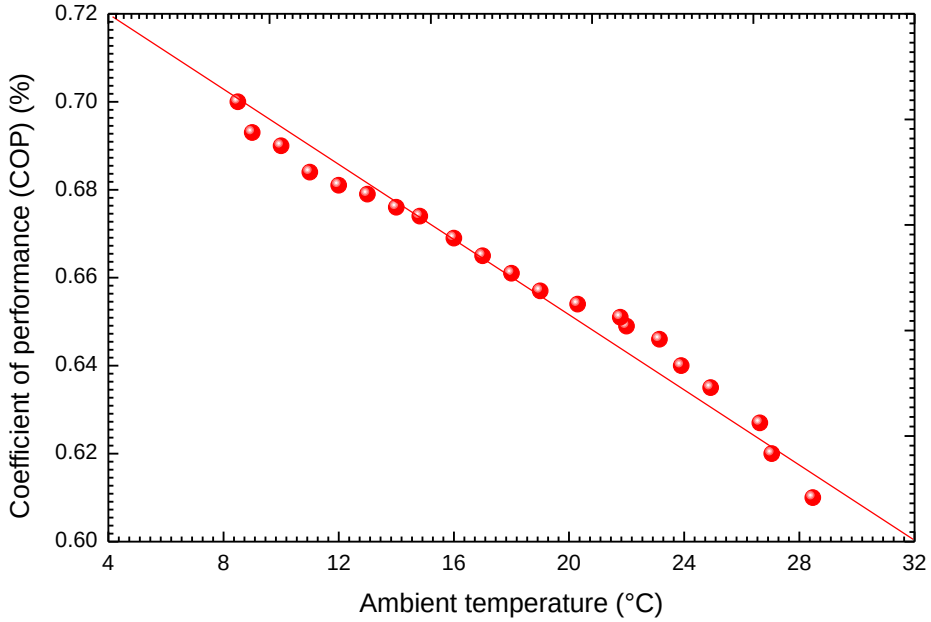

Figure 3-11 COP variation of FPSC with the different ambient temperature (T_a) (material of cold head is copper; L=180 mm; D=40 mm)

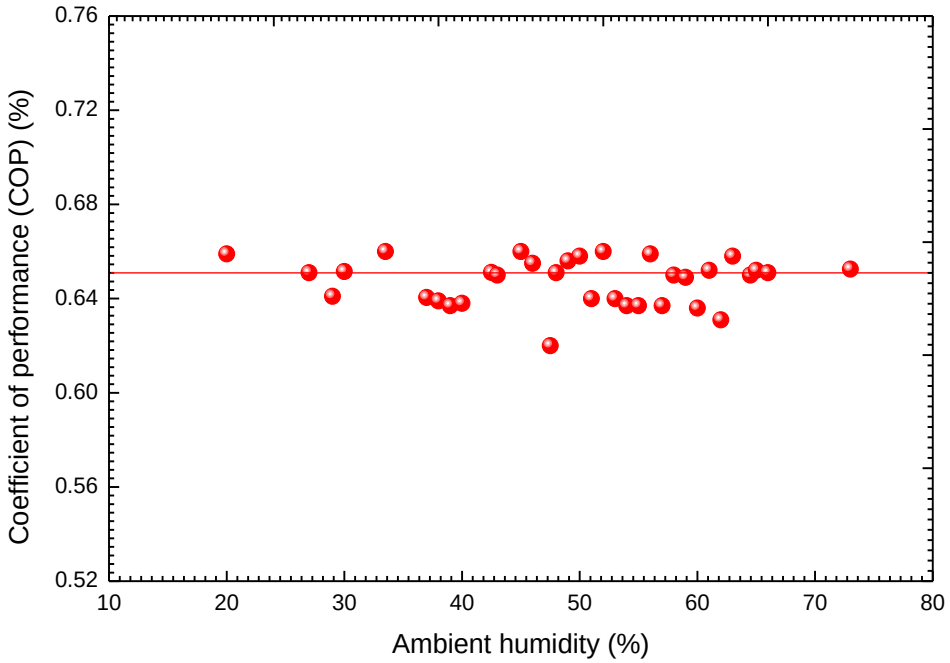

Figure 3-12 COP variation of FPSC with different ambient humidity (h_a) (material of cold head is copper; L=180 mm; D=40 mm)

5.3 COP of the cryogenic CO_2 capture system

In order to make a significant calculation on the COPS of the system, the energy consumption units in the CO_2 capture system is summarized in Table 3-2. Additionally, the COP variation of the FPSCs (FPSC-1, 2 and 3) and the whole system is shown in Figure 3-13. From the results, it can be found that the COPs of three FPSCs were different. That is for the reason that due to the different functions in the cryogenic CO_2 capture system, the length of the cold head of the FPSCs is also different. When the temperature of the cold head for FPSC-2 was cooled to -140 ℃, the COPs of FPSC-1, 2 and 3 were 0.82, 0.78 and 0.79, respectively. Meanwhile, due to the other energy consumption units (such as vacuum pump, control panel and scraper), the COP of the whole system was 0.70.

Table 3-2 Summary of the energy consumption units in the cryogenic CO_2 capture system.

Units	Power (W)
FPSC-1	150
FPSC-2	150
FPSC-3	150
Vacuum pump	400
Control panel	56
Scraper	12

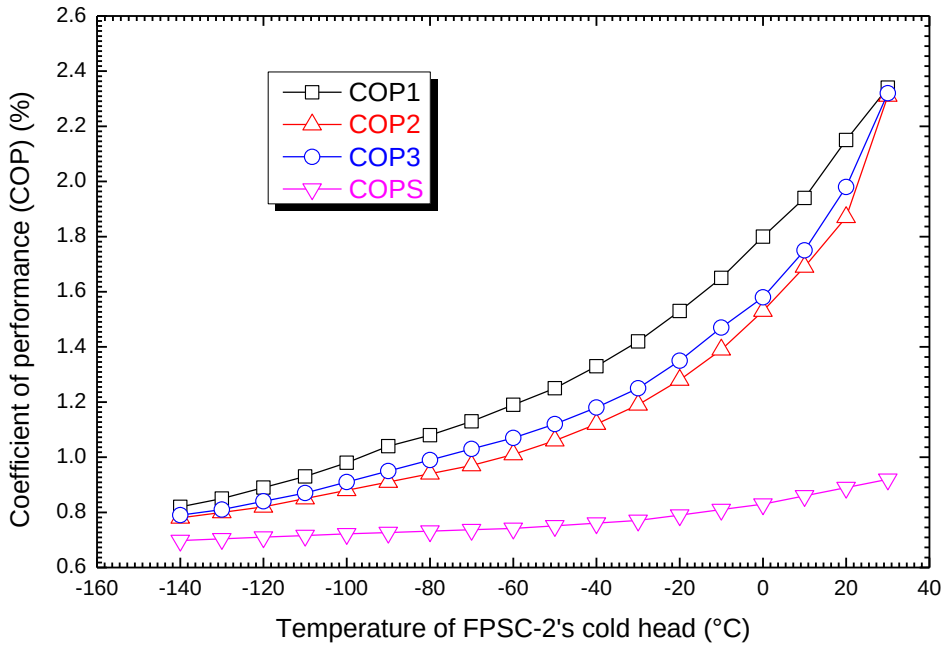

Figure 3-13 COP variation of the FPSCs and system with the root temperature of FPSC-2's cold head (material of cold head is copper; L=180 mm; D=40 mm). COP-1, COP-2, COP-3 and COPS represent the coefficient of performance for FPSC-1, FPSC-2, FPSC-3 and the whole system, respectively.

6. CONCLUSION

In the present work, the theoretical analysis of the working mechanism of FPSC has been conducted in detail. Meanwhile, the COP of the FPSC was numerically deduced. In order to improve the COP of FPSC, the key parameters that affect the COP were also investigated. Based on the experimental results, the conclusions are summarized as follows:

1) From the experiment of the materials, it can be concluded that when the cold head was made by copper, the temperature loss of the cold head was 13.38 ℃ and the COP of FPSC was 0.82 (with the root temperature was -140 ℃). By contrast, the temperature difference for the aluminium cold head was 33.31 ℃, and the COP of FPSC was 0.61. However, it is worth noting that due to the weight of copper is further greater than aluminium. Therefore, the oscillation phenomenon is also dramatic and which would result in a higher energy loss.

2) The length of cold head should be as short as possible to improve the COP of FPSC. When the length of the cold head was set at 270 mm, the temperature difference and COP of FPSC were 15.73 ℃ and 0.59 (with the root temperature is -140 ℃), respectively. When the length was shortened to 180 mm, the temperature difference reduced to 9.92 ℃. Meanwhile, the COP of FPSC increased to 0.82. By contrast, the diameter should be as big as possible to enhance the COP. When the diameter of the cold head was set at 30 mm, the temperature difference was 20.28 ℃ and the COP of FPSC was 0.52 (with the root temperature is -140 ℃). With the diameter thickening to 40 mm, the temperature difference decreased to 15.73 ℃ and the COP of FPSC increased to 0.59.

3) In addition, the ambient temperature also has a significant influence on the COP

of FPSC. When the ambient temperature varied from 8℃ to 28℃, the COP of FPSC reduced from 0.7 to 0.6. Nevertheless, the effect of ambient humidity on the COP is not significant. With the ambient humidity increasing from 20% to 75%, the COP of FPSC varied in the range of 0.62 to 0.68.

4) Although the FPSCs in the system had high COPs, the COP of the system was around 0.70 due to other energy consumption units (such as vacuum pump and control panel). For the future work, the energy penalty of the main units should be avoided and the latent heat associated with frost CO_2 should also be recovered.

REFERENCES

M.R.M. Abu-Zahra, L.H.J. Schneiders, J.P.M. Niederer, P.H.M. Feron, G.F. Versteeg, 2007. CO_2 capture from power plants Part I. A parametric study of the technical performance based on monoethanolamine. International Journal of Greenhouse Gas Control 1, 37-46.

B. Belaissaoui, Y.L. Moullec, D. Willson, E. Favre, 2012. Hybrid membrane cryogenic process for post-combustion CO_2 capture. Journal of Membrane Science 415-416, 424-434.

D.M. Berchowitz, 1992. Free-Piston Stirling Coolers. International Refrigeration Conference Energy Efficiency and New Refrigerants, July, Purdue University.

D.M. Berchowitz, D. Kiikka, B.D. Mennink, 1995. Recent advances in Stirling cycle refrigeration. 19th International Congress on Refrigeration Exhibition. August 20-25, The Hague, The Netherlands.

D. Clodic, M. Younes, 2002. A new method for CO_2 capture: frosting CO_2 at atmospheric pressure. Sixth International Conference on Greenhouse Gas Control Technologies, GHGT6, Kyoto, Japan, 1-4 October, pp.155-160.

L. Dumée, C. Scholes, G. Stevens, S. Kentish, 2012. Purification of aqueous amine solvents used in post combustion CO_2 capture: A review. International Journal of Greenhouse Gas Control 10, 443-455.

O. Ercan Ataera, H. Karabulut, 2005. Thermodynamic analysis of the V-type Stirling-cycle refrigerator. International Journal of Refrigeration 28, 183-189.

C. Gouedard, D. Picq, F. Launay, P.L. Carrette, 2012. Amine degradation in CO_2 capture. I. A review. International Journal of Greenhouse Gas Control 10, 244-270.

IPCC. Summary for policymakers. In: climate change 2007: the physical science basis, contribution of working group i to the fourth assessment report of the intergovernmental panel on climate change. Geneva: World Meteoro-logical Organization/United Nations Environment Program; 2007.

H. Karabulut, 2011. Dynamic analysis of a free piston Stirling engine working with closed and open thermodynamic cycles. Renew Energy 36, 1704-1709.

Z.H. Lee, K.T. Lee, S. Bhatia, A.R. Mohamed, 2012. Post-combustion carbon dioxide capture: Evolution towards utilization of nanomaterials. Renew Sustainable Energy Reviews 16, 2599-2609.

P. Luis, T.V. Gerven, B.V. Bruggen, 2012. Recent developments in membrane-based technologies for CO_2 capture. Progress in Energy and Combustion Science 38, 419-448.

B.D. Mennink, W.J. Goossen, 1995. The free-piston Stirling cooling system improving the energy efficiency of refrigerators. 19th International Congress on Refrigeration Exhibition. August 20-25, The Hague, The Netherlands.

C.F. Song, Y. Kitamura, S.H. Li, K.J. Ogasawara, 2012a. Design of a cryogenic CO_2 capture system based on Stirling coolers. International Journal of Greenhouse Gas Control 7, 107-114.

C.F. Song, Y. Kitamura, S.H. Li, 2012b. Evaluation of Stirling cooler system for cryogenic CO_2 capture. Applied Energy 98, 491-501.

M.J. Tuinier, M. van Sint Annaland, J.A.M. Kuipers, 2011. A novel process for cryogenic CO_2 capture using dynamically operated packed beds—An experimental and numerical study. International Journal of Greenhouse Gas Control 5, 694-701.

P. Versteeg, E.S. Rubin, 2011. A technical and economic assessment of ammonia-based post-combustion CO_2 capture at coal-fired power plants. International Journal of Greenhouse Gas Control 5, 1596-1605.

CHAPTER 4

PARAMETRIC STUDY OF THE CRYOGENIC CO_2 CAPTURE SYSTEM

In previous chapter, a novel desublimation CO_2 capture process has been exploited making use of three free piston Stirling coolers (namely, SC-1, SC-2 and SC-3, respectively). In the present chapter, the novel system was applied on CO_2 capture from post-combustion flue gas and different process parameters (*i.e.* flow rate of feed gas, temperature of Stirling cooler and operating condition) were investigated to obtain the optimal performance (CO_2 recovery and energy consumption). From the extensive experiments, it was concluded that the cryogenic system could realize CO_2 capture without solvent and pressure drop condition. Meanwhile, The optimal conditions for the system are as follows: idle operating time is 240 min, flow rate is 5 L/min, vacuum degree of the interlayer is 2.2×10^3 Pa and temperature of SC-1, 2 and 3 are -30 ℃, -120 ℃ and -120 ℃, respectively. Under these conditions, the energy consumption of the system is around 0.5 $MJ_{electrical}$ /kg CO_2 with above 90 % CO_2 recovery.

1. INTRODUCTION

The emission of huge amounts of industrial CO_2 into the atmosphere has led to the issue of global climate change. The consensus that a complete arrangement to reduce CO_2 release must be implemented as soon as possible has been formed. As a primary alternative to control CO_2 emission, CO_2 capture and storage (CCS) technology has been widely researched. There are three main technologies to capture CO_2 from coal-fired power plants, including: post-combustion, pre-combustion and oxy-combustion (Olajire, 2010; Khoo and Tan, 2006). The post-combustion capture method, in particular, plays an important role in the development of CCS (Puxty, 2009). Since it eliminates the need for substantial modifications to existing combustion processes and facilities it provides an alternative approach for near-term CO_2 capture for new and existing stationary fossil fuel fired power plants (Thiruvenkatachari et al., 2009; Lucquiaud and Gibbins, 2011; Bhown and Freeman, 2011). With the rapid development of capture technologies and their maturity, the requirement of capture efficiency and cost becomes more and more prominent (Rubin and Zhai, 2012). The U.S. Department of Energy (DOE) has set a capture and sequestration target of 90% CO_2 capture from power plants for its development program (Figueroa et al., 2008). In 2011, Clausse et al. also reported that with high CO_2 recovery (above 90%), energy consumption should be reduced as low as possible (around 1 $MJ_{thermal}$ /kg CO_2) (Clausse et al., 2011).

The main reasons for the high cost of capturing CO_2 from power plant flue gas include the following: 1) low concentration of CO_2 in flue gas; The diluted CO_2 in flue gas from gas turbine is typically 3 vol.%, while the CO_2 concentration in the coal combustion process is approximately 13 vol.% (Simmonds et al., 2003). 2) low

pressure of feed gas; Generally, the flue gas is at atmospheric pressure. For coal-fired power plants, the partial pressure of CO_2 is only around 0.13 bar, and it leads to a high energy requirement to sequestrate the CO_2 from flue gas. 3) huge gas flow rates; The enormous flow of flue gas has a high impact on the utilities. At present, a typical 600 MWe coal-fired power plant can emit 500 m^3/s of flue gas containing approximately 13 vol.% CO_2, which amounts to about 11,000 ton CO_2/day (Merkel et al., 2010). Obviously, it is a huge challenge for capture utilities. To make a large reduction in CO_2 emission sources and with a low-cost energy consumption is a significant challenge. Amine based scrubbing has commercial applications as a mature candidate technology, and it has been proven a successful technology to treat industrial flue gas in the last few years (Rao and Rubin, 2002). Nevertheless, some research shows that the energy penalty of the amine process is currently in the range of 3-4 $MJ_{thermal}$ /kg CO_2 (Abu-Zahra et al., 2007; Pellegrini et al., 2010; Belaissaoui et al., 2012; Choi et al., 2011). And in which, the energy consumption of compression unit for transport is approximately 0.5-1 $MJ_{thermal}$ /kg CO_2 (Posch and Haider, 2012). Therefore, the energy cost for amine CO_2 capture process without compression section is around 2-3.5 $MJ_{thermal}$ /kg CO_2. This cost and energy investment is mainly due to the necessary input of thermal energy for the regeneration of the solvent in the traditional chemical absorption process (Adams and Davison, 2007; Klara, 2007; Echeverri and Hoppock, 2012).

Cryogenic capture process has significant potential to become a low energy cost solution for CO_2 capture from flue gas, since it avoids the requirement of solvents and pressure drop. In recent years, cryogenic CO_2 capture technology using the liquid nitrogen (LN_2) and liquefied natural gas (LNG) evaporation process has attracted interest (Clodic and Younes, 2002; Tuinier et al., 2011; Lively et al., 2012). However,

there are still some areas in need of improvement. Such as: 1) the frosted CO_2 on heat exchanger surfaces would adversely affect heat transfer and reduce capture efficiency in the process developed by Clodic et al. in 2004. 2) An important quality concerning coolers is the coefficient of performance (COP). It is defined as the ratio of the cooling capacity and the input power of the system. The COP of the process exploited by Tuiniers et al. is around 0.5, and it is relatively low. Free piston Stirling cooler (SC) has attracted the interest of researchers due to its specific advantages. The working fluid of SC can be air, helium or hydrogen, which have zero ozone depletion potential in contrast to conventional refrigerants such as CFCs, HCFCs and HFCs. In an ideal case, the Stirling cycle is reversible which means that heat can be put into the machine and electric power will be produced or as with the SC, electric power can be put in and heat will be removed. Another advantage is that the SC can be utilized within a wide temperature range (-120 ℃ to +70 ℃ of the cold head) and the COP can reach higher than 2.5 at low heat loads (Oguz and Ozkadi, 2002).

Based on the above discussion, a concept of cryogenic CO_2 capture technology based on SCs has been constructed. In this chapter, this novel desublimation process is experimentally validated in detail. The objective of our work is to investigate the influence of process parameters on the capture performance. The effect of operating conditions (*i.e.* ambient temperature and humidity, vacuum degree of the interlayer, idle operating time of the system, temperature of SC-1 and flow rate of flue gas) are discussed and the feasible operating condition of the system is also estimated.

The structure of this chapter is as follows. Section 2 describes the base case of cryogenic CO_2 capture process in brief. Section 3 simulates the detailed mass and heat transfer process in the cryogenic system. Section 4 introduces the key parameters that influence the capture performance of the system. Section 5 describes the materials

used in the system and the experimental conditions. Section 6 investigates the influence of the selected parameters on the capture efficiency. Section 7 summarizes the main conclusions in this chapter.

2. PROCESS DESCRIPTION

The schematic of the cryogenic process based on SCs is described in Figure 4-1. In the process, the feed gas is separated into three flows: condensate water, dry ice and residual gas. At the first step, the water in flue gas condenses in the pre-cool process by SC-1 and then moves through the condensing pipe to the outlet to avoid plugging the vessel, which is the key issue of cryogenic separation technologies. Meanwhile, the other gas flows into the main freezing tower, at atmospheric pressure and the cryogenic temperature, CO_2 gas anti-sublimates into solid form. At last, the solid CO_2 frosts onto the heat exchanger of SC-2, and by spinning the scraping rod on the heat exchanger of SC-2, it falls down to the storage column, where SC-3 provides a cryogenic condition for storage. On the other hand, residual gas exhausts from the gas outlet. Finally, the cold energy of sweep gas is recovered by a heat exchanger with the subsequent flue gas.

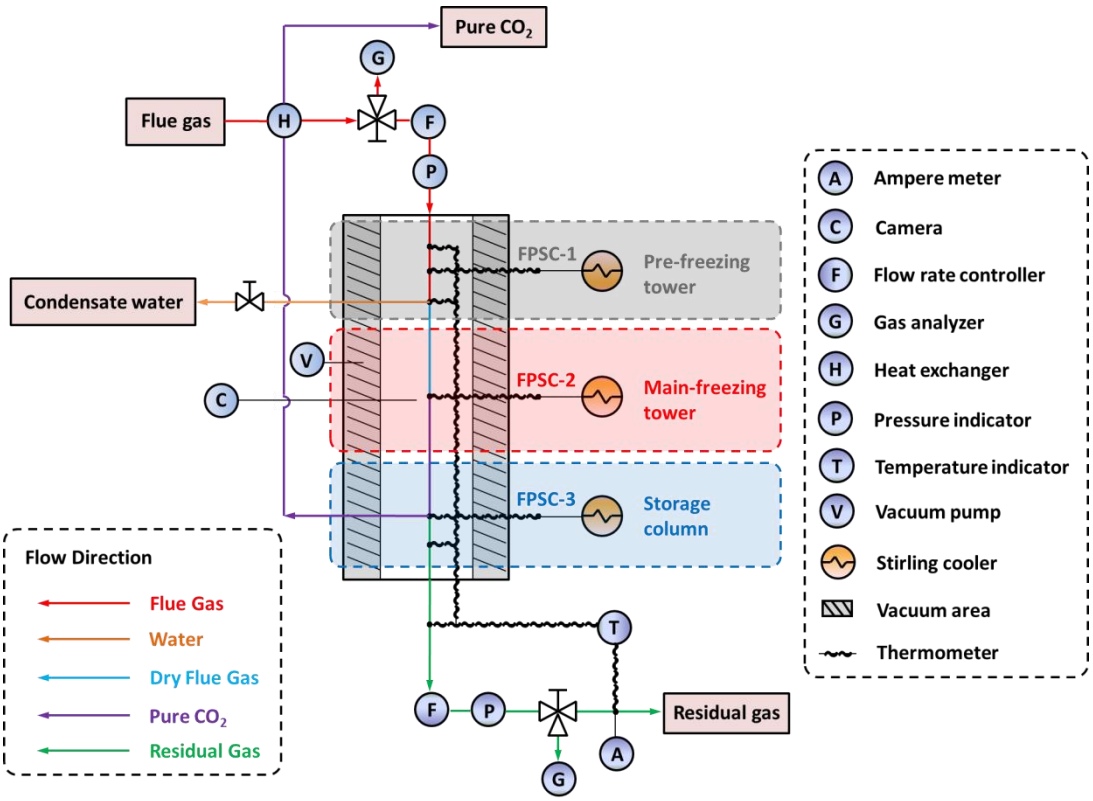

Figure 4-1 Schematic diagram of the whole capture process

3. SIMULATION WORK

In order to deepen the understanding of capture characteristic and improve the capture efficiency, the CO_2 frost formation process was simulated in this section. The process was described by a numerical model. The frost formation process involves simultaneous heat and mass transfer during varying thermo physical properties. To simplify the complex process, some assumptions were employed: 1) Frost layer distribution is homogeneous over the cooling fin; 2) The frosting process takes place at a quasi-steady state; 3) Frost thermal conductivity of the frost layer varies only with frost density; 4) Radiation heat transfer between flue gas and frost layer is negligible. The structure in the main freezing tower and the direction of airflow has been described in Figure 4-2(a), and the temperature distribution in the main freezing tower has been simulated in Figure 4-2(b). The detail description of the simulation process can be found in the previous work (Song et al., 2012a).

3.1 Energy balance

The heat transfer from influent gas stream to the frost layer contains two parts: sensible (Q_{sen}) and latent heat (Q_{lat}). The latent heat (Q_{lat}) represents the energy due to sublimation of deposited CO_2 at the frost surface. According to the research of Fossa and Tanda, latent heat can be defined as:

$$Q_{lat} = 2.88 \times 10^6 - 195 T_f \qquad (4\text{-}1)$$

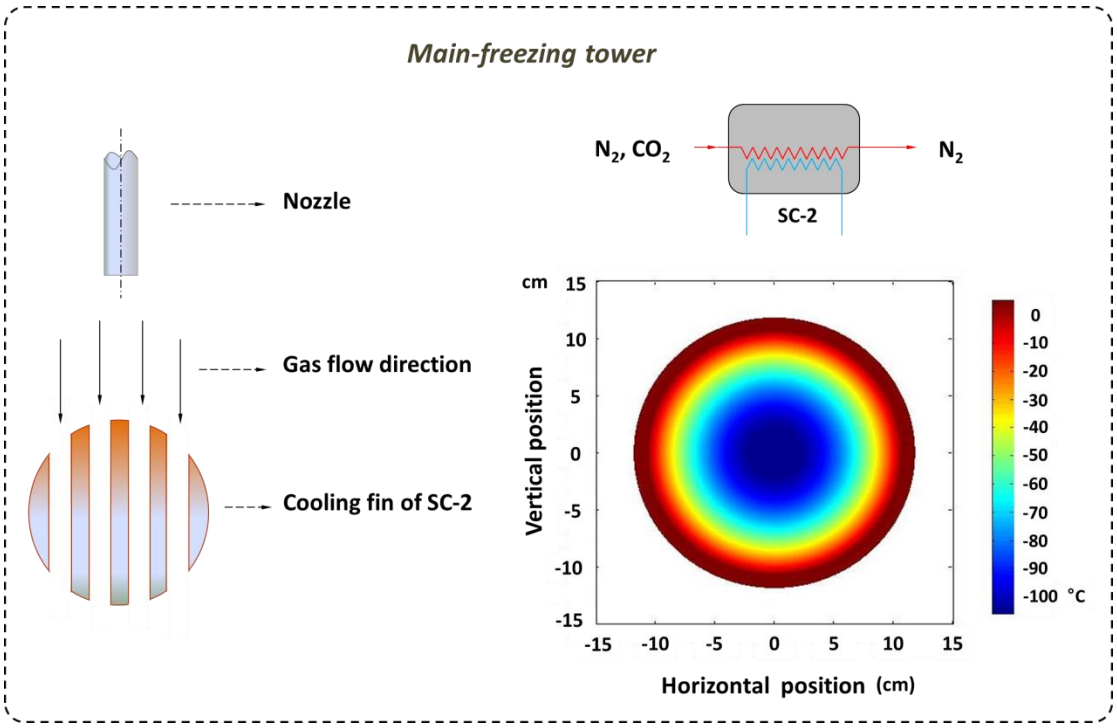

(a) (b)

Figure 4-2 The structure and temperature distribution in the main freezing tower.

Besides the latent heat transfer, sensible heat is another important part of energy transmission. It is defined as the energy transferred from the gas phase to the frost layer, and can be calculated as follows:

$$Q_{sen} = Q_c + Q_p \tag{4-2}$$

where Q_c represents the energy by convection heat transmission and can be obtained according to the following equation:

$$Q_c = h_c \cdot (T_g - T_f) \tag{4-3}$$

$$h_c = \left| h_{nc}^{\ 3} + h_{fc}^{\ 3} \right|^{1/3} \tag{4-4}$$

where h_c is the heat transfer coefficient of convection. T_g and T_f are the temperature of gas phase and frost layer, respectively. In addition, the empirical equations to calculate the heat transfer coefficient of natural convection (h_{nc}) and forced convection (h_{fc}) have been introduced by Cengel in 2003:

$$h_{nc} = \frac{Nu_{nc} \cdot k_g}{L} = \left\{ 0.825 + \frac{0.387 Ra^{1/6}}{\left[1 + (0.492/Pr)^{9/16} \right]^{8/27}} \right\}^2 \tag{4-5}$$

$$h_{fc} = \frac{Nu_{fc} \cdot k_g}{W} = 0.3 + \frac{0.62 Re^{2/3} Pr^{1/3}}{\left[1 + (0.4/Pr)^{2/3} \right]^{1/4}} \left[1 + \left(\frac{Re}{282000} \right)^{5/8} \right]^{4/5} \tag{4-6}$$

here k_g is the thermal conductivity of the gas stream. L and W are the length and width of the cooling fin of the heat exchanger. Nu, Pr, Ra and Re are the Nusselt number, Prandtl number, Rayleigh number and Reynolds number, respectively. In contrast, the heat transfer caused by phase change (Q_p) is expressed as follows (Kim et al., 2009):

$$Q_p = h_m \cdot (\rho_f - \rho_g) \cdot Q_{lat} \tag{4-7}$$

here h_m is the mass transfer coefficient. ρ_f and ρ_g are the density of the frost layer and gas phase, respectively. The mass transfer coefficient (h_m) and can by calculated as

follows:

$$h_m = \frac{h_c}{\rho \cdot c_p \cdot Le^{2/3}} \tag{4-8}$$

where ρ and c_p are the density and the specific heat at constant air pressure. *Le* is the Lewis number. In addition, the frost density (ρ_f) is the function of frost thickness (Ogunbameru et al., 1973):

$$\rho_f = -\frac{\ln(GI / I_0)}{\mu_m \cdot \delta_f} \tag{4-9}$$

From the above, the energy balance of the desublimation process is the sum of the sensible (Q_{sen}) and latent heat (Q_{lat}), and can be expressed by Eq. (4-10):

$$Q = Q_{sen} + Q_{lat} \tag{4-10}$$

3.2 Mass balance

The desublimation of CO_2 on the frost layer (m_f) can also be divided into two parts: first, part of the CO_2 deposits on the surface of the frost layer, which increases the frost layer thickness (m_t). Second, part of the CO_2 diffuses in the frost layer and increases the density of the frost layer (m_d). Therefore, the mass balance of the capture process can be described as follows:

$$m_f = m_t + m_d \tag{4-11}$$

the m_t and m_d can be calculated by Eq.(4-12) and (4-13)

$$m_t = \rho_f \frac{d\delta_f}{dt} \tag{4-12}$$

$$m_d = \delta_f \frac{d\rho_f}{dt} \tag{4-13}$$

Here, σ_f is the thickness of the frost layer. It has been described by Qu et al. in 2006:

$$\delta_f = \frac{k_f (T_f - T_g)}{Q_p} \tag{4-14}$$

In addition, the detailed equations for solution of the heat and mass transfer process have been described in our previous work (Song et al., 2012b).

4. PARAMETERS STUDY

The key process parameters that influence the capture performance are: flow rate, temperature of SC-1, operating time and vacuum condition.

Flow rate of gas stream (v). From the description of the system, it can be seen that the optimum area for CO_2 frost is limited. Thus, the research on the flow rate is beneficial to find the optimum capture condition.

Temperature of SC-1 (T). CO_2 capture is realized by cryogenic CO_2 capture technology based on the principle of temperature variation. Temperature is considered as a process parameter according to this essence. It should be noted that due to the different function of SCs, the temperature of SC-2 and SC-3 must operate at the minimum thresholds to separate and store CO_2.

Operating time (t). It is obvious that the developed cryogenic process is based on the consumption of electrical energy. Therefore, operating time is critical parameter to determine capture efficiency. Meanwhile, it needs to be pointed out that operating time (t) of the whole process can be divided into two parts, idle operating time (t_1) and capture time (t_2). Since the capture time (t_2) is a constant for different experiment in this research, idle operating time (t_1) is set as the parameters that affect capture performance.

Vacuum condition (Pa). It is noteworthy that there is an interlayer between tower wall and capture column. Due to large temperature difference between the

inside and outside, the vacuum degree in the interlayer is an important factor that affects heat loss and capture performance.

In addition, the performance of the whole capture process is represented by CO_2 recovery and energy consumption.

CO_2 recovery (η). As an important parameter to measure the efficiency of capture process, CO_2 recovery has been investigated widely in various CO_2 capture process. In this research, it also is selected as a representation of performance.

Energy consumption (EC). This parameter is an essential element for each CO_2 capture technologies. It is one of the central concerns for the capture process and the key issue needs to be improved. For this reason, energy consumption is identified as another dependent factor.

5. EXPERIMENTAL SECTION

5.1 Materials

The thermal insulation material used in the system is foam foil insulation sheet. The out and middle layer are aluminium foil and Expand Aple Poly Ephylene (EPE), respectively. The cold head of SCs are made by pure copper (Tanabe Engineering Ltd, Japan). In addition, the flue gas of post-combustion was simulated by synthetic gas mixture (N_2 82 vol.%, CO_2 13 vol.% and H_2O 5 vol.%). It is noted that no pollutants in the flue gas such as SO_x and NO_x were assumed. The temperature of the simulated flue gas is 50 ℃.

5.2 Methods

The experiments are based on four parameters. These are the vacuum degree of the interlayer, idle operating time, flow rate of influent gas and temperature of SC-1. For the vacuum degree experiment, the value is set as 1.0×10^5 Pa (without the vacuum pump), 2.5×10^3 Pa and 2.2×10^1 Pa, respectively. Simultaneously, the other conditions remained unchanged (The temperature of SC-1, 2 and 3 are set at -60 ℃, -120 ℃ and -120 ℃; idle operating time is 180 min; flow rate is 2 L/min.). For the experiment of idle operating time, the value is set at 120 min, 180 min, 240 min, 300 min and 360 min, respectively. Unaltered conditions are as follows: temperature of SC-1, 2 and 3 are -60 ℃, -120 ℃ and -120 ℃; vacuum degree of interlayer is 2.5×10^3 Pa; flow rate is 2 L/min. For the temperature test of SC-1, the variation range is between -60 to -20 ℃. Meanwhile, the vacuum degree of interlayer is set at 2.5×10^3 Pa. The idle operating time of the system is 240 min. The temperature of SC-2 and 3 both are -120 ℃. The flow rate of gas stream is 5 L/min. For the experiment of flow rate, it varied from 1 to 6 L/min with other conditions as constant (vacuum degree is 2.5×10^3 Pa; idle operating time is 240 min; temperature of SC-1, 2 and 3 are -30 ℃, -120 ℃, -120 ℃, respectively).

6. RESULTS AND DISCUSSION

6.1 The influence of ambient condition

The ambient condition considered in this work mainly contains: ambient temperature and humidity. The effect of ambient temperature on the temperature variation of SC-2's cold head is depicted in Figure 4-3. The result demonstrates that the temperature of SC-2's cold head decreases with the ambient. That is because the

cryogenic principle of Stirling cooler is based on heat transfer. Consequently, a low ambient temperature is in favor of generating large temperature difference, and then convenient for heat transfer from inside of the system to the outside. The relation between the ambient humidity and the temperature of the cold head of SC-2 is shown in Figure 4-4. Due to the distribution of humidity of the experimental data is uniform, it can be concluded that its influence of on the temperature of SC-2 is weak.

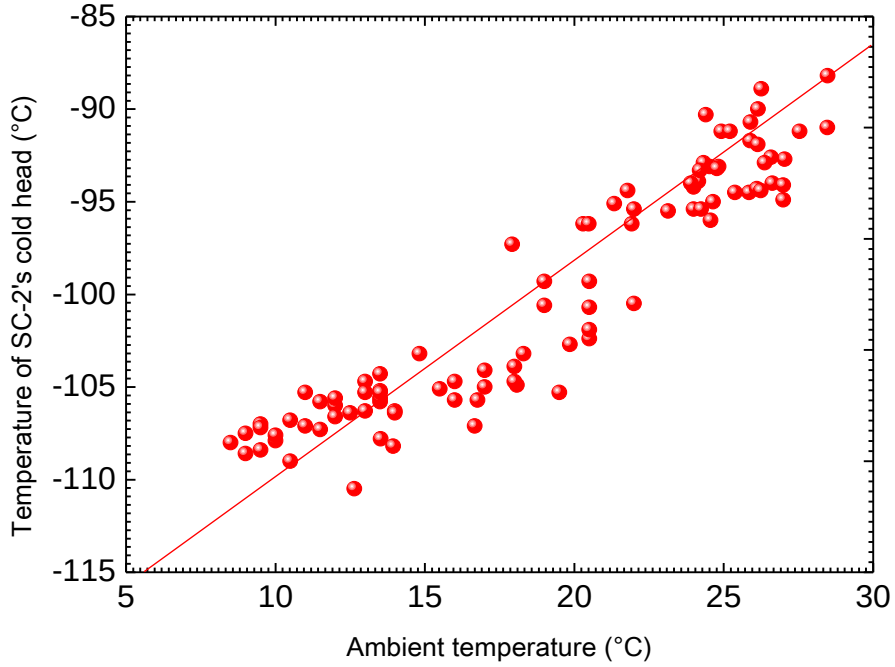

Figure 4-3 Effect of ambient temperature on the temperature variation of SC-2' cold head.

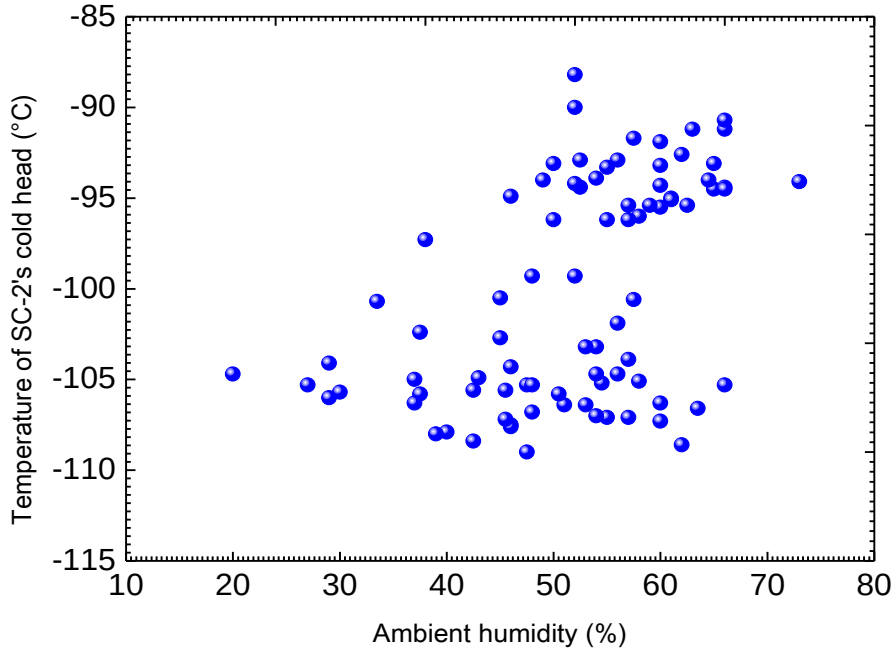

Figure 4-4 Effect of ambient humidity on the temperature variation of SC-2' cold head

.

6.2 The influence of the vacuum condition

In order to investigate the influence of the interlayer on the temperature variation process, an experiment on the vacuum degree of the interlayer was carried out as well as the parameters (CO_2 recovery and energy consumption) used for evaluating capture performance. It should be pointed out that the energy consumption in this work only considered the capture process. The compression energy for transport was not considered. The calculation of the parameters used the following equations:

$$CO_2\ recovery\ (\eta) = 1 - \frac{v_{out}\omega_{CO_2,out}}{v_{in}\omega_{CO_2,in}} \qquad [\%] \qquad (4\text{-}15)$$

$$Energy\ consumption\ (EC) = \frac{\int_0^{(t_1+t_2)} UIdt}{(v_{in}\omega_{CO_2,in} - v_{out}\omega_{CO_2,out})\rho_{CO_2}t_2} \qquad [MJ/kg\ \ CO_2] \qquad (4\text{-}16)$$

where v is the flow rate of the gas stream. ω is the percentage of CO_2 in flue gas. ρ is the density of frosted CO_2. t_1 and t_2 represent the idle operating time and capture time, respectively. U and I are the voltage and current during the experiment period. When the flow rate is 5 L/min, the U and I of the system are 94.1 V and 5.4 A, respectively.

The characteristic of the vacuum pump is listed in Table 4-1. The effect of the vacuum condition on temperature variation in the system is shown in Table 4-2 and 4-3. It indicates that when the vacuum degree of the interlayer is 2.2×10^1 Pa, the temperature of the cold head of SC-1, gas cooling tube and water condensing tube is the lowest among the three different vacuum degrees. That can be explained by the fact that the vacuum interlayer is in favor of heat transfer. Consequently, when the vacuum degree of the interlayer is low (2.2×10^1 Pa), the inside of the tower can be maintained at a lower temperature than the other conditions (1.0×10^5 and 2.5×10^3 Pa). The effect of the vacuum condition on the capture performance (CO_2 recovery and energy consumption) is shown in Figure 4-5 and 4-6. One-way ANOVA results for CO_2 recovery, 1.0×10^5 Pa ($P=0.425>0.05$) and 2.2×10^1 Pa ($P=0.444>0.05$) have no

significant difference compared to 2.5×10^3 Pa. With respect to energy consumption, 1.0×10^5 Pa (P=0.000<0.05) and 2.2×10^1 Pa (P=0.000<0.05) both have significant difference compared to 2.5×10^3 Pa. As previously discussed, it can also be seen that with the vacuum degree dropping, the temperature in the pre-freezing tower decreased rapidly. However, this does not mean the lower temperature is better. Although the vacuum degree of 2.2×10^1 Pa the temperature of the pre-freezing part is slightly lower than the other conditions, the capture performance (CO_2 recovery and energy consumption) reduces significantly. That is because the energy penalty of keeping a vacuum condition increases with the reduction of vacuum degree.

6.3 The influence of the idle operating time

Investigation of the idle operating time for the system is necessary for the purpose of energy conservation. According to the different operating purpose, the operating time (t) of the whole process can be divided into two parts: idle operating time (t_1) and capture time (t_2). The function of the idle operating section is to allow the cooler to reach the cryogenic condition to solidify CO_2, and there is no heat load in this period. After the temperature is low enough, the process is switched to capture mode and flue gas is introduced into the system. In this research, the idle operating time (t_1) is tested on 5 levels, and has been introduced in the experimental design section. Meanwhile, the capture time (t_2) is always controlled as 60 min.

Table 4-1 Specification of the vacuum pump.

Power (W)	400 (4 pole)	
Frequency (Hz)	50	60
Voltage (V)	100/200	100/200
Current (A)	6.8/3.4	6.0/3.0
RPM (r/min)	1420	1720

Table 4-2 Experimental condition of the vacuum degree of the interlayer in the tower.

Experiments	Pressure (Pa)
$1^{\#}$ (without ⓥ*)	1.0×10^{5}
$2^{\#}$	2.5×10^{3}
$3^{\#}$	2.2×10^{1}

* ⓥ represents the vacuum pump.

Table 4-3 Effect of vacuum condition on the variation of temperature in the system*.

	Temperature (℃)				
Experiments	Cold head of SC-1	Gas cooling tube	Water condensing tube	Cooling fin of SC-2	Storage column
$1^{\#}$	-23.29	11.79	13.68	-99.3	-82.38
$2^{\#}$	-28.31	1.40	4.23	-101.9	-83.35
$3^{\#}$	-31.75	0.03	2.82	-100.6	-82.42

* The temperature of SCs is set as (SC-1: -60 ℃; SC-2: -120 ℃; SC-3: -120 ℃). The operating time is 180 min.

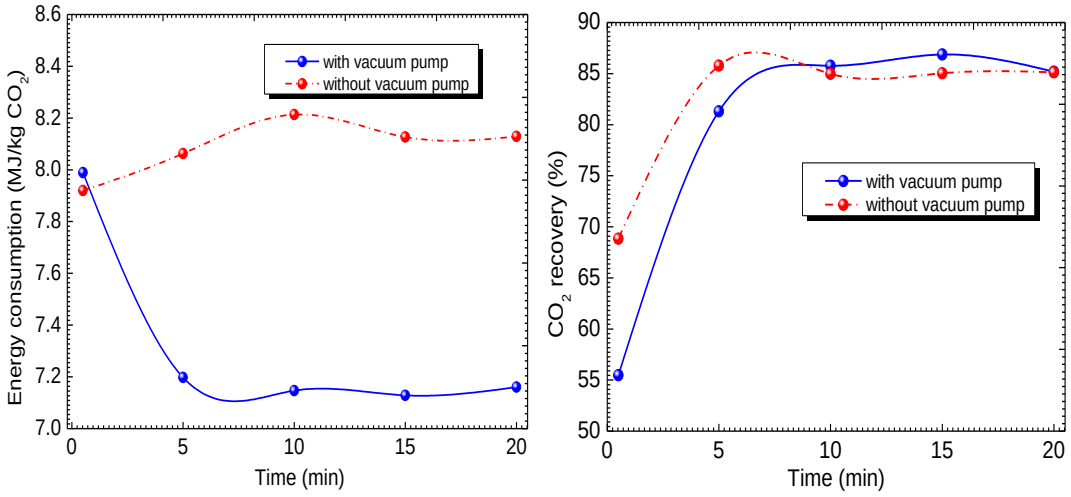

(a) (b)

Figure 4-5 The variation of energy consumption (EC) (a) and CO_2 capture efficiency (η) (b) with the conjunction of a vacuum pump and without a vacuum pump(T_{sc-1}= -60 ℃; T_{sc-2}= -120 ℃; T_{sc-3}= -90 ℃; v_{in}=1.5 L/min).

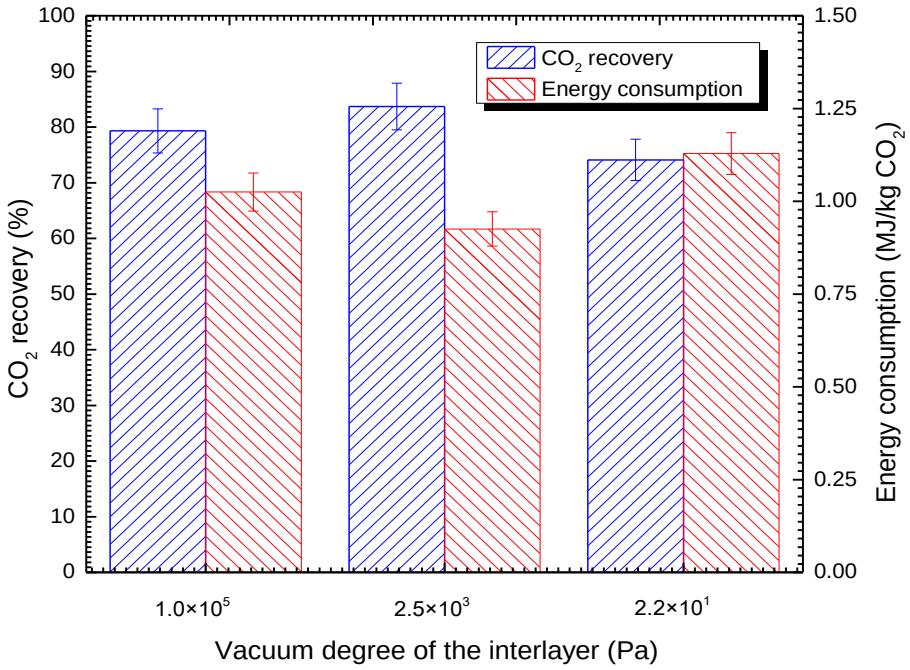

Figure 4-6 Effect of vacuum condition on CO_2 recovery (%) and energy consumption (MJ/kg CO_2) (v= 2 L/min; T_{SC-1}= -60 ℃; T_{SC-2}= -120 ℃; T_{SC-3}= -120 ℃)

The influence of idle operating time on temperature variation in the system is shown in Table 4-4. As time passes, the temperature of the main parts in the system gradually decreases. The effect of the idle operating time on the CO_2 capture performance was statistically analyzed using one-way ANOVA. The experiment results are listed in Figure 4-7. For CO_2 recovery, 180 min ($P=0.000<0.05$), 200 min ($P=0.000<0.05$), 240 min ($P=0.005<0.05$) and 300 min ($P=0.017<0.05$) have a significant difference compared to 360 min. With respect to energy consumption, there is a very significant difference for 180 min ($P=0.000<0.05$) and 200 min ($P=0.000<0.05$) compared to 360 min; but for 240 min ($P=0.418>0.05$) and 300 min ($P=0.532>0.05$) both are not significant. Therefore, for the aim of reducing the cost of avoided CO_2 (with 90% CO_2 recovery), 240 min is considered as the optimum operating time in future experiments.

Table 4-4 Effect of idle operating time on the variation of temperature in the system*.

Experiments	Temperature (℃)				
	Cold head of SC-1	Gas cooling tube	Water condensing tube	Cooling fin of SC-2	Storage column
120 min	-25.99	4.64	6.63	-99.3	-73.72
180 min	-31.75	0.03	2.82	-100.6	-82.42
240 min	-31.62	0.44	3.48	-100.5	-85.95
300 min	-39.23	-7.04	-3.60	-103.9	-89.29
360 min	-40.10	-7.76	-3.97	-105.3	-88.49

* The temperature of SCs is set as (SC-1: -60 ℃; SC-2: -120 ℃; SC-3: -120 ℃) with the vacuum degree of 2.2×10^{1} Pa.

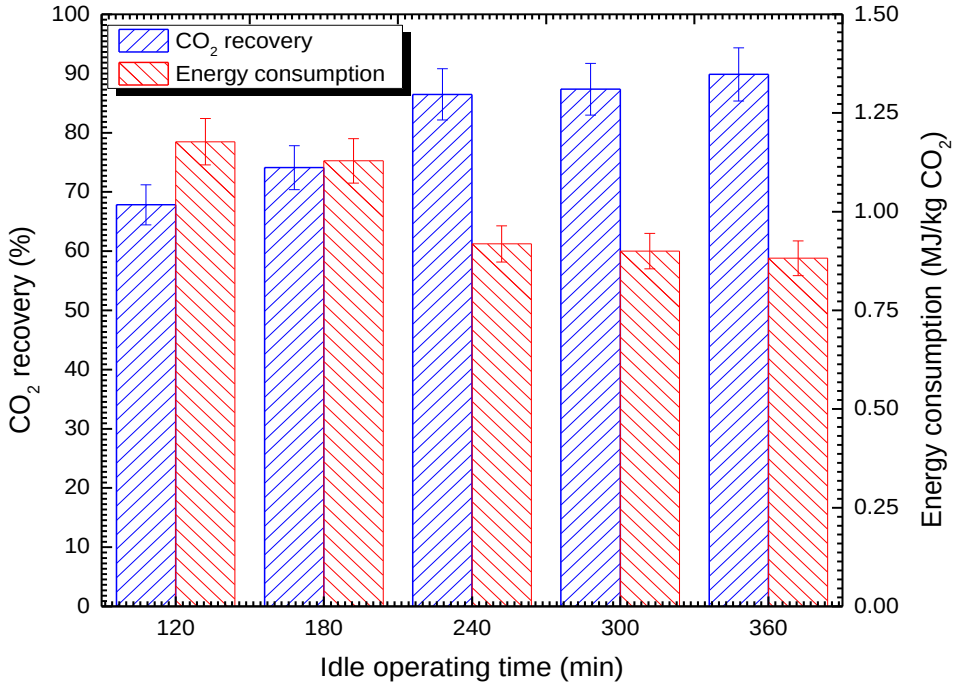

Figure 4-7 Effect of idle operating time on CO_2 recovery (%) and energy consumption (MJ/kg CO_2). Experimental conditions are: flow rate of gas stream is 2 L/min; vacuum degree of the interlayer is 2.5×10^3 Pa; the temperature of SC-1 is -60 ℃; the temperature of SC-2 is -120 ℃; the temperature of SC-3 is -120 ℃.

6.4 The influence of the temperature of SC-1

The anti-sublimation system was operated under a different temperature threshold for SC-1. Its influence on CO_2 recovery and energy consumption is shown in Figure 4-8. Meanwhile, the one-way ANOVA statistical analysis was carried out to investigate the influence. With respect to CO_2 recovery, -30 ℃ (P=0.093>0.05), -40 ℃ (P=0.080>0.05), -50 ℃ (P=0.152>0.05) and -60 ℃ (P=0.832>0.05) showed no significant difference compared to -20 ℃. For energy consumption, -30 ℃ (P=0.151>0.05) showed no significant difference compared with -20 ℃. By contrast, a difference of -40 ℃ (P=0.002>0.05), -50 ℃ (P=0.000>0.05) and -60 ℃ (P=0.000>0.05) is very significant. It can be concluded that the high temperature of SC-1 results in more efficient CO_2 capture. Meanwhile, it needs to be noted that the temperature of SC-1 does not indicate that higher is best. That is because one of the functions of the pre-freezing tower is dehydration and its temperature depends on SC-1. Therefore, the temperature of the water condensing tube should be maintained under the frost point (0 ℃).

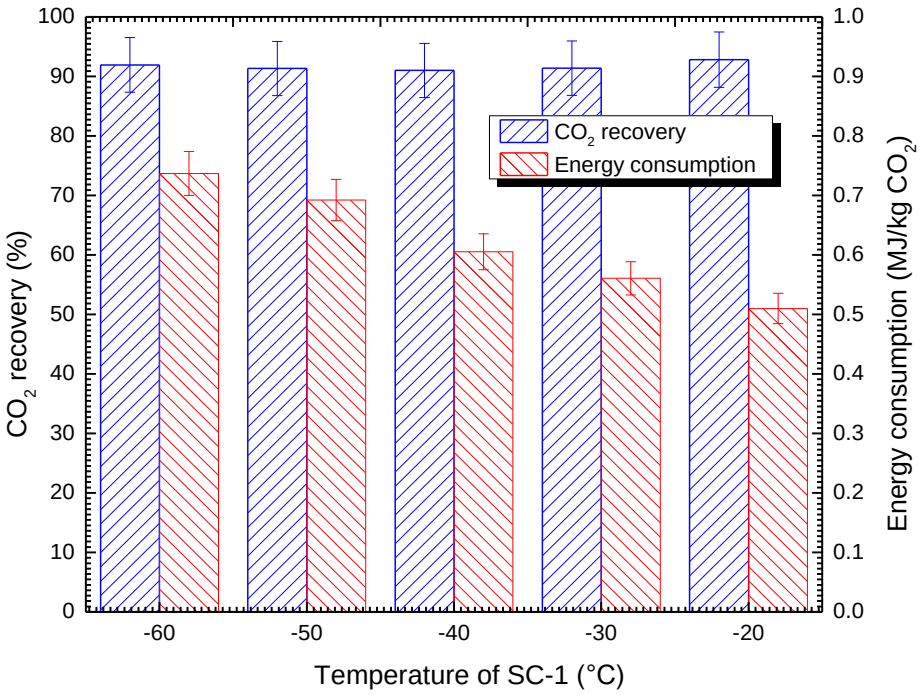

Figure 4-8 Effect of temperature of SC-1 on CO_2 recovery (%) and energy consumption (MJ/kg CO_2). The unaltered conditions of the experiments are: the flow rate of gas stream is 5 L/min; vacuum degree of the interlayer is 2.5×10^3 Pa; the idle operating time of the system is 240 min; the temperature of SC-2 is -120 ℃; the temperature of SC-3 is -120 ℃.

6.5 The influence of the flow rate of flue gas

The effect of the flow rate of flue gas on the performance of the system is summarized in Figure 4-9. At a low flow rate, the energy requirement for capturing per CO_2 unit was high. With increasing flow rate, the energy consumption per kg CO_2 removed declined. When the flow rate was set at 5 L/min, the energy consumption is around 0.5 $MJ_{electrical}$ /kg CO_2 with above 90% CO_2 recovery. Compared to the condition of 1 L/min, the recovery efficiency is increased 9% with a saving of 1.08 MJ to capture per kilogram CO_2. A one-way ANOVA test was also undertaken to assess significance. The test results showed that for CO_2 recovery, 1 L/min ($P=0.001<0.05$), 2 L/min ($P=0.000<0.05$), 3 L/min ($P=0.000<0.05$), 4 L/min ($P=0.000<0.05$) and 6 L/min ($P=0.000<0.05$) show significant difference compared to 5 L/min. For energy consumption, 1 L/min ($P=0.000<0.05$), 2 L/min ($P=0.000<0.05$), 3 L/min ($P=0.008<0.05$), 4 L/min ($P=0.013<0.05$) and 6 L/min ($P=0.007<0.05$) also show significant difference compared to 5L/min. It needs to be pointed out that when the flow rate was set at 6 L/min, the CO_2 recovery decreased 13.60% and simultaneously energy consumption increased 27.48% compared to 5 L/min. That is because that although the flue gas can also flow via the cooling fin, it is too fast for most of it to undergo the frosting process. Therefore, the capture efficiency decreases in this case.

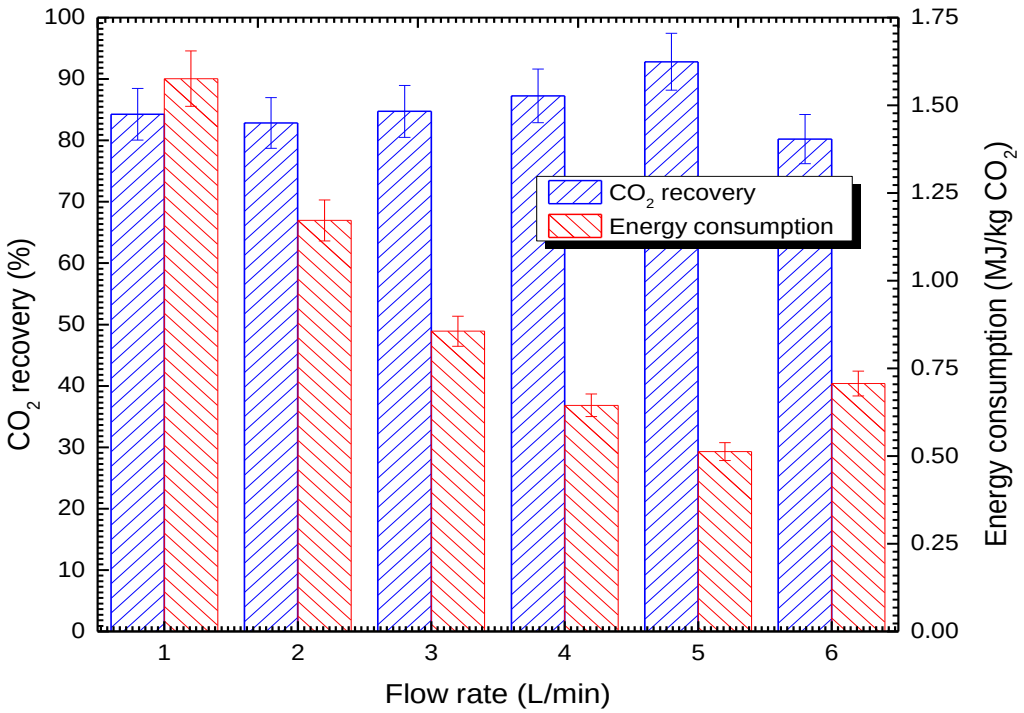

Figure 4-9 Effect of flow rate on CO_2 recovery (%) and energy consumption (MJ/kg CO_2). The experiment was carried out under the identical conditions. The vacuum degree of the interlayer is 2.5×10^3 Pa; the idle operating time of the system is 240 min; the temperature of SC-1 is -30 ℃; the temperature of SC-2 is -120 ℃; the temperature of SC-3 is -120 ℃.

7. CONCLUSION

In summary, the key parameters that affect capture performance were experimentally investigated in this chapter. Through the experiments of process parameters, it was found that the optimal conditions for the system were: idle operating time before gas inflow of 240 min, flow rate of 5 L/min, temperature of SC-1 of -30 ℃ and a vacuum degree 2.2×10^3 Pa (other conditions: temperature of SC-2 and 3 are both set as -120 ℃). Under these conditions, the EC of the system is around 0.5 $MJ_{electrical}$ /kg CO_2 with above 90% CO_2 recovery. In addition, for further improvement of capture performance, the latent heat of condensate water should be recovered.

REFERENCES

A.A. Olajire, 2010. CO_2 capture and separation technologies for end-of-pipe applications-A review. Energy 35(6), 2610–2628.

H.H. Khoo, R.B.H. Tan, 2006. Life Cycle Investigation of CO_2 Recovery and Sequestration. Environmental Science & Technology 40 (12), 4016–4024.

G. Puxty, R. Rowland, A. Allport, Q. Yang, M. Bown, R. Burns, M. Maeder, M. Attalla, 2009. Carbon Dioxide Postcombustion Capture: A Novel Screening Study of the Carbon Dioxide Absorption Performance of 76 Amines. Environmental Science & Technology 43 (16), 6427-6433.

R. Thiruvenkatachari, S. Su, H. An, X.X. Yu, 2009. Post combustion CO_2 capture by carbon fibre monolithic adsorbents. Progress in Energy and Combustion Science 35 (5), 438-455.

M. Lucquiaud, J. Gibbins, 2011. Effective retrofitting of post-combustion CO_2 capture to coal-fired power plants and insensitivity of CO_2 abatement costs to base plant efficiency. International Journal of Greenhouse Gas Control 5(3), 427-438.

A.S. Bhown, B.C. Freeman. 2011. Analysis and Status of Post-Combustion Carbon Dioxide Capture Technologies. Environmental Science & Technology 45 (20), 8624-8632.

E.S. Rubin, H. Zhai, 2012. The Cost of Carbon Capture and Storage for Natural Gas Combined Cycle Power Plants. Environmental Science & Technology 46 (6), 3076–3084.

J.D. Figueroa, T. Fout, S. Plasynski, H. McIlvried, R.D. Srivastava, 2008. Advances in CO_2 capture technology - the U.S. Department of Energy's Carbon Sequestration program. International Journal of Greenhouse Gas Control 2 (1), 9-20.

M. Clausse, J. Merel, F. Meunier, 2011. Numerical parametric study on CO_2 capture by indirect thermal swing adsorption. International Journal of Greenhouse Gas Control 5 (5), 1206-1213.

M. Simmonds, P. Hurst, M.B. Wilkinson, S. Reddy, S. Khambaty, 2003. Amine based CO_2 capture from gas turbine. In: Klara, S. (Ed.), Second Annual Conference on Carbon Sequestration. USDOE, Alexandria, VA, pp. 1-10.

T.C. Merkel, H. Lin, X. Wei, R. Baker, 2010. Power plant post-combustion carbon dioxide capture: an opportunity for membranes. Journal of Membrane Science 359 (1-2), 126-139.

A.B. Rao, E.S. Rubin, 2002. A Technical, Economic, and Environmental Assessment of Amine-Based CO_2 Capture Technology for Power Plant Greenhouse Gas Control. Environmental Science & Technology 36 (20), 4467-4475.

M.R.M. Abu-Zahra, J.P.M. Niederer, P.H.M. Feron, G.F. Versteeg, 2007. CO_2 capture from power plants Part II. A parametric study of economical performance based in mono-ethanolamine. International Journal of Greenhouse Gas Control 1 (2), 135–42.

G. Pellegrini, R. Strube, G. Manfrida, 2010. Comparative study of chemical absorbents in postcombustion CO_2 capture. Energy 35 (2), 851–857.

B. Belaissaoui, G. Cabot, M.S. Cabot, D. Willson, E. Favre, 2012. An energetic analysis of CO_2 capture on a gas turbine combining flue gas recirculation and membrane separation. Energy 38 (1), 167–175.

S. Choi, J.H. Drese, P.M. Eisenberger, C.W. Jones, 2011, Application of Amine-Tethered Solid Sorbents for Direct CO_2 Capture from the Ambient Air. Environmental Science & Technology 45 (6), 2420–2427.

S. Posch, M. Haider, 2012. Optimization of CO_2 compression and purification units (CO_2CPU) for CCS power plants. Fuel 101, 254–263.

D. Adams, J. Davison, Capturing CO_2, International Energy Agency Greenhouse Gas R&D Programme. 2007.

J.M. Klara, Cost and Performance Baseline for Fossil Energy Plants, vol. 1. Bituminous Coal and Natural Gas to Electricity. 2007.

D.P. Echeverri, D.C. Hoppock, 2012. Reducing the Energy Penalty Costs of Postcombustion CCS Systems with Amine-Storage. Environmental Science & Technology 46 (2), 1243–1252.

D. Clodic, M. Younes, A new method for CO_2 capture: frosting CO_2 at atmospheric pressure. Sixth International Conference on Greenhouse Gas Control Technologies, GHGT6, Kyoto, Japan, 2002, 1-4 October, pp.155–160, [CD ROM].

M.J. Tuinier, M. van Sint Annaland, J.A.M. Kuipers, 2011. A novel process for cryogenic CO_2 capture using dynamically operated packed beds—An experimental and numerical study. International Journal of Greenhouse Gas Control 5 (4), 694–701.

R.P. Lively, W.J. Korosand, J.R. Johnson, 2012. Enhanced cryogenic CO_2 capture using dynamically operated low-cost fiber beds. Chemical Engineering Science 71, 97–103.

D. Clodic, M. Younes, A. Bill, Test result of CO_2 capture by anti-sublimation capture efficiency and energy consumption for boiler plants. Seventh International Conference on Greenhouse Gas Control Technologies, GHGT7, Vancouver, Canada, 2004, 6-9 September.

E. Oguz, F. Ozkadi, Experimental investigation of a Stirling cycle cooled domestic refrigerator, Ninth International Refrigeration and Air Condition Conference at Purdue, USA, 2002, R19-3.

C.F. Song, Y. Kitamura, S.H. Li, K. Ogasawara, 2012. Design of a cryogenic CO_2 capture system based on Stirling coolers. International Journal of Greenhouse Gas Control 7, 107–114.

K.H. Kim H.J. Ko, K. Kim, Y.W. Kim, K.J. Cho, 2009. Analysis of heat transfer and frost layer formation on a cryogenic tank wall exposed to the humid atmospheric air. Applied Thermal Engineering 29, 2072-2079.

Y.A. Cengel. Heat Transfer: A Practical Approach, second ed., McGraw-Hill, 2003.

M. Fossa, G. Tanda, 2002. Study of free convection frost formation on a vertical plate, Experimental Thermal Fluid Science 26, 661-668.

A.N. Ogunbameru, B.P.L. Thibaut, R.C. Reid, 1973. On Carbon Dioxide Frost Formation. Ind. Eng. Chemical Fundamental 12, 385–387.

K. Qu, S. Komori, Y. Jiang, 2006. Local variation of frost layer thickness and morphology. International Journal of Thermal Sciences 45, 116–123.

C.F. Song, Y. Kitamura, S.H. Li, 2012b. Evaluation of Stirling cooler system for cryogenic CO_2 capture. Applied Energy 98, 491-501.

CHAPTER 5

MODELING ANALYSIS OF CO_2 FROST PROCESS

With the development of CO_2 capture technologies, the cryogenic approach provides a promising alternative for greenhouse effect mitigation. In previous work, a novel CO_2 capture process was developed based on Stirling coolers (SC). However, the properties of frosted CO_2 that deposits onto the heat exchanger of SC are not completely understood but it plays an important role as a heat transfer medium and affects subsequent CO_2 deposition. In order to improve the system performance and capture efficiency, a thorough analysis of the CO_2 frost process becomes especially significant. Based on this aim, numerical and experimental analysis of CO_2 frost formation in the cryogenic capture process has been investigated in the present chapter. The results show that the frosted CO_2 layer significantly influences the heat transfer between the gas stream and cooling fins. Over time (from 0 to 60 min), the thickness of the frost layer increased from 0 to 3.0 mm. The thermal conductivity increased from 0 to 0.4 W/(m·K). When the flow rate was set at 1 L/min, the temperature of the cold head of the SC varied from -105.2 ℃ to -102.1 ℃. When the flow rate was 3 L/min, the temperature rose from -106.3 ℃ to -98.0 ℃.

1. INTRODUCTION

CO_2 capture and storage (CCS) is proposed as an important strategy to help mitigate the increasing serious issue of global warming. CCS consists of three steps: capture, transport and storage. Of these three steps, CO_2 capture has attracted the most attention due to the technical challenges associated with its implementation. Currently, the main CO_2 capture technologies contain chemical absorption, membrane separation, cryogenic distillation and physical adsorption. Among these technologies, amine based absorption is the most technically mature and commercially viable to be integrated into coal-fired power plants (Liang et al., 2011). The main advantages of this technology are that it can be retrofitted to existing power plants and other industrial stations with minimum modification. Furthermore, amine scrubbing is suitable for low CO_2 partial pressure in flue gas (Luis et al., 2012). However, there are still some drawbacks: 1) the energy consumption required for regeneration; 2) the corrosion of the installations; 3) the environmental impact (Davison, 2007; Huang et al., 2011). For this reason, various researches have been carried out on the improvement of existing technologies and the exploitation of novel processes.

Cryogenic CO_2 separation technology is attracting increased attention due to its significance in recent years. As a promising alternative, this technology has several advantages: 1) to avoid the energy penalty in the regeneration process; 2) to prevent the issue of corrosion caused by solvent; 3) to realize a CO_2 capture method that is environmental friendly without causing degradation. In previous work (Song et al., 2012a), a novel CO_2 capture process based on Stirling coolers (SC) was exploited. The whole system is chilled by SCs, and the moisture and CO_2 in flue gas were captured at different places. Simultaneously, the residual gas (such as N_2) passes through the

system without phase change. The core part of the process is that CO_2 in the flue gas is captured in solid form. When exposed to the heat exchanger under the frost point of CO_2, the CO_2 in the gas stream will anti-sublimate and frost on the surface of the cold head. With the purpose of enhancing capture efficiency, intensive study on CO_2 frost properties is an imperative task.

Frost formation is a common phenomenon that exists in various fields, such as cryosurgery, meteorology, agriculture, aerospace industry, refrigeration industry, civil engineering (Lee and Ro, 2005). The investigation of the frost process in different engineering processes has been widely implemented (Seker et al., 2004; Kim et al., 2009; Schmelzer, 2003). It is worth noting that in spite of this a relatively large amount of literature has investigated the frost formation process, however most relate to moisture and there are still gaps and inconsistencies (O'Neal and Tree, 1985). Reports with respect to the frosting process of CO_2 in the greenhouse gas control field are few (Shchelkunov et al., 1986; Sumarokov et al., 2003). According to Ogunbameru et al. in 1973, the frost behavior of CO_2 is different from moisture. In the moisture frost process, the density increases continuously with the total mass of the deposition (Na and Webb, 2004a). By contrast, the initial increase rate in density for the frosted CO_2 is large but in the later stages it decreased (Brian et al., 1969). Meanwhile, the thermal conductivity of solid CO_2 is related to the variation of the layer density (Cook and Davey, 1976). Therefore, the frost formation of CO_2 is an intricate deposition process. In light of these characteristics, it is necessary to investigate the CO_2 frost formation process in order to improve cryogenic CO_2 capture performance.

The objective of this chapter is to numerically analysis the properties of the CO_2 frost formation process by the SC based cryogenic CO_2 capture technology. In order to achieve this aim, the influence of the frost layer on thermal conductivity and

temperature variation has also been investigated in detail. Moreover, the variation of the frost layer thickness has been simulated.

This chapter is organized as follows: In the section 2, the base case of CO_2 capture is described. In the section 3, the whole frost formation process is explained in three sections. In the section 4, the experimental conditions and the structure of the heat exchanger for CO_2 frost are introduced. In the section 5, the variation of frost layer (thickness and thermal conductivity) and temperature in the capture process is simulated and analyzed in detail. In the section 6, the main conclusion of this chapter is summarized.

2. BASE CASE

The schematic of the exploited CO_2 capture process is shown in Figure 5-1. The whole capture process can be described as follows: Prior to CO_2 recovery, the gas stream from the combustion furnace flows through the removal units. There the acid gases (such as SO_x and NO_x) and particulate can be separated as they affect the capture performance and installation. SO_x removal is usually achieved in a flue gas desulphurization (FGD) unit. Particulate matter such as fly ash is removed by electrostatic precipitators (ESP). NO_x is removed using selective catalytic reduction (SCR). Then, the gas mixture is fed to the developed cryogenic capture system which is mainly composed of three SCs. By the first SC, the flue gas is chilled to (between 40 and 50 ℃) from a high initial temperature (around 60 ℃ after desulphurization). The function of this section is to decrease the mechanical shock of the gas stream to the installation. It should be pointed out that as the temperature of the flue gas decreases rapidly to the freezing point of H_2O, the moisture in the gas condenses and is recovered at the condensate water outlet. After the pre-chilling step, the gas stream

is introduced into the CO_2 separation tower. In this section, the CO_2 in the flue gas frosts onto the heat exchanger of the SC-2 under the cryogenic condition (around -105 ℃) and the residual gas (mainly as N_2) is exhausted without phase change. In this way, the CO_2 is recovered from flue gas. In the last step, the captured CO_2 is stored in the column chilled by SC-3 to avoid sublimation. Furthermore, since the temperature of residual gas and condensate water is low, it can be used to cool down the follow-up gas stream by heat exchanger for energy conservation. In addition, the flue gas in my research is simulated by synthetic gas (N_2/82 vol.%, CO_2/13 vol.% and H_2O/5 vol.%). After the cryogenic CO_2 capture process, the composition of the residual gas is N_2/99.38 vol.% and CO_2/0.62 vol.%. Furthermore, the average flow rates of the initial and final gas stream are 3 L/min and 2.47 L/min, respectively. The details of the capture process can be found in previous work (Song et al., 2012a).

3. CO_2 FROST FORMATION PROCESS

3.1 Frost formation

As mentioned in the relevant research, the whole CO_2 frost formation process can be divided into three periods (Hayashi et al., 1977). 1) Crystal growth period. 2) Frost growth period. 3) Frost formation period. The sketch of the frost formation process is depicted in Figure 5-2.

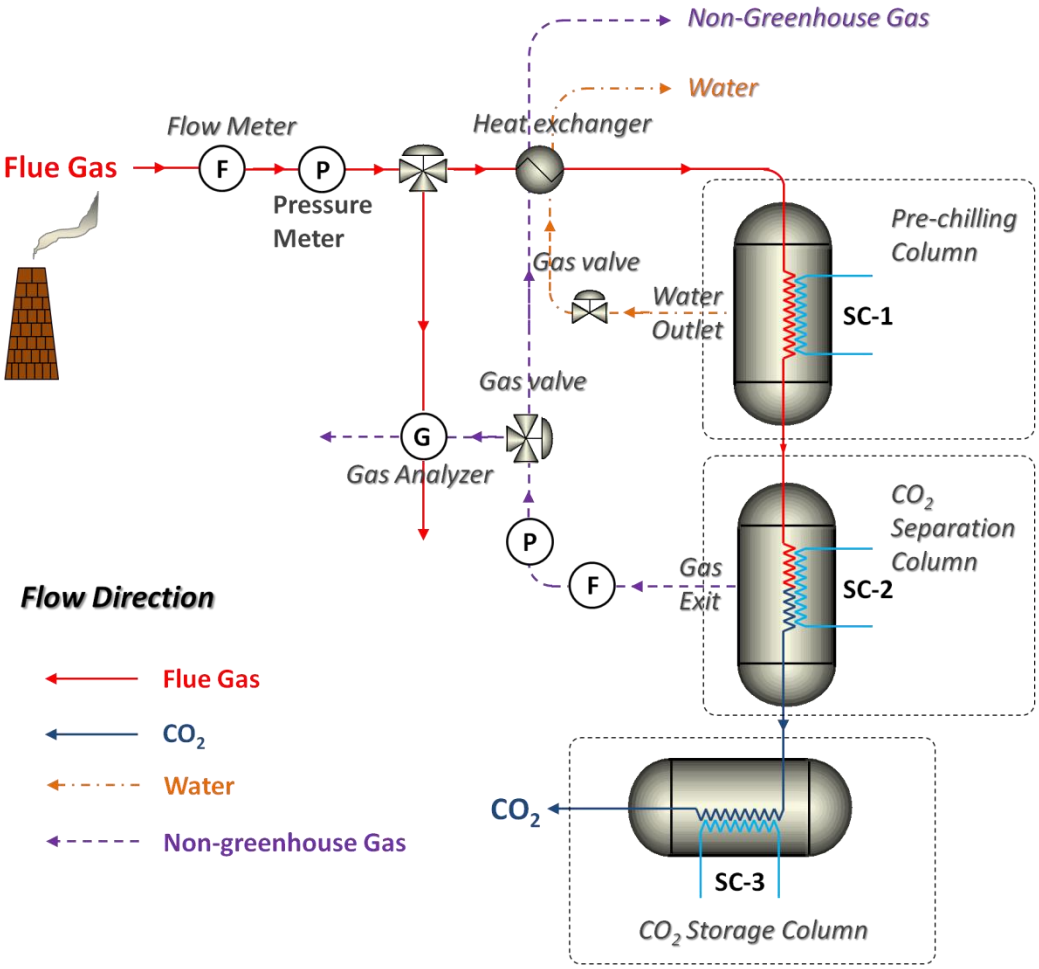

Figure 5-1 Schematic diagram of SC based cryogenic CO_2 capture process

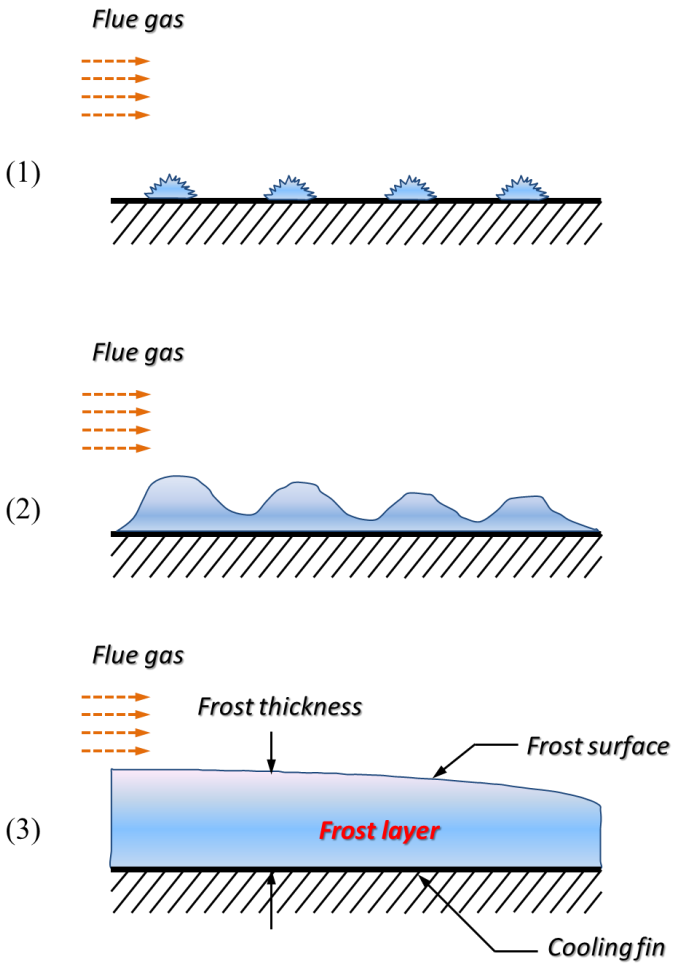

Figure 5-2 Sketch diagram of CO_2 frost formation process. (1) Crystal growth period. (2) Frost growth period. (3) Frost densification period (Cui et al., 2011)

3.1.1 Crystal growth period

This is a relatively short period during the early stage of the frosted CO_2 formation process. At the beginning, the CO_2 in the flue gas anti-sublimates into small crystals and is simultaneously extracted from the gas stream by frosting onto the cooling fin of the heat exchanger. The frosted CO_2 plays a role as the nucleus for further crystallization. New CO_2 crystal grows on the previous nucleus and spreads in all directions. It needs to be pointed out that this period has a significant influence on the further frost growth process. However, the characteristics of this period are complexity and instantaneity. Therefore, the effect of this period on the whole capture performance is taken into account by setting appropriate initial parameters (Cui et al., 2011).

3.1.2 Frost growth period

The frost growth period is characterized by a porous frost structure growing. The structure consists of solid CO_2 (99.89 mol.%), a small quantity of residual gas (around 0.04 mol.%) and a trace of H_2O (approximate 0.07 mol.%). Thus, in this period, the frost layer becomes visibly rugged due to new crystal formation on the surface. The subsequent CO_2 crystal leads to further growth and densification of the frost layer. The thickness of the frost deposition increases rapidly.

3.1.3 Frost formation period

In the last period, the frost formation is fully developed. The increasing rate of deposition slows and the density increases gradually. As the frost layer grows, the heat resistance of the frost layer also rises. This reflects in the decrease in the effective thermal conductivity of the cold head and causes a surface temperature increase. When the temperature of the frost layer surface becomes higher than the freezing point, the

CO_2 in the subsequent gas stream cannot frost. Meanwhile, the following feed gas can cause that part of the frosted CO_2 on the layer surface to sublimate. The sublimation results in a thinning layer, and then enhances the thermal conductivity of the layer. The CO_2 in the gas stream frosts again until a dynamic equilibrium of anti-sublimation and sublimation of the whole frost process is achieved.

3.2 Numerical model of the frost process

According to previous discussion, knowledge of the characteristics of CO_2 frost is important to improve the capture performance and decrease the energy penalty of the cryogenic system. In order to simplify the intricate CO_2 frost process, some assumptions are mentioned as follows: 1) the water in the frost layer is neglected due to its fractional content. 2) the density of the frost layer on the heat exchanger is homogeneous. 3) radiation effect within the frost layer is negligible.

The CO_2 frost process on the cold surface is simulated in Figure 5-3. The mass and heat transfer processes have been introduced in our previous work (Song et al., 2012b). The thermal dynamic behavior of the frosted CO_2 layer is described using empirical models. The summaries of the frost density (ρ_f) and thickness (δ_f) correlation model are listed in Tables 5-1 and 5-2. The correlations published in the literature for thermal conductivity (λ_f) calculations are shown in Table 5-3.

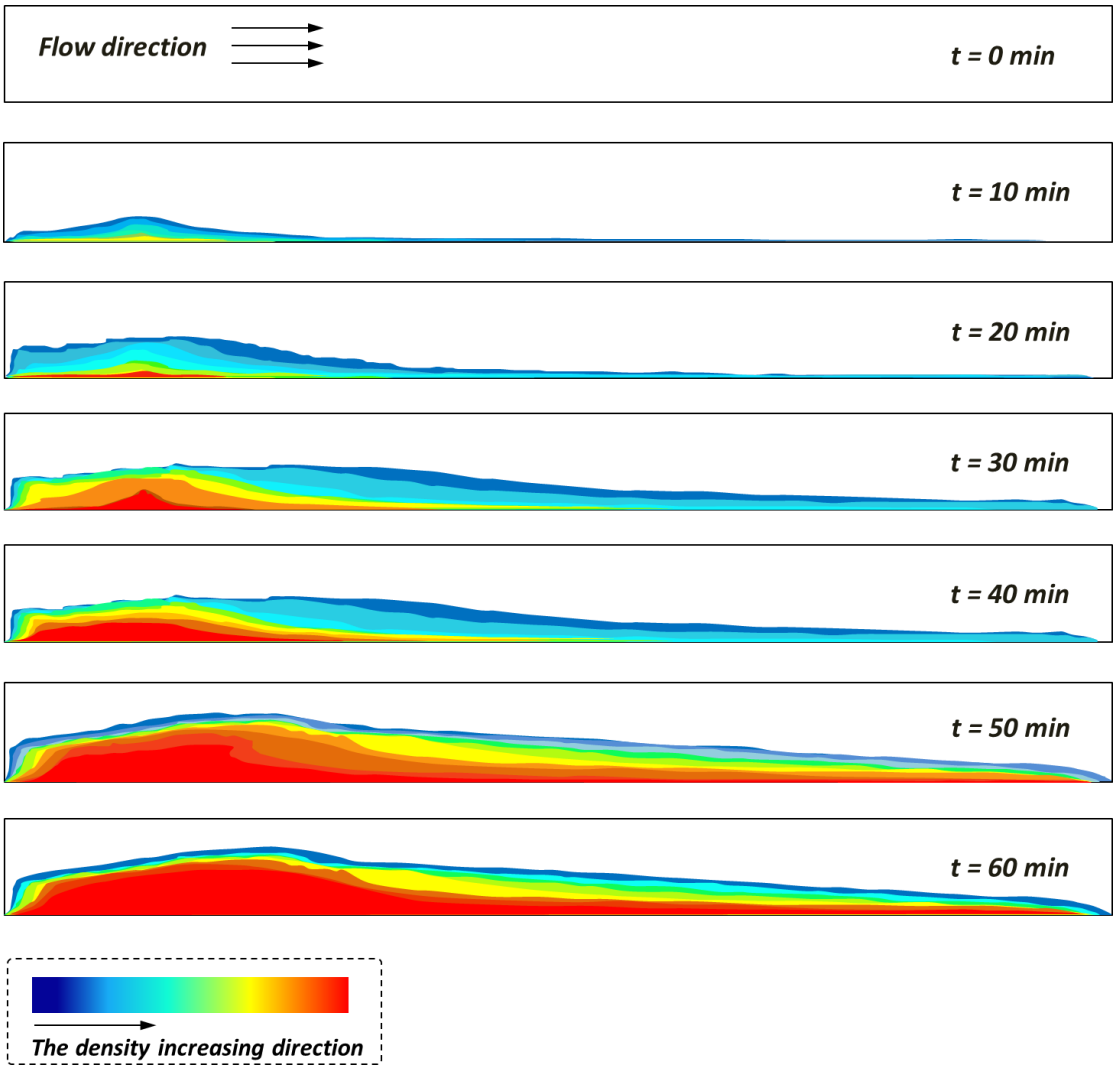

Figure 5-3 The growth process of the CO_2 frost layer on the heat exchanger of SC-2. The difference in color represents the direction of the increase in density of the frost layer (from blue to red)

Table 5-1 Calculation models for the density of the frost layer.

1) Average frost density calculated by Ogunbameru et al., 1973:

$$\rho_f = -\ln(GI / I_0) / \mu_m \cdot x$$

In which G is the dimensionless geometrical correction factor. I is the number of γ-radiation counts. I_0 is the number of counts without frost deposit. μ_m is mass attenuation factor. x is the thickness of frost layer.

2) Frost density is determined from empirical correlation by Hayashi et al., 1977:

$$\rho_f\Big|_t = 650 \cdot \exp\left[0.277 \cdot T_f(t)\right]$$

3) Calculation of frost density proposed by Cui et al. in 2011:

$$\rho_f(\vec{x},t) = \rho_g \cdot \left[1-\alpha_i \cdot (\vec{x},t)\right] + \rho_i \cdot \alpha_i \cdot (\vec{x},t)$$

Where ρ_g and ρ_i are the density of gas phase and crystal, respectively. α_i is the volume fraction of frosted droplets.

4) The local density of the frost layer (Na and Webb, 2004b; Lenic et al., 2009):

$$\rho_f = \varepsilon \cdot \rho_g + (1-\varepsilon)\rho_s$$

Here ε is the local porosity of the frost layer. It is defined as following:

$$\varepsilon = \frac{\rho_s - \rho_f}{\rho_s - \rho_g}, \quad 0 \leqslant \varepsilon \leqslant 1$$

In which, ρ_g, ρ_s and ρ_f are the density of gas phase, solid phase and frost layer, respectively.

Table 5-2 Empirical models for the thickness of the frost layer.

1) The frost thickness for each time interval is given by Yun et al., 2002:

$$\delta_f\Big|_{t+\Delta t} = \delta_f + \Delta\delta_f$$

2) The average frost thickness calculated by Cui et al., 2011:

$$\delta_f(t) = \frac{\sum_{j=1}^{n}\left[\delta_j(t)\Delta x\right]}{L}$$

In which $\delta_j(t)$ is the local thickness of frost layer. L is the length of the computational domain.

3) The average layer thickness defined by Lenic et al., 2009:

$$\delta_f = \frac{\sum_{k=1}^{M}\delta_{L,k}}{M}$$

Where $\delta_{L,k}$ is the local thickness of frost layer. M is the number of control volumes in horizontal direction.

Table 5-3 Correlation models for the thermal conductivity of the frost layer.

1) The total thermal conductivity is the sum of surface and inner layer. (Yun et al., 2002):

$$\lambda_{total} = \frac{\lambda_{f,s} \cdot \lambda_{f,in} \cdot (\delta_{f,s} + \delta_{f,in})}{\lambda_{f,in} \cdot \delta_{f,s} + \lambda_{f,s} \cdot \delta_{f,in}}$$

Here, the thermal conductivity of surface is given by:

$$\lambda_{f,s} = \lambda_a + \rho_{a,s} \cdot c_{p,a,s} \cdot u_a^2 \cdot C_f / 2 \cdot [y(t) + \delta_b] / 2.5$$

the thermal conductivity of inner layer is calculated by Woodside in 1958:

$$\lambda_{f,in} = \lambda_a / (1 - 6 \cdot s / \pi)^{1/3} \cdot \left\{1 - \left(c^2 - 1\right) / 2 \cdot \ln\left[(c+1)/(c-1)\right]\right\}$$

2) The frost thermal conductivity is related to temperature as a sole parameter (Sahin, 2000):

$$\lambda_f(T) = 0.131 \times 10^{-6}(1-\beta) \cdot \frac{h_s \cdot P_{atm} \cdot P_g}{T_g^{1.94} \cdot R^2 \cdot T_s^{1.06}} \cdot \exp\left[\frac{h_s}{R} \cdot \left(\frac{1}{T_g} - \frac{1}{T_s}\right)\right]$$
$$+ 1.202 \times 10^{-3} \beta (\rho_c)^{0.963} + (1-\beta)(1.0465 + 0.017 T_s) \times 10^{-5}$$

Where h_s is the latent heat of sublimation. P_g is the partial pressure of specific gas phase at initial temperature (T_g). T_s is the temperature of frost surface. β is the volumetric ratio of frost deposition. ρ_c is the density of crystal.

3) The empirical equation validated by Yonko and Sepsy, 1967:

$$\lambda_f = 0.024248 + 0.00072311 \rho_f + 0.000001183 \rho_f^2$$

In which ρ_f is the density of frost layer.

4) The expression demonstrated by Sanders, 1974:

$$\lambda_f = 1.202 \times 10^{-3} \cdot \rho_f^{0.963}$$

5) The correlation proposed by Lee et al., 2003:

$$\lambda_f = 0.132 + 3.13 \times 10^{-4} \cdot \rho_f + 1.6 \times 10^{-7} \cdot \rho_f^2$$

4. EXPERIMENTAL SECTION

4.1 Materials

In order to measure the temperature distribution, eight K-type thermocouples were placed on different places in the system, and all the thermocouples are connected to a data-acquisition system. Commercial software is used to record and process data in a database format using a computer. The temperature data measured by the thermocouples is recorded every 0.1 s during the total testing time. The ambient temperature (T_a) and humidity (ω_a) are measured with the thermo hygrometer in the laboratory. All the heat exchangers in the system are made from copper. The structure of the heat exchanger of SC-2 is shown in Figure 5-4(a). The details of its size are described in Figure 5-4(b). The length and diameter of the cold head are 230.0 and 36.0 mm, respectively. The length and width of the cooling fin are 15.0 and 1.0 mm, respectively. The interval between the fins is 6.0 mm.

4.2 Methods

The formation of the frost layer has a significant influence on the performance of the whole capture process. In order to investigate the variation of the frost layer in the CO_2 capture process, two parameters are considered to represent the characteristics of variation, namely thickness (δ_f) and thermal conductivity (λ_f).

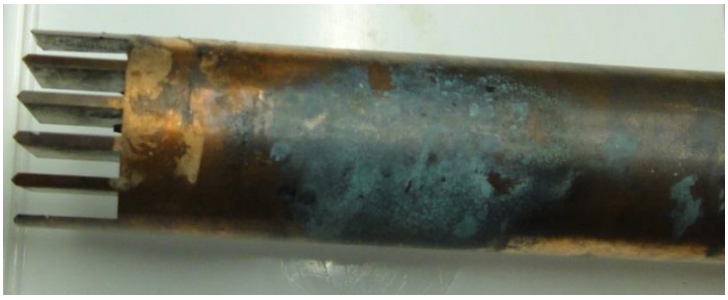

(a)

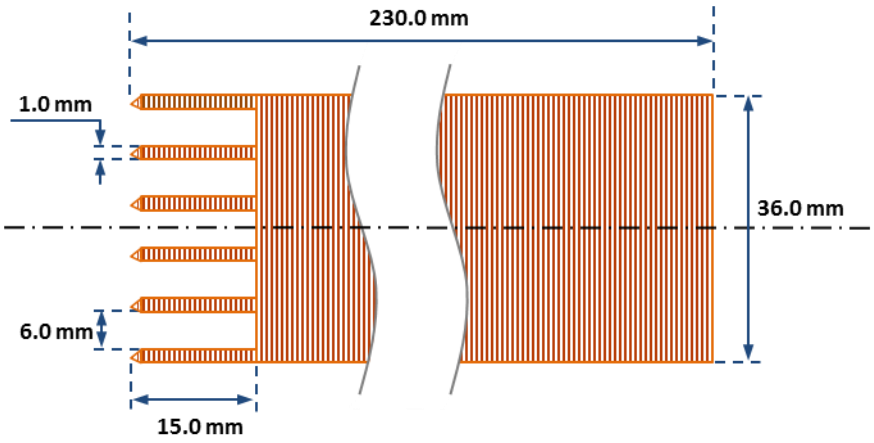

(b)

Figure 5-4 The structure (a) and dimension (b) of the heat exchanger for capturing CO_2.

The thickness of the frost layer is a significant parameter that reflects the properties of the frost process. Its variation process is observed by use of a charge coupled device (CCD) camera. Simultaneously, tick marks are added among the cooling fins of the cold head to facilitate thickness measurement. It is obvious that the deposited frost layer will lead to an increase in thermal resistance. Meanwhile, it influences the heat flux between the cold head of SC-2 and the gas stream, and results in the decrease of capture efficiency. Thus, in order to evaluate the characteristic of the frost layer, the investigation of effective thermal conductivity (λ_f) is necessary. The detail calculation method is described as follows (Lenic et al., 2009):

$$\lambda_f = \frac{\delta_f}{\sum_{c=1}^{\delta} \frac{1}{\lambda_c}} \tag{5-1}$$

where δ_f represents the thickness of the frost layer. λ_c represents the coefficient of the thermal conductivity for individual unit volume.

5. RESULTS AND DISCUSSION

5.1 Frost layer

The formation of frost layer has a significant influence on the performance of the whole capture process. In order to investigate the variation of the frost layer in CO_2 capture process, two significant parameters are considered to represent the characteristic, namely thickness (δ_f) and thermal conductivity (λ_f).

5.1.1 Growth of the frost layer

When the temperature dropped to the freezing point of CO_2, the flue gas was loaded into the system. Initially, there was no frost present on the heat exchanger (as shown in

Figure 5-5(a)). As time went on, the frost began to form, temperature increased and the crystals of frosted CO_2 became gradually larger (as shown in Figure 5-5(b)). Then, as the crystal of solid CO_2 gathered, frost grew on the heat exchanger and its volume expanded rapidly (as shown in Figure 5-5(c)). At the full growth stage, the captured CO_2 almost totally covered the cooling fin of the heat exchanger (as shown in Figure 5-5(d)).

The effect of the gas flow rate on the thickness of the frost layer is shown in Figure 5-6. The result indicates that the thickness of the frost layer increased continuously with time however the rate of deposition was not constant. Initially, the growth rate was slow and then increased rapidly. That can be explained by the fact that during the stage of crystal growth (described in section 3.1), the variation in deposition was moderate. When the CO_2 crystal covered the cooling fin, the growth rate of the frost layer accelerated. In the frost formation period, the frost layer increased sufficiently. Meanwhile, the rate of frost deposition decreased again and eventually approached zero. In this period, the variation of the frost layer mainly presented in density. After 60 minutes, the thickness of frost layer reached 3.0 mm. Additionally, it can also be seen that along with the increase in the flow rate, the thickness of the frosted CO_2 grew accordingly.

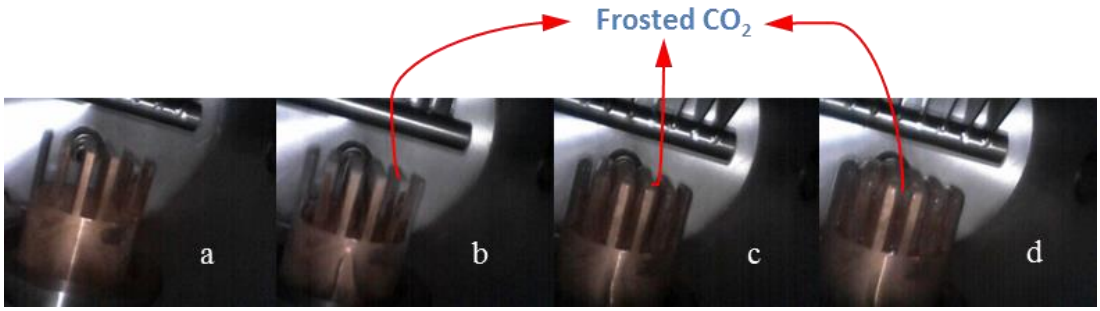

Figure 5-5 CO_2 frosting process: (a) no frost; (b) initial frost; (c) growth of the frost; (d) full growth

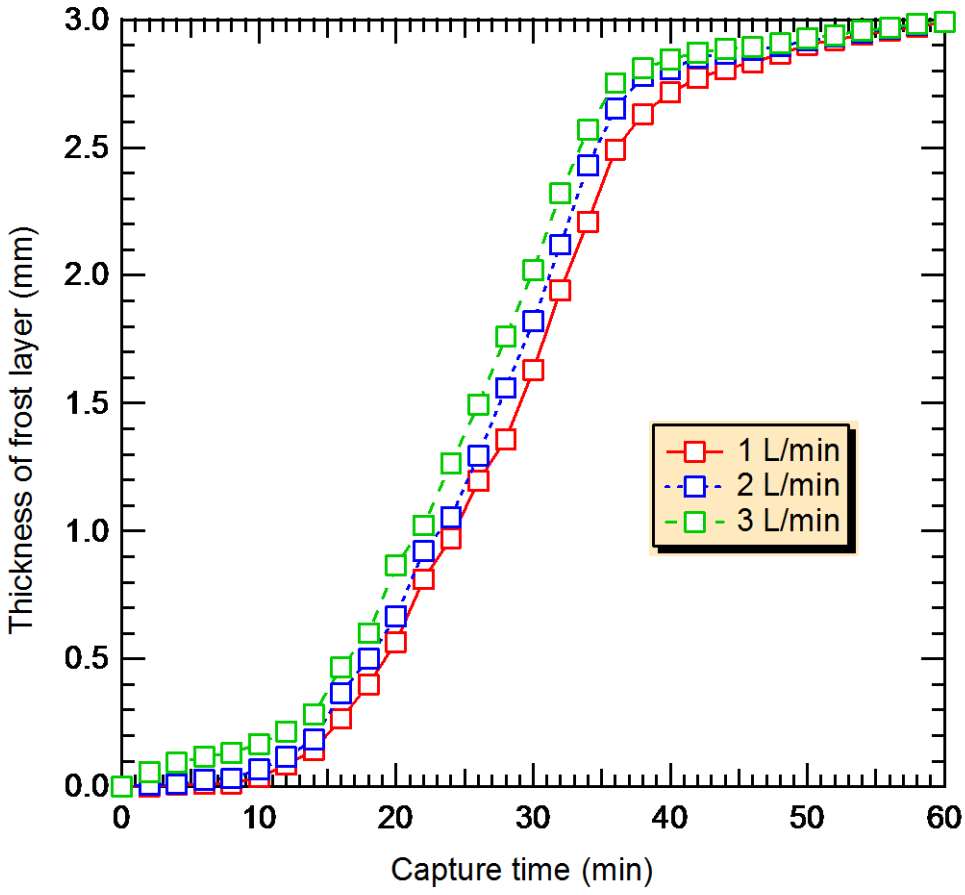

Figure 5-6 Effect of the flow rate on thickness of the CO_2 frost layer. (T_{SC-1}= -30 ℃; T_{SC-2}= -120 ℃; T_{SC-3}= -120 ℃; t_1=240 min; t_2=60 min)

5.1.2 Conductivity of the frost layer

The influence of the flow rate for the gas stream on the thermal conductivity (λ_f) of the frost layer is shown in Figure 5-7. From the results, it indicates that the thermal conductivity increased with capture time passed. At the beginning of the capture process, the effective conductivity of the frost layer increased quickly, and with time decelerated. In addition, with the increase in the flow rate of feed gas, the increase rate of the thermal conductivity obviously accelerated. It is worth noting that after 20 minutes the variation of the thermal conductivity of the frost deposition amplified slowly, and reached around 0.4 W/(m·K) after 60 min. This can be explained by the fact that the rise in thermal conductivity with time is due to the variation of the thickness and density of the frost layer. At the initial period (from 0 to 20 min), the CO_2 crystals deposited on the surface of the cold head and the growth rate of frost layer was fast. Consequently, the thermal conductivity increased and the rate was also fast. At a subsequent time (from 20 to 60 min), more CO_2 crystal groups formed around the existing crystals and the gas pores were filled up. The solid phase became denser through internal diffusion. However, the variation of the thickness for the frost layer slowed down. Therefore, the increase rate in the thermal conductivity decelerated.

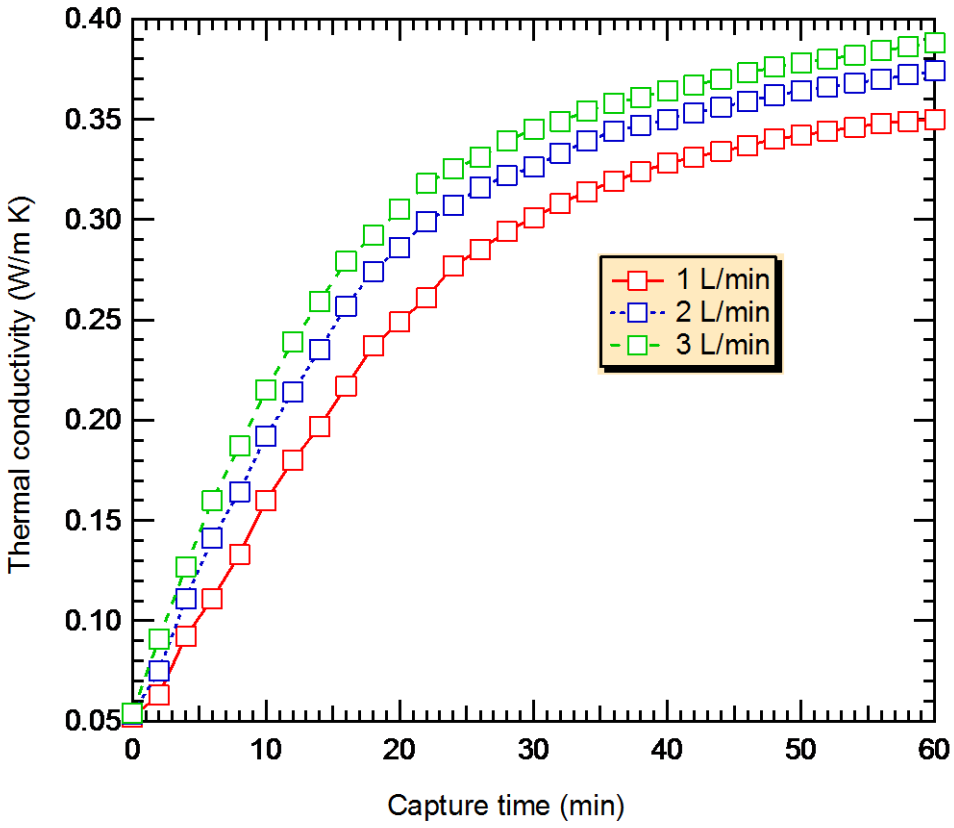

Figure 5-7 Effect of the flow rate on thermal conductivity (λ_f) of the CO_2 frost layer. (T_{SC-1}= -30 ℃; T_{SC-2}= -120 ℃; T_{SC-3}= -120 ℃; t_1=240 min; t_2=60 min)

5.2 Temperature variation

As the frosted CO_2 layer grows, a gradual increase in the frost surface temperature occurs due to the augmentation of heat resistance which is unfavorable to the capture process. This is because the temperature driving force is reduced due to the frost insulation on the heat exchanger surface, and hence energy and mass transfer rates drop. As a consequence, this results in a decrease of CO_2 capture efficiency.

Figure 5-8 indicates that SC-1 has a significant influence on the temperature of SC-2, and impacts the whole capture performance. During the capture process, SC-1 played a part in pre-chilling the flue gas and preventing the rapid increase of the temperature in the capture tower. The temperature of SC-2 is lower when SC-1 is working compared to stop.

Figure 5-9 indicates the influence of flue gas flow rate on the temperature of SC-2. At the initial stage of gas inflow, the temperature of the heat exchanger of SC-2 increased quickly. As the frost layer formed on the surface of the cold head, the increase in speed trended to constant. From the results, it can be concluded that if flow rate was controlled slightly, the lower the temperature in the system can be maintained. This is because a high flow rate would lead to a high increase speed in the CO_2 frost layer. Due to the frost point of CO_2 being far above the temperature of the heat exchanger, when the frost formed, the temperature of the heat exchanger increased rapidly. Along with the increase in flow rate, the temperature change also increased gradually.

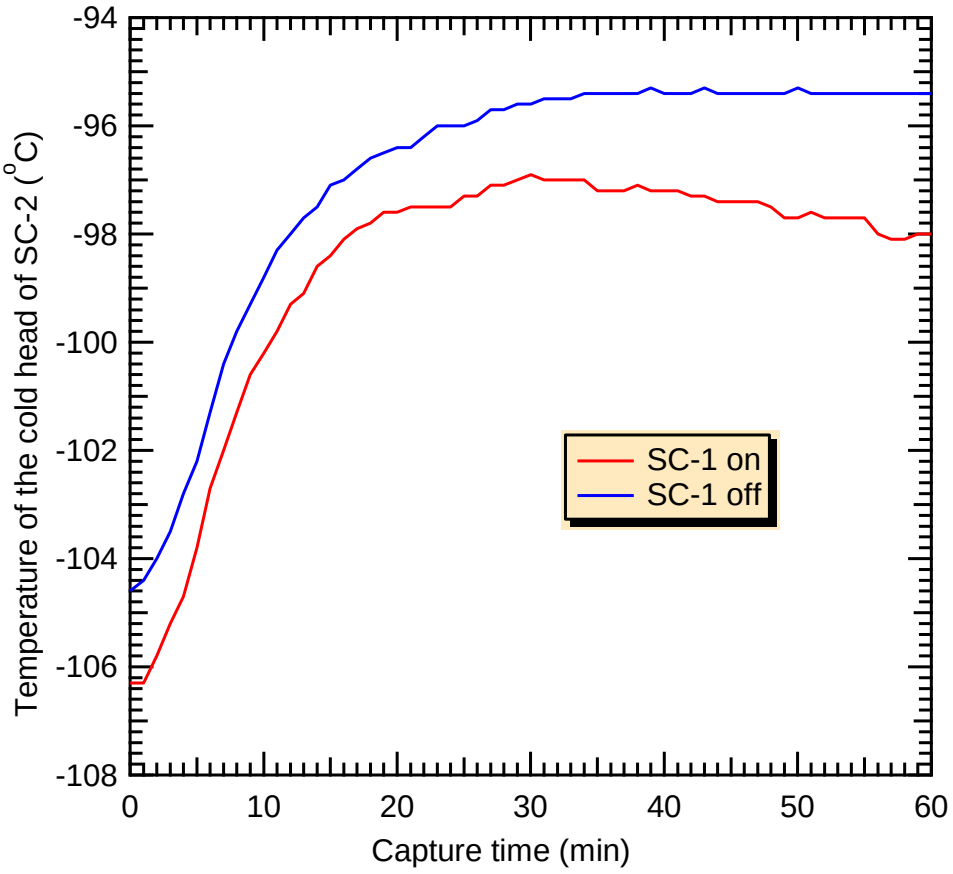

Figure 5-8 Effect of SC-1 on the temperature variation of the SC-2's cold head. (T_{SC-1}= -30 ℃; T_{SC-2}= -120 ℃; T_{SC-3}= -120 ℃; v=2 L/min; t_1=240 min; t_2=60 min)

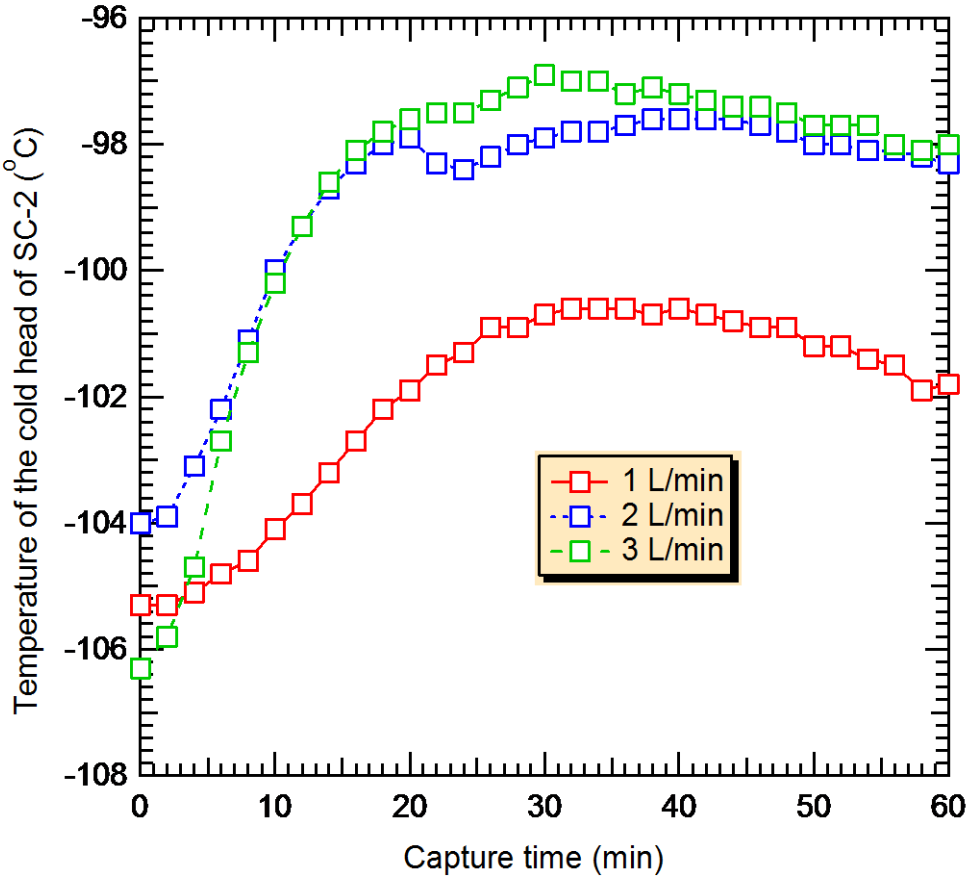

Figure 5-9 Effect of flow rate on the temperature variation of SC-2's cold head. (T_{SC-1}= -30 ℃; T_{SC-2}= -120 ℃; T_{SC-3}= -120 ℃; t_1=240 min; t_2=60 min)

The influence of temperature variation of SC-1 on the properties of the frost layer is investigated in Figure 5-10 and 5-11. In Figure 5-10, with the decrease in the temperature of SC-1, the rate of frost growth increases. When the temperature of SC-1 was set to -20 ℃, the frost deposited slowly during the initial 20 minutes. Then the layer grew rapidly in the following 20 minutes. Finally, the rate of deposition decreased again and tended to zero. This is because during the initial 20 minutes, the CO_2 formed crystals on the surface of the cold head. Therefore, the frost layer changed slightly. From the 20 minute mark, the CO_2 crystal fully covered the surface of the cold head and the density of frost layer grew rapidly. When the frost layer had increased sufficiently, the rate decreased again from the 40 minutes mark. With the decreasing temperature of SC-1, the crystal formation stage became shorter and the rate of deposition faster. When the temperature dropped down to -60 ℃, the variation of frost thickness stabilized after 30 minutes. In Figure 5-11, at the initial period the thermal conductivity was almost zero due to little frosted CO_2 on the cold head. While capture time passed, the heat transfer coefficient of the frost layer increased rapidly but the increase rate decelerated due to the decrease in the densification rate. After 60 minutes, the thermal conductivity of deposited CO_2 was around 0.4 W/(m·K). Meanwhile, with the decrease in temperature of SC-1, the thermal conductivity of the deposition increased. That is because the lower temperature of SC-1 facilitates the pre-chilling of the flue gas, and CO_2 solidification onto the cold surface.

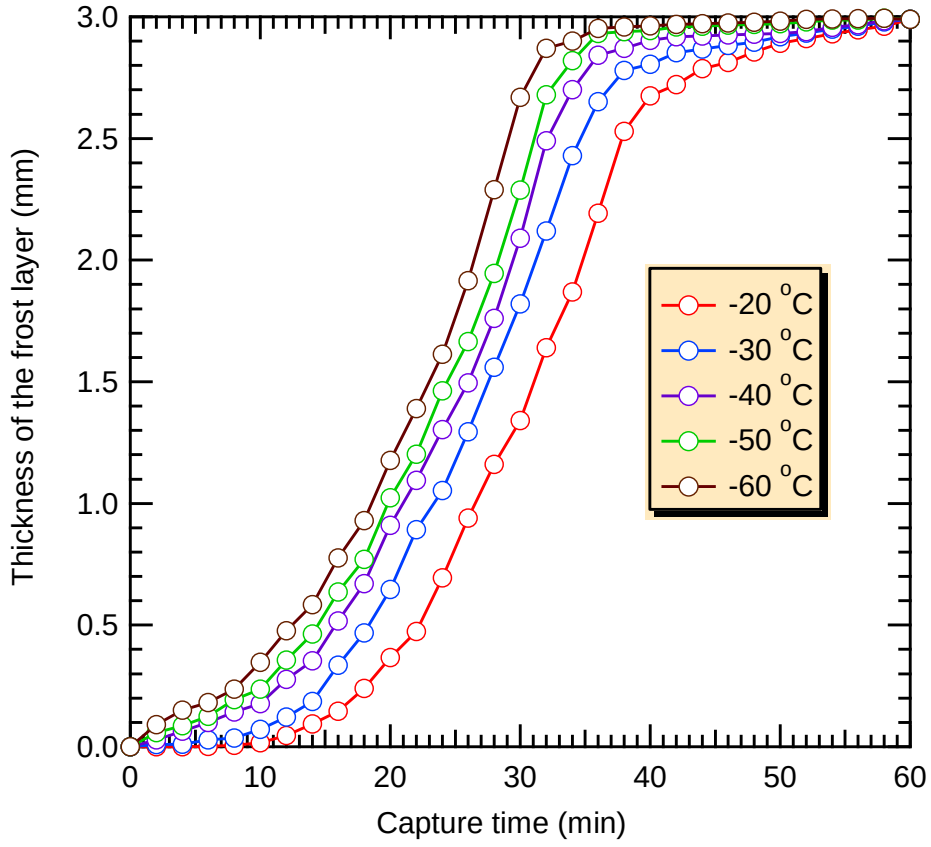

Figure 5-10 Effect of temperature variation of SC-1 on the thickness of the frost layer. (T_{SC-2}= -120 ℃; T_{SC-3}= -120 ℃; v=2 L/min; t_1=240 min; t_2=60 min)

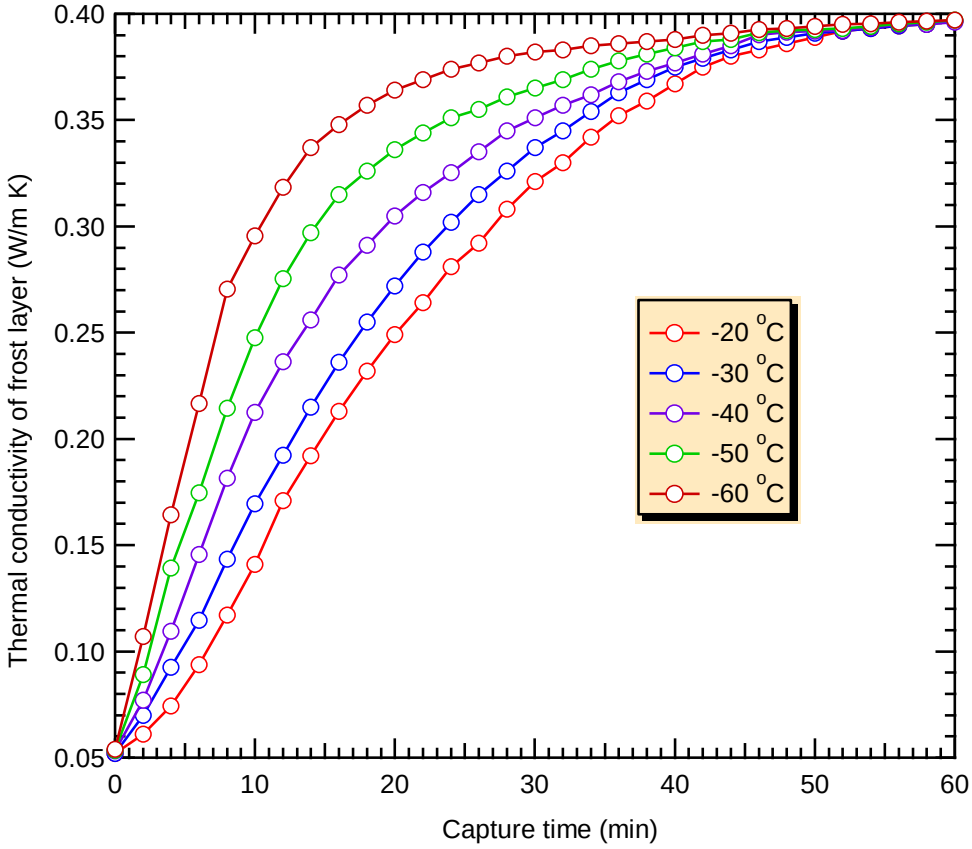

Figure 5-11 Effect of temperature variation of SC-1 on the thermal conductivity of the frost layer. (T_{SC-2}= -120 ℃; T_{SC-3}= -120 ℃; v=2 L/min; t_1=240 min; t_2=60 min)

6. CONCLUSION

Frost formation is a vital consideration in cryogenic CO_2 capture technology, and the phenomenon of CO_2 frosts on the surface of the heat exchanger has an important influence on capture performance. Based on this, the growth processes of the CO_2 frost layer and its effect on temperature variation have been numerically analyzed in this paper. The effect of frost layer growth on thermal conductivity and temperature variation was also investigated. According to the results of simulation and experiments, the following conclusions are given:

1) The thickness of the frost layer increased with time but the rate of CO_2 deposition decreased gradually. Furthermore, with the increase in the flow rate, the frost growth also accelerated. After 60 minutes, the thickness of frost layer was 3.0 mm.

2) The thermal conductivity of the frost layer increased due to the growth of the frost layer. Nevertheless, as time passed, its increase rate reduced. After 60 minutes, the thermal conductivity of the frost layer increased to around 0.4 W/(m·K).

3) The frost surface temperature increased rapidly as frost insulated the heat exchanger. Meanwhile, with the decrease in the flow rate, the increase rate of temperature decelerated. When the flow rate was set at 1 L/min, the temperature of the cold head for the SC varied from -105.2 ℃ to -102.1 ℃ after 60 minutes. When the flow rate was 3 L/min, the temperature rose from -106.3 ℃ to -98.0 ℃. However, the rate of the increase declined and approached zero when the energy balance between the gas stream and frost layer was reached.

REFERENCES

H. Liang, Z. Xu, F. Si, 2011. Economic analysis of amine based carbon dioxide capture system

with bi-pressure stripper in supercritical coal-fired power plant. International Journal of Greenhouse Gas Control 5, 702-709.

P. Luis, T. Van Gerven, B. Van der Bruggen, 2012. Recent developments in membrane-based technologies for CO_2 capture. Progress in Energy and Combustion Science 38, 419-448.

J. Davison, 2007. Performance and costs of power plants with capture and storage of CO_2. Energy 32, 1163-1176.

Y. Huang, M. Wang, P. Stephenson, S. Rezvani, D. McIlveen-Wright, A. Minchener, N. Hewitt, A. Dave, A. Fleche, 2011. Hybrid coal-fired power plants with CO_2 capture: A technical and economic evaluation based on computational simulations. Fuel, doi:10.1016/j.fuel.2010.12.012.

C.F. Song, Y. Kitamura, S.H. Li, K.J. Ogasawara, 2012a. Design of a cryogenic CO_2 capture system based on Stirling coolers. International Journal of Greenhouse Gas Control 7, 107-114.

C.F. Song, Y. Kitamura, S.H. Li, 2012b. Evaluation of Stirling cooler system for cryogenic CO_2 capture. Applied Energy 98, 491-501.

Y.B. Lee, S.T. Ro, 2005. Analysis of the frost growth on a flat plate by simple models of saturation and supersaturation. Experimental Thermal and Fluid Science 29, 685-696.

D. Seker, H. Karatasa, N. Egrican, 2004. Frost formation on fin-and-tube heat exchangers. Part I-Modeling of frost formation on fin-and-tube heat exchangers. International Journal of Refrigeration 27, 367-374.

K.H. Kim, H.J. K, K. Kim, Y.W. Kim, K.J. Cho, 2009. Analysis of heat transfer and frost layer formation on a cryogenic tank wall exposed to the humid atmospheric air. Applied Thermal Engineering 29, 2072-2079.

J.W.P. Schmelzer, 2003. Kinetic and thermodynamic theories of nucleation. Materials Physics and Mechanics 6, 21-33.

D.L. O'Neal, D.R. Tree, 1985. A review of frost formation in simple geometries. ASHRAE Transactions 91, 267-272.

V.N. Shchelkunov, N.Z. Rudenko, Y.V. Shostak, V.I. Dolganin, 1986. Surface desublimation of carbon dioxide from binary gas mixtures. Translated from Inzhenerno-Fizicheskii Zhurnal 51 (6), 965-970.

V.V. Sumarokov, P. Stachowiak, A. Jezowski, 2003. Low-temperature thermal conductivity of solid

carbon dioxide. FIzika Nizkikh Temperatur 29 (5), 603-605.

A.N. Ogunbameru, P.L.T. Brian, R.C. Reid, 1973. On carbon dioxide frost formation. Industrial & Engineering Chemistry Fundamentals 12, 385-387.

B. Na, R.L. Webb, 2004a. Mass transfer on and within a frost layer. International Journal of Heat and Mass Transfer 47, 899-911.

P.L.T. Brian, R.C. Reid, I. Brazinsky, 1969. Cryogenic frost properties. Cryogenic Technology 5, 205.

T. Cook, G. Davey, 1976. The density and thermal conductivity of solid nitrogen and carbon dioxide. Cryogenics 363-369.

Y. Hayashi, K. Aoki, H. Yuhara, 1977. Study of frost formation based on a theoretical model of the frost layer. Heat Transfer - Japanese Research 6, 79-94.

J. Cui, W.Z. Li, Y. Liu, Z.Y. Jiang, 2011. A new time- and space-dependent model for predicting frost formation. Applied Thermal Engineering 31, 447-457.

B. Na, R.L. Webb, 2004b. New model for frost growth rate. International Journal of Heat and Mass Transfer 47, 925-936.

K. Lenic, A. Trp, B. Frankovic, 2009. Transient two-dimensional model of frost formation on a fin-and-tube heat exchanger. International Journal of Heat and Mass Transfer 52, 22-32.

W. Woodside, 1958. Calculation of the thermal conductivity of porous media. Canadian Journal of Physics 36, 815-823.

A.Z. Sahin, 2000. Effective thermal conductivity of frost during the crystal growth period. International Journal of Heat and Mass Transfer 43, 539-553.

C.T. Sanders, 1974. Frost formation: the influence of frost formation and defrosting on the performance of air coolers, Ph. D. thesis, Technische Hogeschool, Delft, The Netherlands.

K. Lee, S. Jhee, D. Yang, 2003. Prediction of the frost formation on a cold flat surface. International Journal of Heat Mass Transfer 46, 3789-3796.

J.D. Yonko, C.F. Sepsy, 1967. An investigation of the thermal conductivity of frost while forming on a flat horizontal plate. ASHRAE Transactions 73, 567-579.

R. Yun, Y.C. Kim, M.K. Min, 2002. Modeling of frost growth and frost properties with airflow over a flat plate. International Journal of Refrigeration 25, 362-371.

CHAPTER 6

ENERGY ANALYSIS OF THE CRYOGENIC CO_2 CAPTURE SYSTEM

For the existing coal-fired power plant, energy penalty associated with CO_2 capture process is an important challenge. Energy analysis has been widely used as a powerful tool to overcome this problem and reduce the energy consumption of CO_2 capture process. In this chapter, the process simulation and energy analysis of the cryogenic CO_2 capture system has been implemented. The whole capture process is composed of three energy sections, namely pre-chilling, CO_2 anti-sublimation and storage. According to the first and second laws of thermodynamic, the influence of each section on the overall energy efficiency was also investigated. The performance of the typical coal-fired power plant with and without CO_2 capture units is also compared. The simulation results show that the energy requirement of the pre-chilling, main freezing and storage sections is 15.58 J/s, 30.34 J/s and 30.34 J/s, respectively. The total energy requirement of the cryogenic CO_2 capture system is 30.34 J/s.

1. INTRODUCTION

At present, a number of large industrial stations become the dominant greenhouse gas (GHG) emission sources, and coal-fired power plant has been paid wide attention as an important one. According to the Word Energy Outlook 2009 of International Energy Agency (IEA), by 2030 coal will account for approximately 44% of the word energy (IEA, 2009). In face of this situation, integration of CO_2 capture and storage (CCS) technologies into the CO_2 emission sources is an effective strategy to mitigate the increasing climate issues.

Currently, several CO_2 capture and storage technologies for post-combustion power plants have been developed, such as solvent absorption, sorbent adsorption, membrane permeation and cryogenic fractionation (Rubin et al., 2012). Chemical absorption method has been researched as the most mature technology, and it can be used to different CO_2 sources even for a dilute CO_2 concentration (3 vol.% for gas turbine) (Zhao et al., 2012). Adsorption is a promising alternative for CO_2 capture, and the common solid adsorbents are activated carbon, zeolite, CaO, etc. (Wang et al., 2011). Application of polymeric membrane on CO_2 separation has been widely investigated in the last years due to its significant characteristics (i.e. high selectivity and high driving force) (Criscuoli et al., 2011). Cryogenic fractionation is a well know technique for air separation (Smith and Klosek, 2001) and also has been utilized in oxy-fuel combustion CO_2 capture process (Markewitz et al., 2012).

On the other hand, the major challenge of CO_2 capture technologies is to lessen the energy consumption of the capital and operational cost. Therefore, a growing attention has been paid on the energy reduction of CO_2 capture and storage technologies. Amrollahi et al. (2012) and Cousins et al. (2011) investigated different chemical

absorption process configurations to reduce the energy requirement. Chaffee et al. (2007) reduced the energy penalty of adsorption process by developing novel materials. Luis et al. (2012) summarized the current situation of membrane CO_2 capture technologies. As they pointed out that the existing permeation processes are still expensive and few membrane modules are commercially available. Tuinier et al. (2011) evaluated the energy requirement of a novel post-combustion CO_2 capture process based on cryogenic packed beds. Although the research of the CO_2 capture technologies has made remarkable progress, the energy penalty for the existing technologies is still high. Meanwhile, CO_2 capture is an intricate and integrated process, and various forms of energy are utilized. Therefore, in order to improve capture efficiency and reduce energy penalty, energy analysis of the capture process is significant. Therefore, the investigation on the energy requirement is particularly significant.

In light of these concerns, efforts are implemented to reduce the energy penalty of CO_2 capture processes. The objective of this chapter is to simulate and analyze the energy efficiency of the developed cryogenic CO_2 system. In order to achieve the aim, the detailed energy requirement of different stages in the process has been investigated. With the purpose of decreasing the energy consumption, the energy of the cryogenic CO_2 process based on Stirling coolers is particularly significant.

This chapter is structured as follows: Section 2 describes the typical coal-fired power plant and cryogenic CO_2 capture unit. Section 3 analyzes the overall energy demand of the process and simulates the characteristics of the cryogenic system. Section 4 numerically investigates the energy requirements of different stages in the system. Section 5 discusses the energy efficiency of the system and its influence on the efficiency of the power plant. Section 6 summarizes the main conclusions and

prospects the future work.

2. BASE CASE DESCRIPTION

2.1 Pulverized coal-fired power plant

The base case in this research is simulated to 600 MWe pulverized coal-fired power plant. The process flow diagram of the power plant is described in Figure 6-1. Initially, the coal is pulverized in the mill and blew into the furnace. The milled black coal is combusted with pre-heated air and the resulting flue gas heats up feed-water in water-tubes inside the boiler producing sub-critical steam. The stream is sent to a series of turbines to utilize the heat to produce electricity. The first turbine is high pressure (HP), and in which the stream is bled from an appropriate section to heat up feed water before entering the furnace. The steam from the outlet of the turbine is returned back to the furnace to be pre-heated and move to the intermediate pressure (IP) turbine in steam cycle. This turbine may also have some bleeds to supply heat for feed water heating or deaerator. The exiting steam from the IP turbine is directed to the low pressure (LP) turbines, and which have usually different bleeds for primary heating of feed water. The low pressure low temperature (LPLT) steam at the outlet of the turbine is condensed, heated, deaerated, chemically adjusted, pressurized and returned back to the furnace. After the fly ash is deposited, the impurities in the flue gas are separated by the removal units. For instance, selective catalytic reduction (SCR) is used to remove NOx, electrostatic precipitation (ESP) is used to particulate deposition and flue gas desulfurization (FGD) is used to separate the component of SOx. The detailed performance of the plant is listed in Table 6-1.

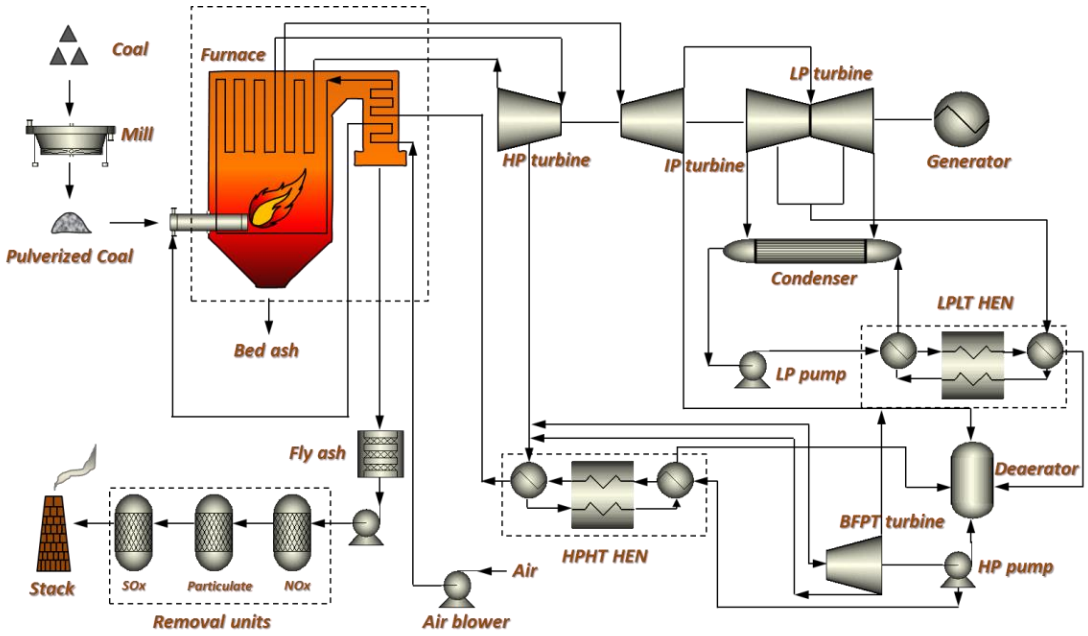

Figure 6-1 A typical flow sheet of pulverized coal fired power plant without CO_2 capture

Table 6-1 Performance of a typical coal-fired power plant.

Description	Value	Unit
Gross power output	580	MW
Net power output	550	MW
Net efficiency	39.1	%
HHV	30776	kJ/kg
Flue gas mass flow	670	m^3/s
Flue gas temperature	110	℃
Flue gas pressure	95	kPa
Flue gas composition		
N_2	75	vol. %
CO_2	13	vol. %
O_2	5	vol. %
H_2O	7	vol. %
SOx	220	ppm
NOx	< 50	ppm

2.2 Cryogenic CO_2 capture process

The detailed cryogenic CO_2 capture process integrated with coal-fired power plant is illustrated in Figure 6-2. Forward the CO_2 capture process, a series of purification treatment are required to remove the relevant impurities (e.g. SOx, NOx and fly ash). But it worth noting that these removal processes are not considered in this work. The purified flue gas is pumped into the pre-chilling tower and cooled by SC-1. In this stage, the moisture in the gas stream condenses and exhausts from the outlet. After the pre-chilling process, the treated gas is sent to the CO_2 anti-sublimation column and simultaneously the cold energy of condensate water is recovered by heat exchanger to chill the subsequent flue gas. In the anti-sublimation column, the CO_2 in the flue gas frosts onto the surface of the cold head and the residual gas (such as N_2 and O_2) exhausts from the outlet. Meanwhile, the latent heat associated with exhaust gas is also recovered by the heat exchanger. Finally, the deposited CO_2 is scraped down by a motor driven scraper and gathered in the storage column. The detailed description of the cryogenic system has been introduced in the previous work (Song et al. 2012). The performance of the cryogenic CO_2 capture process is listed in Table 6-2.

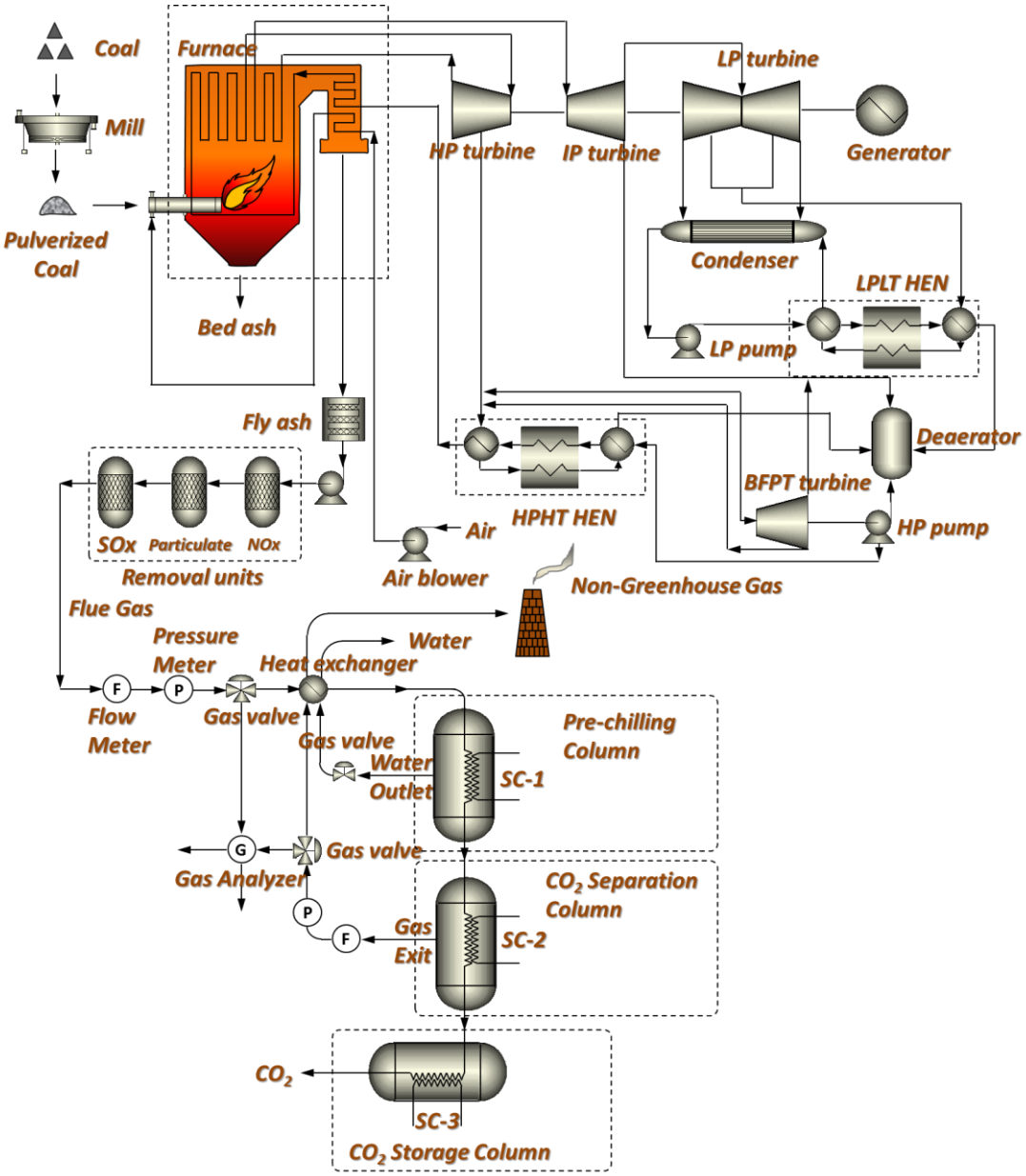

Figure 6-2 The schematic diagram of the cryogenic CO_2 capture process.

Table 6-2 Performance of the cryogenic CO_2 capture unit.

Description	Value (W)
Pre-chilling column (SC-1)	150
CO_2 anti-sublimation column (SC-2)	150
Storage column (SC-3)	150
Auxiliaries	
Vacuum pump	400
Control panel	50
Scraper	20

3. THEORETICAL ANALYSIS

3.1 Overall energy requirement of the process

The energy flow diagram of the cryogenic CO_2 capture process is shown in Figure 6-3. First, the flue gas from coal fired power plant is introduced into pre-chilling section. In the stage, SC-1 provides a cold energy (Q_{C-1}) to the pre-chilling tower. Under the low temperature condition, the moisture in the gas stream can be condensed into water and separated from the outlet of condensate tube. Then, the treated gas is introduced into the main freezing column, and which is chilled by the SC-2. With the cold energy Q_{C-2}, the CO_2 in the gas stream can anti-sublimate into the solid form (namely, dry ice) on the surface of the cold head. Simultaneously, the residual gas (mainly as N_2) exhausts from the system without phase change. According with the CO_2 deposition process, a motor driven scrapping rod is used to scrape the frosted CO_2 down to the storage column. The fallen CO_2 droplets is gathered and preserved by the cold energy from SC-3 (Q_{C-3}). Finally, the cold energy of condensate water, N_2 and captured CO_2 are recovered by heat exchangers. The recovered cold energy of the three stages is represented by H_{R-1}, H_{R-2} and H_{R-3}, respectively. Meanwhile, the heat loss associated with the three flows is represented by H_{L-1}, H_{L-2} and H_{L-3}, respectively.

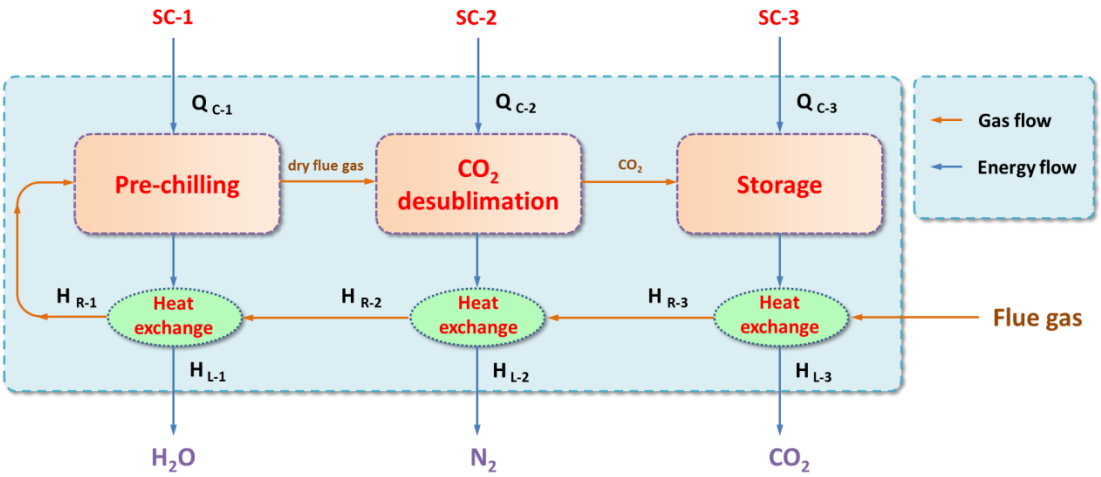

Figure 6-3 The overall mass and energy flow in the cryogenic CO_2 capture process.

3.2 Cryogenic performance of cryogenic CO_2 capture system

In order to understand intricate CO_2 capture process better and improve the capture efficiency. The cryogenic performances of the three stages in the system are numerically studied in this section. Some geometrical assumption is put forward to simplify the intricate process. The detail structure of the columns used in the system is depicted in Figure 6-4.

The distribution of temperature in the pre-chilling, CO_2 anti-sublimation and storage columns is simulated in Figure 6-5. The temperature field of the three columns is labeled in radial position. The diameters of the columns are 32, 32 and 16 cm, respectively. Because the function of the pre-chilling section is to reduce the temperature of feed gas and separate moisture, the lowest temperature is around -30 ℃. By contrast, the minimum temperature in the main-freezing tower can drop to -105 ℃ to anti-sublimate the CO_2 from the flue gas. For the storage column, it needs to maintain the condition below -78 ℃ to avoid the frosted CO_2 sublimation.

4. METHODOLOGY

Energy analysis is an effective measurement of energy quality or thermodynamic irreversibility related to the isolated processes (Liszka, et al., 2012). In order to grasp the energy flow in the system and improve the energy efficiency, the detailed energy requirement of the whole process is numerically investigated in this section.

4.1 Energy requirement

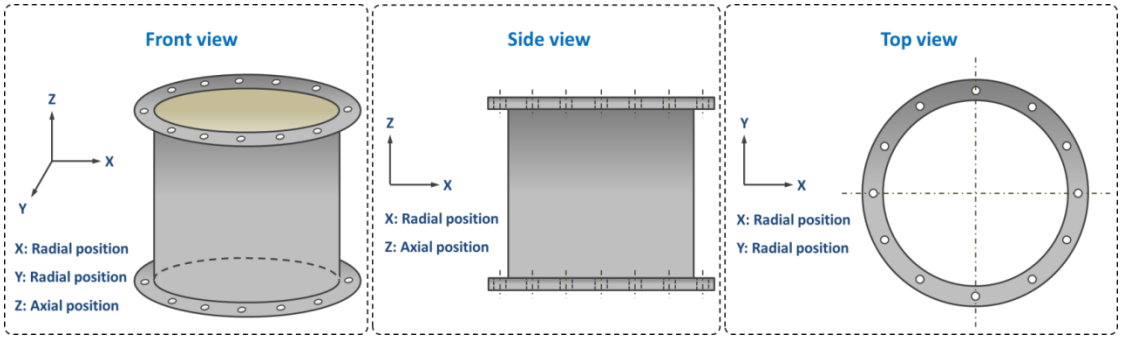

Figure 6-4 The geometrical structure of the columns in the system.

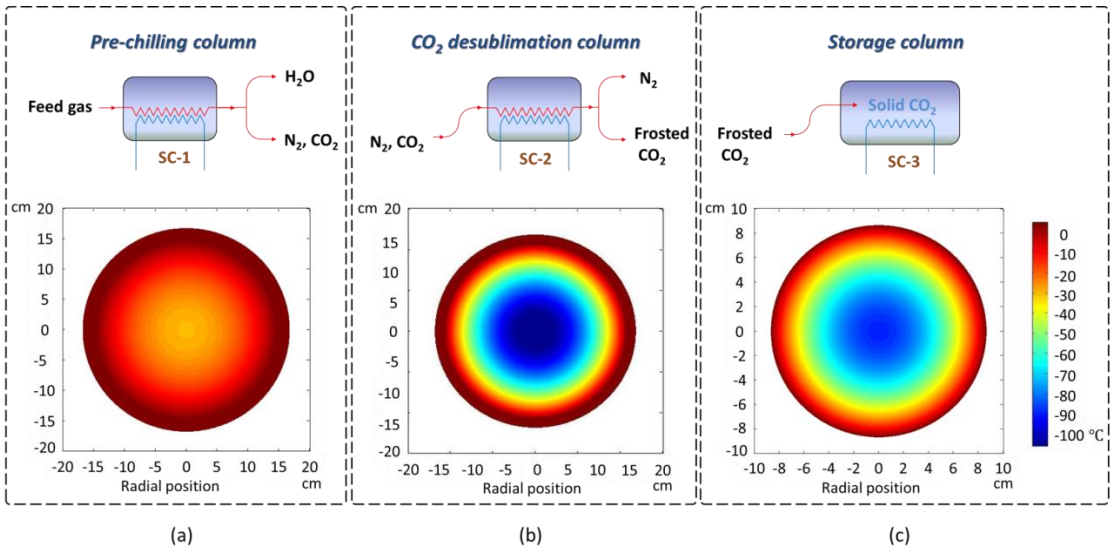

Figure 6-5 Temperature distributions in pre-cooling tower, main-freezing tower and storage column.

4.1.1 Characteristics of flue gas

In order to simplify the investigation of energy requirement for the system, some assumption is implemented.

The mass flow rate of the simulated flue gas (φ_M) can be calculated as follows:

$$\varphi_{\mathrm{M}} = \frac{\varphi_V \cdot \rho_g}{V_M} \quad \text{(kg/s)} \tag{6-1}$$

where φ_M and φ_V are the mass (kg/s) and volume (m^3/s) flow rates of gas mixture, respectively. V_M is the mole volume (L/mol) of ideal gas. ρ_g is the density (kg/m^3) of gas mixture and can be calculated as follows:

$$\rho_{\mathrm{g}} = \omega_{N_2} \cdot \rho_{N_2} + \omega_{CO_2} \cdot \rho_{CO_2} + \omega_{H_2O} \cdot \rho_{H_2O} \quad \text{(kg/m}^3\text{)} \tag{6-2}$$

here, ω_{N2}, ω_{CO2}, ω_{H2O} are the percentage (%) of N_2, CO_2, water vapor in the flue gas, respectively. ρ_{N2}, ρ_{CO2} and ρ_{H2O} are the density (kg/m^3) of N_2, CO_2 and H_2O, respectively.

The average heat capacity of gas mixture (C_g) is expressed as follows:

$$C_g = \omega_{N_2} \cdot C_{N_2} + \omega_{CO_2} \cdot C_{CO_2} + \omega_{H_2O} \cdot C_{H_2O} \quad \text{(J/kg·℃)} \tag{6-3}$$

here, C_g is the heat capacity of gas mixture. C_{N2}, C_{CO2}, C_{H2O} are the heat capacity of N_2, CO_2 and water vapor, respectively.

4.1.2 Energy requirement of the pre-chilling column

The total energy requirement of the pre-chilling column (Q_1) can be mainly divided into two parts: sensible heat of gas stream (Q_{S1}) and latent heat of evaporation for water vapor (Q_{L1}). Hereinto, the sensible heat for SC-1 (Q_{S1}) can be calculated as follows:

$$Q_{S1} = \varphi_M \cdot C_g \cdot \Delta T_1 \quad \text{(J/s)} \quad \text{(6-4)}$$

here ΔT_1 is the temperature variation from the inlet to the outlet of pre-chilling column.

The calculation method for the latent heat of the condensate water (Q_{L1}) is presented in Equation (5-5):

$$Q_{L1} = \varphi_{m\ H_2O} \cdot H_{H_2O} \quad \text{(J/s)} \quad \text{(6-5)}$$

here, H_{H2O} is the heat of vaporization for H_2O. The mass flow rate of H_2O ($\varphi_{m\ H2O}$) can be calculated as follows:

$$\varphi_{m\ H_2O} = \frac{\omega_{H_2O} \cdot \varphi_V \cdot M_{H_2O}}{V_M} \quad \text{(kg/s)} \quad \text{(6-6)}$$

where M_{H2O} is the mole mass of H_2O. Thus, the total energy requirement of the pre-chilling column (Q_1) can be calculated by the sum of the sensible heat and latent heat.

$$Q_1 = Q_{S1} + Q_{L1} \quad \text{(J/s)} \quad \text{(6-7)}$$

4.1.3 Energy requirement of the CO_2 anti-sublimation column

For the CO_2 capture column, the total energy requirement (Q_2) can be divided in the sensible heat of gas stream (Q_{s2}) and latent heat of anti-sublimation for CO_2 (Q_{L2}). The sensible heat (Q_{s2}) can be calculated as follows:

$$Q_{S2} = \varphi_M \cdot C_g \cdot \Delta T_2 \quad \text{(J/s)} \quad \text{(6-8)}$$

here, ΔT_2 is the temperature difference between the inlet and outlet of the main freezing column.

In addition, the latent heat (Q_{L2}) can be calculated as follows:

$$Q_{L2} = \varphi_{m\,CO_2} \cdot H_{CO_2} \quad \text{(J/s)} \quad \text{(6-9)}$$

here, H_{CO2} is the heat of sublimation for CO_2. The mass flow rate of CO_2 ($\varphi_{m\,CO2}$) can be calculated as follows:

$$\varphi_{m\,CO_2} = \frac{\omega_{CO_2} \cdot \varphi_V \cdot M_{CO_2}}{V_M} \quad \text{(kg/s)} \quad \text{(6-10)}$$

The total energy requirement of the CO_2 anti-sublimation column (Q_2) is the sum of the sensible heat and latent heat:

$$Q_2 = Q_{S2} + Q_{L2} \quad \text{(J/s)} \quad \text{(6-11)}$$

4.1.4 Energy requirement of the storage column

Due to there is no phase change in the storage column, the energy requirement (Q_3) is mainly used to maintain the preserving condition to avoid captured CO_2 sublimation.

$$Q_3 = \varphi_{m\,CO_2} \cdot C_{CO_2} \cdot \Delta T_3 \quad \text{(J/s)} \quad \text{(6-12)}$$

4.2 Exergy

Exergy is an effective measurement of energy quality or thermodynamic irreversibility related to the isolated processes (Liszka, et al., 2012). In order to grasp the energy flow in the system and improve the energy efficiency, the detailed exergy requirement of the whole process is numerically investigated in this section.

The calculation approaches for exergy efficiency in the published references are summarized in Table 6-3.

Table 6-3 The calculation approaches of exergy efficiency

1) The simple efficiency is the ratio of the total outgoing exergy flow ($E_{x\ out}$) to the total incoming

exergy flow ($E_{x\ in}$) (Cornelissen, 1997):

$$\eta = \frac{E_{x_{out}}}{E_{x_{in}}}$$

2) The calculation defined by Torres and Gallo in 1998 is described as following:

$$\eta = \frac{E_{x_{out}} - E_{x_{loss}}}{E_{x_{in}}}$$

here $E_{x\ loss}$ represents the exergy loss in the system.

3) The traditional form of exergy efficiency (Ghannadzadeh et al., 2012):

$$\eta = \frac{E_{x_{desired\ output}}}{E_{x_{used}}}$$

where $E_{x\ desired\ output}$ represents the desired result produced in the system without the external exergy loss. $E_{x\ used}$ is defined as the net resources which were spent to generate the product. The relationship of $E_{x\ desired\ output}$ and $E_{x\ used}$ can be expressed as:

$$E_{x_{used}} = E_{x_{desired\ output}} + I$$

here, I is the irreversibility of the system.

4) The exergy efficiency with transiting exergy is introduced by Brodyansky et al. (1994):

$$\eta = \frac{E_{x_{out}} - E_{x_{tr}}}{E_{x_{in}} - E_{x_{tr}}}$$

where $E_{x\ tr}$ is the transiting exergy that can be considered as the part of the exergy which traverses a system without taking any part in the mechanical, thermal or chemical changes which take place in the system.

5. RESULTS AND DISCUSSION

5.1 Effect of the cryogenic temperature of SC-1

The variation of the energy requirement for the different sections according with the temperature of SC-1 is summarized in Table 6-4. From the results, it indicates that with the decreasing of the temperature for SC-1, the energy requirement of pre-chilling column increased and simultaneously the energy requirement of CO_2 anti-sublimation column decreased obviously. With the temperature of SC-1 varied from -20℃ to -60℃, the energy requirement of pre-chilling stage increased from 14.50 $_{thermal}$ J/s to 18.78 $_{thermal}$ J/s. By contrast, the energy requirement of the CO_2 anti-sublimation stage decreased from 32.03 $_{thermal}$ J/s to 25.90 $_{thermal}$ J/s due to the sufficient pre-treatment, and the energy requirement of the storage column varied from 7.20 $_{thermal}$ J/s to 12.73 $_{thermal}$ J/s. The relationship of the detailed energy requirement with the temperature of SC-1 is described in Figure 6-6.

Table 6-4 Effect of the temperature of SC-1 on the energy efficiency for the cryogenic CO_2 capture system *

Energy requirement (J/s)	Temperature of SC-1 (℃)				
	-20	-30	-40	-50	-60
Pre-chilling stage					
Sensible heat	8.09	9.24	10.40	11.55	12.71
Latent heat (condensate water)	7.57	7.57	7.57	7.57	7.57
Heat removal	15.66	16.81	17.97	19.12	20.28
Energy requirement (electric)	5.80	6.23	6.66	7.08	7.51
Energy requirement (thermal)	14.50	15.58	16.65	17.70	18.78
CO_2 anti-sublimation stage					
Sensible heat	11.03	9.92	8.82	7.72	6.62
Latent heat (frosted CO_2)	12.03	12.03	12.03	12.03	12.03
Heat removal	23.06	21.95	20.85	19.75	18.65
Energy requirement (electric)	12.81	12.19	11.58	10.97	10.36
Energy requirement (thermal)	32.03	30.48	28.95	27.43	25.90
CO_2 storage column					
Sensible heat	5.18	6.21	7.33	8.20	9.17
Energy requirement (electric)	2.88	3.45	4.07	4.56	5.09
Energy requirement (thermal)	7.20	8.63	10.18	11.40	12.73
Total energy requirement (thermal)	53.73	54.69	55.78	56.53	57.41

* The flow rate of the gas stream is set at 5 L/min. The temperature of SC-2 and 3 are both set at -120 ℃. The COP of SC-1, 2 and 3 are 2.7, 1.8 and 1.8, respectively. The concentration of CO_2 is set at 13%. The conversion efficiency from electric power to thermal energy is defined as 40%.

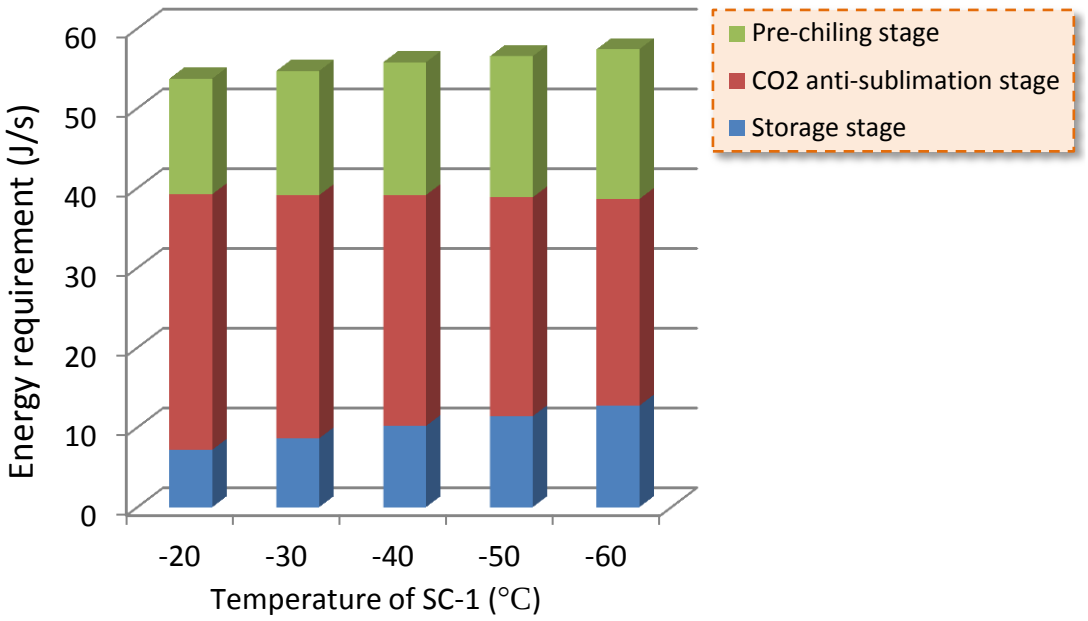

Figure 6-6 The influence of temperature of SC-1 on the energy requirement of the pre-chilling, CO_2 anti-sublimation and storage stages.

5.2 Effect of the flow rate of gas stream

The variation of the energy requirement for the different units according with the flow rate of gas stream is summarized in Table 6-5. From the results, it indicates that with the increasing of the flow rate, the energy requirement of pre-chilling column increased rapidly. When the flow rate was set at 1 L/min, the energy requirement of the pre-chilling stage was 2.95 $_{thermal}$ J/s. With the flow rate increasing to 5 L/min, the energy requirement of pre-chilling stage increased to 15.58 $_{thermal}$ J/s. Meanwhile, the energy requirement of CO_2 anti-sublimation column also increased according to the flow rate. When the flow rate increased from 1 to 5 L/min, the energy requirement of the CO_2 anti-sublimation stage varied from 6.18 $_{thermal}$ J/s to 30.48 $_{thermal}$ J/s. Additionally, the energy requirement of the storage column also increased from 2.28 $_{thermal}$ J/s to 11.40 $_{thermal}$ J/s. The detail of the energy variation of the three stages (pre-chilling, CO_2 anti-sublimation and storage) is shown in Figure 6-7.

Table 6-5 The effect of flow rate on the energy efficiency for the cryogenic CO_2 capture system *

Energy requirement (J/s)	Flow rate of the gas stream (L/min)				
	1	2	3	4	5
Pre-chilling stage					
Sensible heat	1.68	3.36	5.88	7.56	9.24
Latent heat (condensate water)	1.51	3.03	4.54	6.05	7.57
Heat removal	3.19	9.39	10.42	13.61	16.81
Energy requirement (electric)	1.18	3.48	3.86	5.04	6.23
Energy requirement (thermal)	2.95	8.70	9.65	12.60	15.58
CO_2 anti-sublimation stage					
Sensible heat	2.01	4.02	6.03	8.04	9.92
Latent heat (frosted CO_2)	2.44	4.88	7.32	9.75	12.03
Heat removal	4.45	8.90	13.35	17.79	21.95
Energy requirement (electric)	2.47	4.94	7.42	9.88	12.19
Energy requirement (thermal)	6.18	12.35	18.55	24.70	30.48
CO_2 storage column					
Sensible heat	1.64	3.28	4.92	6.56	8.20
Energy requirement (electric)	0.91	1.82	2.73	3.64	4.56
Energy requirement (thermal)	2.28	4.55	6.83	9.10	11.40
Total energy requirement (thermal)	11.41	25.60	35.03	46.40	57.46

* The temperature of SC-1, 2 and 3 are set at -30 ℃, -120 ℃ and -120 ℃, respectively. The COP of SC-1, 2 and 3 are 2.7, 1.8 and 1.8, respectively. The concentration of CO_2 is set at 13%. The conversion efficiency from electric power to thermal energy is defined as 40%.

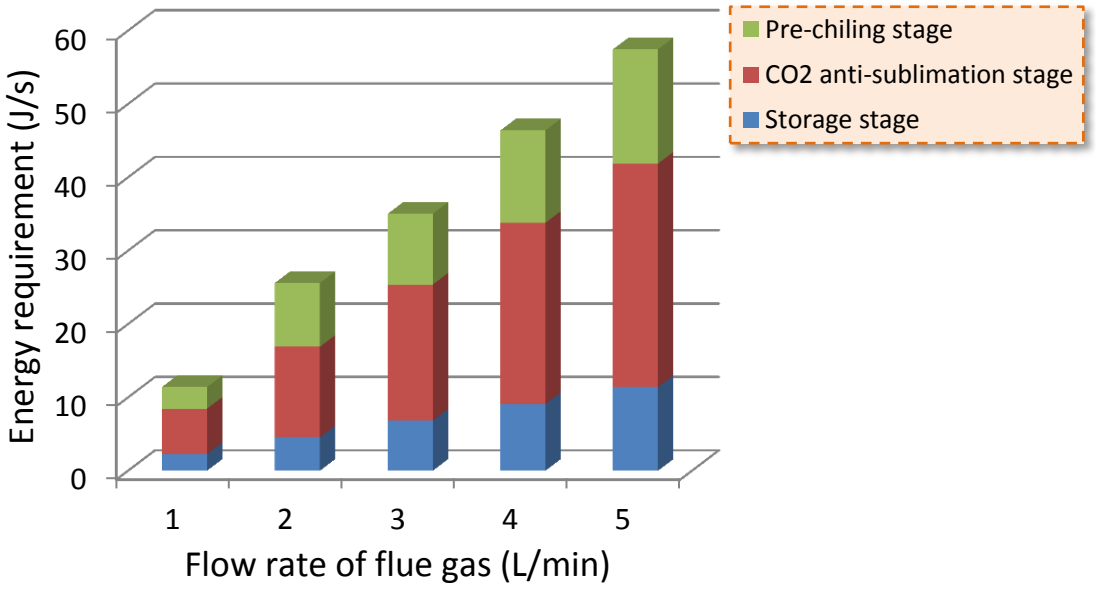

Figure 6-7 The influence of flow rate on the energy requirement of the pre-chilling, CO_2 anti-sublimation and storage stages.

5.3 Effect of the CO_2 concentration

The variation of the energy requirement for the different units according with the flow rate of gas stream is summarized in Table 6-6. From the results, it indicates that with the increasing of the CO_2 concentration, the energy requirement of pre-chilling column increased slowly. When the CO_2 concentration was set at 5 %, the energy requirement of the pre-chilling stage was 15.38 $_{thermal}$ J/s. With the CO_2 concentration increasing to 40 %, the energy requirement of pre-chilling stage increased to 16.38 $_{thermal}$ J/s. By contrast, the energy requirement of CO_2 anti-sublimation column increased rapidly associated with the concentration of CO_2. When the concentration increased from 5 % to 40 %, the energy requirement of the CO_2 anti-sublimation stage varied from 18.50 $_{thermal}$ J/s to 67.53 $_{thermal}$ J/s. Meanwhile, the energy requirement of the storage column also increased from 4.20 $_{thermal}$ J/s to 40.15 $_{thermal}$ J/s. The energy variation process with CO_2 concentration is illustrated in Figure 6-8.

Table 6-6 The effect of CO_2 concentration on the energy efficiency for the cryogenic CO_2 capture system *

Energy requirement (J/s)	CO2 concentration (%)				
	5	10	20	30	40
Pre-chilling stage					
Sensible heat	9.03	9.20	9.52	9.84	10.12
Latent heat (condensate water)	7.57	7.57	7.57	7.57	7.57
Heat removal	16.6	16.77	17.09	17.41	17.69
Energy requirement (electric)	6.15	6.21	6.33	6.45	6.55
Energy requirement (thermal)	15.38	15.53	15.83	16.13	16.38
CO_2 anti-sublimation stage					
Sensible heat	9.63	10.03	10.40	10.76	11.09
Latent heat (frosted CO_2)	4.69	9.38	18.76	28.14	37.52
Heat removal	13.32	19.41	29.16	38.90	48.61
Energy requirement (electric)	7.40	10.78	16.20	21.61	27.01
Energy requirement (thermal)	18.50	26.95	40.50	54.03	67.53
CO_2 storage column					
Sensible heat	3.02	6.21	13.09	22.66	28.90
Energy requirement (electric)	1.68	3.45	7.27	12.59	16.06
Energy requirement (thermal)	4.20	8.63	18.18	31.48	40.15
Total energy requirement (thermal)	38.08	51.11	74.51	101.64	124.06

* The temperature of SC-1, 2 and 3 are set at -30 ℃, -120 ℃ and -120 ℃, respectively. The COP of SC-1, 2 and 3 are 2.7, 1.8 and 1.8, respectively. The flow rate of flue gas is set at 5 L/min. The conversion efficiency from electric power to thermal energy is defined as 40%.

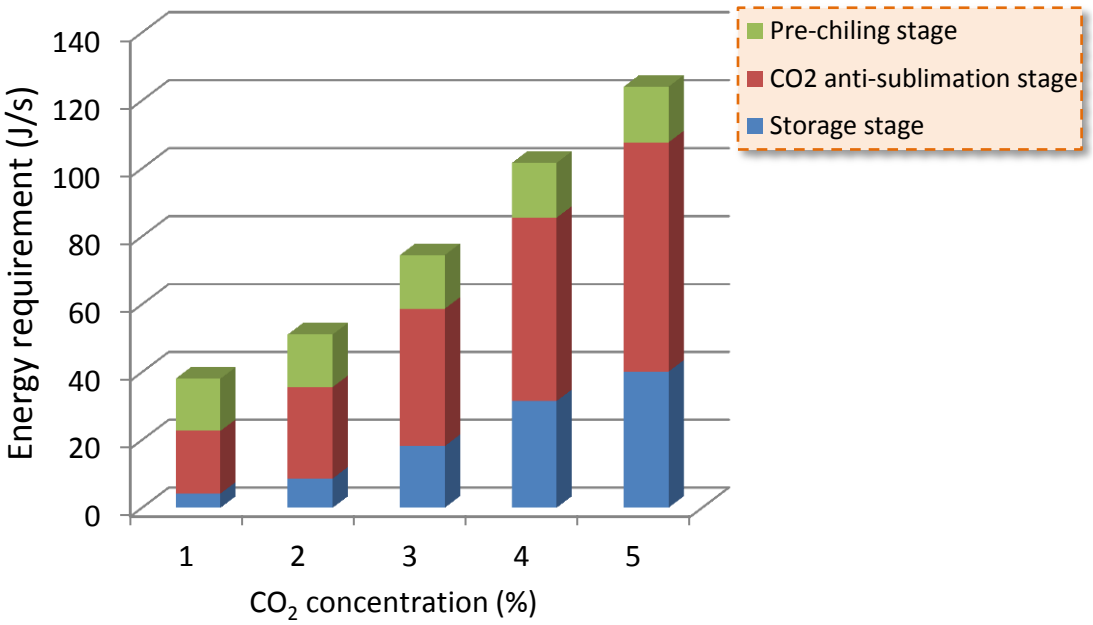

Figure 6-8 The influence of CO_2 concentration on the energy requirement of the pre-chilling, CO_2 anti-sublimation and storage stages.

6. CONCLUSION

The overall energy flow of the Stirling cooler based cryogenic CO_2 capture process was simulated. The theoretical analysis on the energy requirement of each unit in the capture system was also performed. Furthermore, the influence of the CO_2 capture section on the efficiency of the coal-fired power plant was investigated. Finally, the energy performance of the cryogenic system is compared with the reference CO_2 capture technology (amine based absorption process). The main conclusion of the work can be summarized as follows:

1) With the temperature of SC-1 varied from -20 to -60℃, the total energy requirement of the cryogenic CO_2 capture system increased from 53.73 J/s to 57.41 J/s.

2) With the flow rate of flue gas increased from 1 to 5 L/min, the total energy requirement of the cryogenic CO_2 capture system increased from 11.41 J/s to 57.46 J/s.

3) With the CO_2 concentration in the flue gas increased from 5% to 40%, the total energy requirement of the cryogenic CO_2 capture system increased from 30.08 J/s to 124.06 J/s.

4) The energy analysis provides a reliable way to improve capture efficiency and reduce energy penalty. For the future work, the dynamic operating process of system will be simulated, and simultaneously the pilot pant test based on the developed system will also be carried out.

REFERENCES

Z. Amrollahi, I.S. Ertesvåg, O. Bolland, 2011. Thermodynamic analysis on post-combustion CO_2 capture of natural-gas-fired power plant. International Journal of Greenhouse Gas Control 5, 422–426.

M. Liszka, T. Malik, G. Manfrida, 2012. Energy and exergy analysis of hydrogen-oriented coal gasification with CO_2 capture. Energy 45, 142–150.

IEA. (International Energy Agency). World energy outlook 2009. Paris France, 2009.

A. Ghannadzadeh, R. Thery-Hetreux, O. Baudouin, P. Baudet, P. Floquet, X. Joulia, 2012. General methodology for exergy balance in ProSimPlus process simulator. Energy 44, 38-59.

P. Versteeg, E.S. Rubin, 2011. A technical and economic assessment of ammonia-based post-combustion CO_2 capture at coal-fired power plants. International Journal of Greenhouse Gas Control 5, 1596–1605.

Z. Amrollahi, P.A.M. Ystad, I.S. Ertesvåg, O. Bolland, 2012. Optimized process configurations of post-combustion CO_2 capture for natural-gas-fired power plant – Power plant efficiency analysis. International Journal of Greenhouse Gas Control 8, 1–11.

M.J. Tuinier, H.P. Hamers, M. S. Annaland, 2011. Techno-economic evaluation of cryogenic CO_2 capture—A comparison with absorption and membrane technology. International Journal of Greenhouse Gas Control 5, 1559–1565.

A. Cousins, L.T. Wardhaugh, P.H.M. Feron, 2011. A survey of process flow sheet modifications for energy efficient CO_2 capture from flue gases using chemical absorption. International Journal of Greenhouse Gas Control 5, 605–619.

P. Luis, T. V. Gerven, B. V. Bruggen, 2012. Recent developments in membrane-based technologies for CO_2 capture. Progress in Energy and Combustion Science 38, 419–448.

A.L. Chaffee, G.P. Knowl es, Z. Liang, J. Zhang, P. Xiao, P.A. Webley, 2007. CO_2 capture by adsorption: Materials and process development. International Journal of Greenhouse Gas Control 1, 11–18.

E.S. Rubin, H. Mantripragada, A. Marks, P. Versteeg, J. Kitchin, 2012. The outlook for improved carbon capture technology. Progress in Energy and Combustion Science 38, 630 – 671.

C.F. Song, Y. Kitamura, S.H. Li, W.Z. Jiang, 2012. Parametric analysis of a novel cryogenic CO_2 capture system based on Stirling coolers. Environmental Science & Technology 46 (22), 12735–12741.

Q. Wang, J. Luo, Z. Zhong, A. Borgna, 2011. CO_2 capture by solid adsorbents and their applications: current status and new trends. Energy & Environmental Science 4, 42–55.

A. Criscuoli, E. Drioli, 2007. New metrics for evaluating the performance of membrane operations in the logic of process intensifi cation. Industrial & Engineering Chemistry Research 46, 2268-2271.

A.R. Smith, J. Klosek, 2001. A review of air separation technologies and their integration with energy conversion processes. Fuel Processing Technology 70, 115-134.

P. Markewitz, W. Kuckshinrichs, W. Leitner, J. Linssen, P. Zapp, R. Bongartz, A. Schreiber, T.E. Muller, 2012. Worldwide innovations in the development of carbon capture technologies and the utilization of CO_2. Energy & Environmental Science 5, 7281-7305.

B. Zhao, Y. Su, W. Tao, L. Li, Y. Peng, 2012. Post-combustion CO_2 capture by aqueous ammonia: A state-of-the-art review. International Journal of Greenhouse Gas Control 9, 355-371.

M. Clausse, J. Merel, F. Meunier, 2011. Numerical parametric study on CO_2 capture by indirect thermal swing adsorption. International Journal of Greenhouse Gas Control 5, 1206-1213.

M.R.M. Abu-Zahra, L.H.J. Schneiders, J.P.M. Niederer, P.H.M. Feron, G.F. Versteeg, 2007. CO_2 capture from power plants: Part I. A parametric study of the technical performance based on monoethanolamine. International Journal of Greenhouse Gas Control 1, 37-46.

B. Belaissaoui, Y.L. Moullec, D. Willson, E. Favre, 2012. Hybrid membrane cryogenic process for post-combustion CO_2 capture. Journal of Membrane Science 415-416, 424-434.

T.L.P. Dantas, F.M.T. Luna, I.J. Silva Jr, A.E.B. Torres, D.C.S. de Azevedo, A.E. Rodrigues, R.F.P.M. Moreira, 2011. Carbon dioxide–nitrogen separation through pressure swing adsorption. Chemical Engineering Journal 172, 698-704.

M.T. Ho, G.W. Allinson, D.E. Wiley, 2008. Reducing the cost of CO_2 capture from flue gases using pressure swing adsorption. Industrial & Engineering Chemistry Research 47, 4883-4890.

R.L. Cornelissen. Thermodynamics and sustainable development: the use of exergy analysis and the reduction of irreversibility. PhD thesis, University of Twente, The Netherlands; 1997.

E.A. Torres, W.L.R. Gallo, 1998. Exergetic evaluation of a cogeneration system in a petrochemical complex, Energy Convers. Manage. 39 (16–18), 1845–1852.

V.M. Brodyansky, M.V. Sorin, P. Le Goff, 1994. The Efficiency of Industrial Processes: Exergy Analysis and Optimization, Elsevier Science B.V.

CHAPTER 7

CONCLUSION

In this thesis, I exploited a novel cryogenic CO_2 capture system based on Stirling coolers. By the cryogenic system, moisture and CO_2 in the flue gas can be separated at the different places. Meanwhile, the residual gas (such as N_2) exhausts from the system without phase change.

In Chapter 1, the background of our research is introduced. The main CO_2 emission and mitigation technologies are summarized. Furthermore, the advantages and disadvantages of these technologies are illustrated in detail.

In Chapter 2, the principle of operation and advantages of the system were demonstrated and verified in detail. According to the experimental results, an effective separation on the basis of differences in frost points can be achieved without increasing pressure drops and plugging problems. From the performance of system, it demonstrated that the system can separate CO_2 efficiently. Furthermore, the influence of flow rate of gas stream and temperature of SC-1 on the performance of system was investigated. Based on the designed cryogenic system, the recovery of CO_2 can achieve 96% with 1.5 MJ/kg CO_2 energy consumption, which demonstrated that the research of the CO_2 capture process based on Stirling coolers is promising. Meanwhile, further testing has been planned to determine the range and overall performance of the system and solve the problem of heat loss. Besides, the test of CO_2 capture from flue

gas and biogas will be carried out.

In Chapter 3, the theoretical analysis of the working mechanism of FPSC has been conducted in detail. Meanwhile, the COP of the FPSC was numerically deduced. In order to improve the COP of FPSC, the key parameters that affect the COP were also investigated. Based on the experimental results, the conclusions are summarized as follows:

1) From the experiment of the materials, it can be concluded that when the cold head was made by copper, the temperature loss of the cold head was 13.38 ℃ and the COP of FPSC was 0.82 (with the root temperature was -140 ℃). By contrast, the temperature difference for the aluminium cold head was 33.31 ℃, and the COP of FPSC was 0.61. However, it is worth noting that due to the weight of copper is further greater than aluminium. Therefore, the oscillation phenomenon is also dramatic and which would result in a higher energy loss.

2) The length of cold head should be as short as possible to improve the COP of FPSC. When the length of the cold head was set at 270 mm, the temperature difference and COP of FPSC were 15.73 ℃ and 0.59 (with the root temperature is -140 ℃), respectively. When the length was shortened to 180 mm, the temperature difference reduced to 9.92 ℃. Meanwhile, the COP of FPSC increased to 0.82. By contrast, the diameter should be as big as possible to enhance the COP. When the diameter of the cold head was set at 30 mm, the temperature difference was 20.28 ℃ and the COP of FPSC was 0.52 (with the root temperature is -140 ℃). With the diameter thickening to 40 mm, the temperature difference decreased to 15.73 ℃ and the COP of FPSC increased to 0.59.

3) In addition, the ambient temperature also has a significant influence on the COP of FPSC. When the ambient temperature varied from 8 ℃ to 28 ℃, the COP of FPSC

reduced from 0.7 to 0.6. Nevertheless, the effect of ambient humidity on the COP is not significant. With the ambient humidity increasing from 20% to 75%, the COP of FPSC varied in the range of 0.62 to 0.68.

4) Although the FPSCs in the system had high COPs, the COP of the system was around 0.7 due to other energy consumption units (such as vacuum pump and control panel). For the future work, the energy penalty of the main units should be avoided and the latent heat associated with frost CO_2 should also be recovered.

In Chapter 4, the key parameters that affect capture performance were experimentally investigated in this chapter. Through the experiments of process parameters, it was found that the optimal conditions for the system were: idle operating time before gas inflow of 240 min, flow rate of 5 L/min, temperature of SC-1 of -30 ℃ and a vacuum degree 2.2×10^3 Pa (other conditions: temperature of SC-2 and 3 are both set at -120 ℃). Under these conditions, the EC of the system is around 0.5 $MJ_{electrical}$/kg CO_2 with above 90% CO_2 recovery. In addition, for further improvement of capture performance, the latent heat of condensate water should be recovered.

In Chapter 5, the phenomenon of CO_2 frosts on the surface of the heat exchanger has an important influence on capture performance. Based on this, the growth processes of the CO_2 frost layer and its effect on temperature variation have been numerically analyzed. The effect of frost layer growth on thermal conductivity and temperature variation was also investigated. According to the results of simulation and experiments, the following conclusions are given:

1) The thickness of the frost layer increased with time but the rate of CO_2 deposition decreased gradually. Furthermore, with the increase in the flow rate, the frost growth also accelerated. After 60 minutes, the thickness of frost layer was 3.0 mm.

2) The thermal conductivity of the frost layer increased due to the growth of the frost layer. Nevertheless, as time passed, its increase rate reduced. After 60 minutes, the thermal conductivity of the frost layer increased to around 0.4 W/(m·K).

3) The frost surface temperature increased rapidly as frost insulated the heat exchanger. Meanwhile, with the decrease in the flow rate, the increase rate of temperature decelerated. When the flow rate was set at 1 L/min, the temperature of the cold head for the SC varied from -105.2 ℃ to -102.1 ℃ after 60 minutes. When the flow rate was 3 L/min, the temperature rose from -106.3 ℃ to -98.0 ℃. However, the rate of the increase declined and approached zero when the energy balance between the gas stream and frost layer was reached.

In Chapter 6, the overall energy flow of the Stirling cooler based cryogenic CO_2 capture process was simulated. The theoretical analysis on the energy requirement of each unit in the capture system was also performed. Furthermore, the influence of the CO_2 capture section on the efficiency of the coal-fired power plant was investigated. Finally, the energy performance of the cryogenic system is compared with the reference CO_2 capture technology (amine based absorption process). The main conclusion of the work can be summarized as follows:

1) With the temperature of SC-1 varied from -20 ℃ to -60 ℃, the total energy requirement of the cryogenic CO_2 capture system increased from 53.73 J/s to 57.41 J/s.

2) With the flow rate of flue gas increased from 1 to 5 L/min, the total energy requirement of the cryogenic CO_2 capture system increased from 11.41 J/s to 57.46 J/s.

3) With the CO_2 concentration in the flue gas increased from 5% to 40%, the total energy requirement of the cryogenic CO_2 capture system increased from 30.08 J/s to 124.06 J/s.

4) The energy analysis provides a reliable way to improve capture efficiency and reduce energy penalty. For the future work, the dynamic operating process of system will be simulated, and simultaneously the pilot pant test based on the developed system will also be carried out.

Although cryogenic CO_2 capture offers some advantages (such as no chemical absorbents are required and the process can be operated at atmospheric pressures), the cold source for CO_2 liquefaction or anti-sublimation is necessary (Tuinier et al., 2011). At present, the usual cold source is provided by liquid nitrogen (LN_2) and liquefied natural gas (LNG). For the future work, more common cold source should be developed. Meanwhile, in light of the characteristic of cryogenic process, CO_2 concentration is also a limitation (which is more suitable for high CO_2 emission source). Therefore, future work should focus on the integration with other approaches (such as membrane).

SUMMARY

Carbon dioxide (CO_2) is one of the most important greenhouse gases (GHG) for the issue of the climate change. To reduce the effects caused by this environmental problem, several technologies were studied to capture CO_2 from large emission source points: (i) absorption; (ii) adsorption; (iii) gas-separation membranes; and (iv) cryogenic distillation. It is noteworthy that the capture efficiency of the conventional processes does not fit with expected outcomes and energy consumption is still too high. Therefore, developing new methods and technologies that compete with conventional industrial processes for CO_2 capture and recovery is a hot topic in the current research.

In our research, a novel cryogenic CO_2 capture system based on Stirling coolers was developed. During the capture process, the CO_2 in the flue gas can be captured in the solid form and frosts on the surface of the cold head. Then, the captured CO_2 is separate by a motor driven scraper and gathered in the storage column.

The thesis is organized as follows: the background of our research is introduced in Chapter 1. The detailed cryogenic capture is described in Chapter 2. The property of Stirling cooler is investigated in Chapter 3. The performance of the system is evaluated in Chapter 4. The CO_2 frost process is simulated in Chapter 5. The energy analysis of the system is carried out in Chapter 6. Finally, the main conclusion of the thesis is summarized, and the outlook of CO_2 capture technology is prospected in Chapter 7.

要旨(日本語)

温室効果ガスによって引き起こされる世界的な気候変動が懸念されている。温室効果ガスの中で、大気中に占める割合が高い二酸化炭素は温室効果の 6 割に寄与しているとされる。風力や太陽光、バイオマスなど新しい再生可能エネルギーが開発されているものの、世界は今後 10 年間は化石燃料に依存せざるを得ないであろう。よって二酸化炭素の回収は温室効果ガスの制御に極めて有効かつ世界的な優先事項であるであることは明らかである。IPCC により二酸化炭素の回収・貯留（CCS）が温室効果ガス緩和の持続的技術として提唱されている。

近年、多くの研究者らは二酸化炭素の回収効率向上と回収プロセスのコスト削減に努めてきた。現在、二酸化炭素の回収技術として吸収・吸着、冷凍、膜分離といった物理化学的方法が知られている。これらの技術の中で化学溶剤による吸収法が最も良いとされている。しかし本法は高価であり、吸収後の溶液から二酸化炭素を分離するのが困難であり、その適用が限られている。

そこで本研究では、効率的で低コストなスターリングクーラーを活用したシステムを構築し、二酸化炭素の冷凍回収特性を実験的に明らかにした。回収プロセスの概略は以下の通り：初めに供試ガスは二酸化炭素の昇華点以上の温度に達するまで前冷凍処が行われる。主冷凍塔において、そのガス流は二相の混合物に分離される。固体状の二酸化炭素（ドライアイス）は SC-2 における熱交換部上で氷結し、回転式羽根によりかきとられる。ドライアイスは SC-3 によって保冷の可能な温度にまで冷却された貯蔵タンクに落下する。残留ガスはガス出口を通じ大気中に放出される。

先ず、本研究の背景を検討された(第 1 章)。次に、スターリングクーラー(SCs)より構成される新しい二酸化炭素の冷凍回収システムの概要を第 2 章に紹介した。なお、スターリングクーラーの特徴(第 3 章)と重要なパラメタを検討をしった(第 4 章)。また、二酸化炭素固体化のプロセス(第 5 章)とシステムのエネルギー需要量(第 6 章)をモデルに分析した。最後に、本研究の主な結論と将来の二酸化炭素回収技術をまとめした(第 7 章)。

ACKNOWLEDGEMENTS

Three years of overseas study is over. The thesis is written and it implies that my doctoral research will also come to an end. I think it is time to say thank you to the people, who gave me concern and help all the time.

First of all I would like to thank my supervisor, dear professor Yutaka Kitamura, for giving me the opportunity to study for a doctoral degree in Japan and for all his support in the last three years. I also want to thank Mr. Yamano and Mr. Yamasaki of Tanabe Engineering Corporation for their help with technology.

I also would like to thank the China Scholarship Council (CSC). The scholarship let me past a comfortable study life in the last three years.

Thanks to all the members from our laboratory. Thanks for their help in my study and life. Thanks all my friends in Japan, they let me feel the color of the life.

In the end, I would like to express my gratitude to my parents and my wife. My father and mother are the greatest teachers in my life. They taught me how to behave as a human being. Thanks to my wife for her love. Whenever happiness or hardship, she always accompanies me, supports me and cares me. Her smile let me become strong and optimistic.

PUBLICATIONS

JOURNAL PAPERS

[1] Song C.F., Kitamura Y., Li S.H., Ogasawara K.J. Design of a cryogenic CO_2 capture system based on Stirling coolers. International Journal of Greenhouse Gas Control 2012; 7:107-14.

[2] Song C.F., Kitamura Y., Li S.H. Evaluation of Stirling cooler system for cryogenic CO_2 capture. Applied Energy 2012; 98:491-501.

[3] Song C.F., Kitamura Y., Li S.H., Jiang W.Z. Parametric Analysis of a Novel Cryogenic CO_2 Capture System Based on Stirling Coolers. Environmental Science & Technology 2012, 46 (22), pp 12735-12741.

[4] Song C.F., Kitamura Y., Li S.H., Jiang W.Z. Analysis of CO_2 frost formation properties in cryogenic capture process. International Journal of Greenhouse Gas Control 2013; 13:26-33.

[5] Song C.F., Kitamura Y., Li S.H. Performance optimization of a novel cryogenic CO_2 capture process by Response Surface Methodology (RSM). Journal of the Taiwan Institute of Chemical Engineers. Under review.

[6] Song C.F., Kitamura Y., Li S.H. Energy analysis of the cryogenic CO_2 capture process based on Stirling coolers. International Journal of Greenhouse Gas Control. Under review.

[7] Song C.F., Kitamura Y., Li S.H. Study on the COP of Free Piston Stirling Cooler

(FPSC) in the anti-sublimation CO_2 capture process. Applied Energy. Under review.

CONFERENCES PROCEEDINGS

[1] Song C.F., Kitamura Y., Jiang W.Z. A novel desublimation CO_2 capture process based on Free Piston Stirling Cooler (FPSC) system. International Conference on Applied Energy. ICAE 2012, Jul 5-8, 2012, Suzhou, China.

[2] Song C.F., Kitamura Y., Jiang W.Z. Application of Free Piston Stirling Cooler (SC) on CO_2 Capture Process. International Conference on Greenhouse Gas Technologies. GHGT-11, Nov 18-22, Kyoto, Japan.